# LOAD-INDUCED CRACK PREDICTION USING HYBRID MECHANISTIC MACHINE LEARNING MODELS

A Thesis

by

JACOB IAN PAVELKA

Submitted to the Graduate and Professional School of
Texas A&M University
in partial fulfillment of the requirements for the degree of

MASTER OF SCIENCE

| | |
|---|---|
| Chair of Committee, | Stephanie Paal |
| Committee Members, | Maria Koliou |
| | Raymundo Arróyave |
| Head of Department, | Zachary Grasley |

December 2022

Major Subject: Civil Engineering

# ABSTRACT

This thesis implements hybrid mechanistic-machine learning models to predict load-induced cracking in concrete beams without transverse (applied along the depth of the beam) reinforcement. Predicting load-induced cracking is crucial for robustly predicting shear capacity. Mechanistic models lack the flexibility to represent load-induced cracking, and machine learning models lack a sufficient data set to learn load-induced cracking relationships. Hybrid models have the best chance of accurately predicting load-induced cracking. To implement hybrid modeling, we developed the Hybrid Learning theory and identified optimal combinations of mechanistic and machine learning models. Additionally, we developed a framework that has low mechanistic bias and sufficient constraint. This framework will allow for mechanistically consistent predictions. Hybrid models have great potential for modeling in Structural Engineering because of their flexibility and interpretability, and robust prediction of shear capacity will lead to increased design efficiency and understanding of concrete beam failure mechanics.

# CONTRIBUTORS AND FUNDING SOURCES

This work was supported by a thesis committee consisting of Professor Stephanie Paal of the Department of Civil Engineering and Professors Maria Koliou of the Department of Civil Engineering and Raymundo Arróyave of the Department of Materials Science & Engineering. The data used to train machine learning models were provided by Hongrak Pak. All other work conducted for the thesis was completed by the student independently.

# TABLE OF CONTENTS

Page

ABSTRACT ..... ii

CONTRIBUTORS AND FUNDING SOURCES ..... iii

TABLE OF CONTENTS ..... iv

LIST OF FIGURES ..... vi

LIST OF TABLES ..... viii

CHAPTER I: INTRODUCTION ..... 1

CHAPTER II: OVERVIEW OF RELATED WORK ..... 5

- Experimental Programs: Shear Failure, Explained ..... 6
- Mechanistic Models ..... 15
- Machine Learning Models ..... 21

CHAPTER III: DESCRIPTION OF THE PROBLEM ..... 25

CHAPTER IV: METHODOLOGY ..... 28

CHAPTER V: INVESTIGATION OF HYBRID MODELING METHODS ..... 32

- Mechanics as a means of structure ..... 34
- Mechanics as a means of data ..... 44
- Parameter-Free Data-Driven Modeling ..... 46
- Discussion ..... 47
- Hybrid Learning ..... 58
- Application to Shear Failure ..... 62

CHAPTER VI: RECREATING MECHANISTIC SHEAR MODELS ..... 67

- Shear Crack Propagation Theory ..... 67
- Cavagnis et al. (2018) Critical Shear Crack Theory ..... 83

CHAPTER VII: IMPLEMENTATION OF THE DATA-DRIVEN INCLUSION METHOD ..... 83

CHAPTER VIII: ANALYSIS OF CRACK PREDICTIONS ..... 95

CHAPTER IX: INVESTIGATING DIFFERENCES IN MODEL PERFORMANCE ..... 101

Optimal Model Configuration ..... 105
Validation of Hybrid Learning Theory ..... 106
Use in Structural Engineering ..... 108

CHAPTER X: THE BASIS OF MODEL IMPROVEMENT ..... 110

Consideration of multiple cracks ..... 110
Low Bias Mechanistic Models ..... 118

CHAPTER XI: CONSTRAINT EFFECTS ..... 126

Testing the Effect of Constraint ..... 129

CHAPTER XII: CONCLUSIONS AND FUTURE WORK ..... 134

GLOSSARY OF VARIABLES ..... 139

REFERENCES ..... 143

# LIST OF FIGURES

Page

Figure 2.1: Cantilever action in concrete beams without shear reinforcement ..... 7

Figure 2.2: Shear valley explaining variation in shear capacity from beam slenderness ..... 8

Figure 2.3: Typical critical crack configuration ..... 9

Figure 2.4: Shear resisting mechanisms ..... 11

Figure 2.5: Types of load-induced cracking ..... 12

Figure 2.6: Kinematics of a critical crack ..... 14

Figure 2.7: Rigid body equilibrium ..... 16

Figure 3.1: Poor predictions made by mechanistic models for deep beams (a/d<2.5) ..... 26

Figure 4.1: Thesis Methodology and its dependencies ..... 31

Figure 5.1: A decision tree to help clarify the difference in hybrid modeling methods ..... 48

Figure 5.2: Method Purpose ..... 49

Figure 5.3: Comparison of error from Bias and Variance ..... 60

Figure 5.4: Model Space Changes for Data-Driven-Inclusion-Like Methods ..... 61

Figure 5.5: Data-Driven Inclusion Model Layout ..... 65

Figure 6.1: New Crack Geometry Model ..... 71

Figure 6.2: Sensitivity plot of vertical equilibrium ..... 80

Figure 6.3: Validation of the Critical Shear Crack Theory Model ..... 82

Figure 7.1: Shear Mechanics of Concrete Beam ..... 86

Figure 7.2: Model Layouts ..... 89

Figure 7.3: Mechanistic Bounding Expressions ..... 91

Figure 7.4: Data-Driven Inclusion Model ..... 92

Figure 8.1: Connected hybrid model prediction accuracy ..... 95

Figure 8.2: Demonstration of erroneous machine learning predictions ..... 96

Figure 8.3: Crack opening constrained by crack shape and typical Critical Shear Crack Theory values ..... 99

Figure 8.4: Contribution of shear-resisting components over crack openings ..... 99

Figure 9.1: Prediction results ..... 104

Figure 9.2: Model Architecture Comparison with Equivalent Trainable Parameters ..... 106

Figure 9.3: Data Efficiency of Data-Driven Inclusion ..... 107

Figure 9.4: Adverse effects of mechanistic bias ..... 108

Figure 10.1: The effect of predicting multiple cracks and warping caused by shear stresses. ..... 112

Figure 10.2: Crack analysis frameworks ..... 115

Figure 10.3: Crack prediction framework ..... 118

Figure 10.4: Distinction between visible cracks and micro-cracks ..... 122

Figure 11.1: Solutions to non-linear systems of equations ..... 127

Figure 11.2: Source of constraint for experiment ..... 131

# LIST OF TABLES

Page

Table 2.1: Simplified and omitted mechanisms ..... 21

Table 7.1: Input Parameters used to Predict Shear Mechanics Quantities ..... 87

Table 7.2: Bounding Expressions uses ..... 91

Table 7.3: Hyper Parameter Search ..... 93

Table 9.1: Plain Neural Network Configuration ..... 103

Table 9.2: Trainable parameters ..... 105

Table 11.1: Experiment setup for testing the effect of constraint ..... 133

# CHAPTER I: INTRODUCTION

While improving design efficiency is always a goal for structural engineering, it has recently become significantly more important considering recent efforts to reduce carbon emissions. The production of cement (the main constituent of concrete) accounts for 5-7% of global carbon dioxide emissions (Benhelal et al. 2013), and the strategy pertinent to structural engineering for decreasing these emissions is decreasing the quantity of cement and concrete used in construction.

Concrete structures would become significantly lighter with the slightest increase in beam efficiency because beams are the most prolific concrete component found in structures. Beam action is even present when studying other structural components (Wight and MacGregor, 2016). Structural walls, when bent about their weak axis, are considered to have beam-like behavior, and columns, when eccentric loads are applied, are treated as beams with axial loads. Structural slabs, which account for 40% of the concrete used in high-rise buildings (Block et al. 2019), vary only slightly from beam behavior. So, design efficiencies realized for concrete beams would translate to efficiencies in structural members that exhibit beam-like behavior as well.

Without an accurate model to represent concrete beam capacity, extra construction materials will be needed to ensure a design's safety. Conversely, the more accurately concrete beam response can be represented, the more efficiently they can be implemented in design.

Widely accepted models for predicting shear capacity in concrete beams without transverse reinforcement are still sought after, but none have been developed yet (Koscak et al, 2022). This group of concrete beams, which do not contain transverse reinforcement (reinforcement spanning

the depth of the beam), is important to understand because it includes most structural slabs and shares many properties with beams that do contain transverse reinforcement (Zararis and Papadakis, 2001). Models for predicting a concrete beam without transverse reinforcement's capacity are mostly comprised of mechanistic models with empirically fitted relationships, which have limited flexibility in representing any complex mechanism accurately (Classen, 2020). In this thesis, we use the term mechanic or mechanism to describe the phenomena occurring in the beam's response while mechanistic models refer to the mathematical representation of the mechanisms. Even though they do not represent the underlying mechanisms accurately, these mechanistic models accurately describe beam shear capacity (Cavagnis et al., 2018). The main consequence of inaccurately describing underlying mechanisms is a decrease in robustness. Mechanistic models will perform well on the data set they were developed on (slender beams) but their performance deteriorates significantly when tested on beams outside of the data set's range (deep beams).

The main complexity in predicting a concrete beam's capacity is rooted in its addition of other materials, such as deformed steel reinforcement (Ngo and Scordelis, 1967). This addition improves concrete beam performance but complicates their response to loading compared to a beam's response made from either material separately (Kani, 1964). Steel beam capacity is sufficiently understood because steel's isotropic and elastic properties simplify response analysis through much of a steel beam's loading stages (Segui, 2012). If enough steel is added to a concrete beam, its response depends on the properties of the steel. Primarily, Including transverse reinforcement in a concrete beam simplifies the analysis by allowing a beam to be related to a truss structure, as is done in the strut-and-tie method (Schlaich and Schafer, 1991), However, concrete beams only containing

longitudinal reinforcement (not containing transverse reinforcement) are more difficult to analyze (Reineck, 1991; Muttoni and Ruiz 2008; Ruiz et al., 2015). Aside from beams with high slenderness (span-to-depth ratio), concrete beams without transverse reinforcement often do not reach their flexural capacity (making them shear failure driven) and fail suddenly (Yang, 2014), and their response depends mainly on concrete fracture properties and longitudinal reinforcement bond strength mechanics (El-Ariss, 2007). These complex mechanisms determine the crack shape resulting from loading (load-induced cracking), and the crack shape determines the shear capacity (therefore the ultimate capacity).

Load-induced cracking is the most complex mechanism in determining shear capacity. Many of the other mechanisms can be suitably described by mechanistic models, but load-induced cracking must be severely simplified in mechanistic models. Without the flexibility to accurately describe load-induced cracking, mechanistic models will always lack robustness.

Machine learning methods have recently been used to predict shear capacity. These have the flexibility to describe complex relationships but require substantial data sets (Raissi et al, 2019). Additionally, machine learning models have no interpretability (Gondia et al, 2020), so skepticism would be associated with their use in practice.

In the middle of machine learning and mechanistic methods lie hybrid mechanistic-machine learning methods that can represent complex relationships with less data. Hybrid mechanistic-machine learning modeling methods have the best chance of accurately representing load-induced cracking by combining data and mechanics.

Accurate prediction of load-induced cracking would also increase our understanding of the mechanism itself. While machine learning models are not interpretable by themselves, hybrid models provide increased interpretability (Zhang et al., 2020), so if the hybrid model captures an accurate representation of the load-induced cracking mechanism, it can be studied against other mechanism and test data to potentially increase our understanding of load-induced cracking.

Additionally, successfully implementing a hybrid model for this problem will pave the way to increase our understanding of other structural members with mechanisms too complex for mechanistic models. For example, this approach can be applied to timber design, leading to an improved understanding of how moisture conditions affect strength past the empirically derived relationships often used (Breyer et al., 2020).

In this thesis, we implement hybrid mechanistic-machine learning models for accurately predicting load-induced crack propagation of concrete beams without transverse reinforcement. This accurate prediction will remedy the previous poor treatments of crack propagation used in mechanistic models, providing more accurate predictions for all concrete beams without transverse reinforcement and not just the beams the model was developed on. Hybrid models have the flexibility to represent complex relationships, do not require a large data set, and can be interpreted more than machine learning models. Successfully implementing hybrid models for this task allows for more efficient and sustainable concrete design and a greater understanding the crack-induced failure.

# CHAPTER II: OVERVIEW OF RELATED WORK

As we mentioned earlier, shear failure in concrete beams without transverse reinforcement has very complex mechanisms. This section will explore some of the efforts to understand shear failure and its mechanics. In this brief review, we hope to convey the essence of shear failure research and provide a basis for further research.

Through experiments, we prove or identify possible theories about shear failure mechanics. Then, based on those mechanics and gathered experimental data, we develop mathematical relationships, based on the chosen modeling method, to represent the mechanics theorized from experiments. To most clearly reflect the essence of shear failure in concrete members without transverse reinforcement, this review will follow a similar pattern, beginning with experimental programs and their identified mechanics and ending with a description of models developed to predict shear failure. In the *developed models* section, we will not discuss the developed model's mathematical form extensively. Instead, we will identify which mechanics they include and their flaws when predicting shear capacity. Generally, mechanistic models over-simplify mechanisms and limit their robustness. Furthermore, machine learning models robustly predict shear capacity when enough data is available but are uninterpretable. So, mechanistic models will be reviewed to identify what portions they simplify, and machine learning models will be reviewed to identify their limitations in interpretability.

## Experimental Programs: Shear Failure, Explained

Reviewed works in this section perform experiments to determine shear failure mechanics in concrete beams.

One of the first test series studied chronologically was by Kani (1964). These test series lead to the "shear valley" mechanism, which is a term that describes the sudden decrease, then increase, in shear capacity when slenderness increases. In response to ACI committee 426's encouragement to develop a "rational theory", Kani tested 14 beams with varying slenderness ($\frac{a}{d}$) ratios. For ratios under 1.5 and above 5, full flexural capacity was achieved but not for values in between. This matched previous studies from Ferguson (1950), which observed a 225 percent increase in shear stress at failure when the shear arm ratio changed from 2.35 to 1.17. This was unexpected because, from beam theory, an elastic section would have the same shear stress at failure regardless of the shear arm ratio. The unexpected change in shear stress at failure indicated the complexity of shear capacity in concrete beams and provided the basis of the "shear valley".

The shear valley mechanism is caused by two others. The first of these is "cantilever action". When measuring the displacement of plane sections on test beams, they were observed not remaining plane. Instead, severe warping of the cross section was observed, and thus, the cantilever action mechanism was theorized. This mechanism is essentially the bending of concrete "teeth", which are formed when flexural cracks propagate on either side of a section of the concrete beam. The bending of the tooth is caused by beam action, which causes, among other things, increased tensile stresses in longitudinal reinforcement as it tends towards the maximum moment portion of the beam. This causes the cracked beam's teeth, resembling a comb's teeth, to be loaded horizontally like cantilever

beams. Cantilever action causes the beams' stress state to change, especially near the crack, flattening the crack propagation path. A depiction of this action is displayed in Figure 2.1. Results indicate cantilever action is more significant towards the maximum moment, likely due to the decreased flexural resistance of a tooth where larger cracks are present.

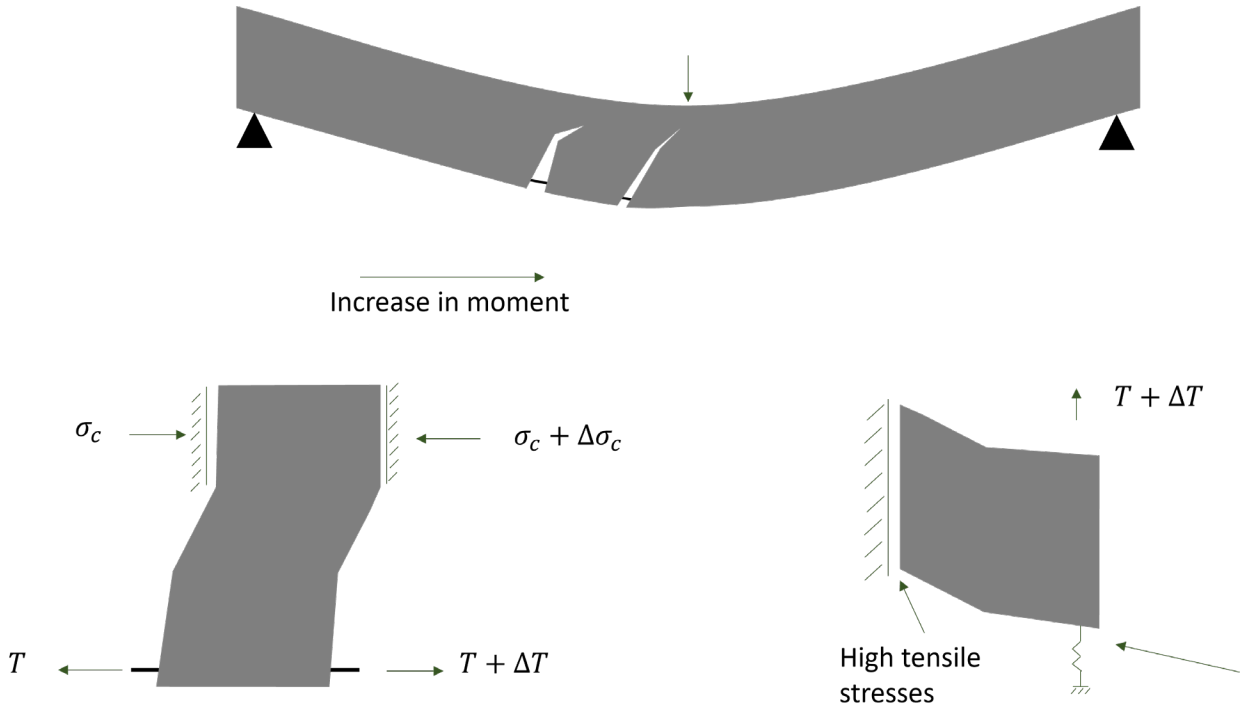


*Figure 2.1: Cantilever action in concrete beams without shear reinforcement*

The other mechanism comprising the "shear valley" mechanism is the remaining arch capacity. To study the compression field of the beam as it progressed towards failure, strain gauges were placed along the beam's depth and oriented parallel to the theoretical compression strut of a tied arch. In deeper beams (shear arm < 2.5), the stain gauges indicated flexural resistance stopped coming from beam action and started coming from the strutting action of a tied arch. This led to the conclusion that after concrete teeth fail in deep beams, the beam's capacity is determined by the arch that remains, whereas the remaining arch's capacity is determined by plasticity theory.

In slender beams, no remaining arch would develop, and in deep beams, the concrete teeth would fail at much lower loads. These two observations construct the shear valley. Deep beam capacity is determined by the capacity of the remaining arch, which decreases as the beam becomes more slender, and the slender beam capacity is determined by tooth capacity, which increases with more slenderness. The lowest shear capacity, and the bottom of the "shear valley", lie at some point of slenderness where capacity transitions from being determined by remaining arch capacity to tooth capacity. Plotting the shear capacity of a beam and varying the slenderness ratio, a valley will form (Figure 2.2).

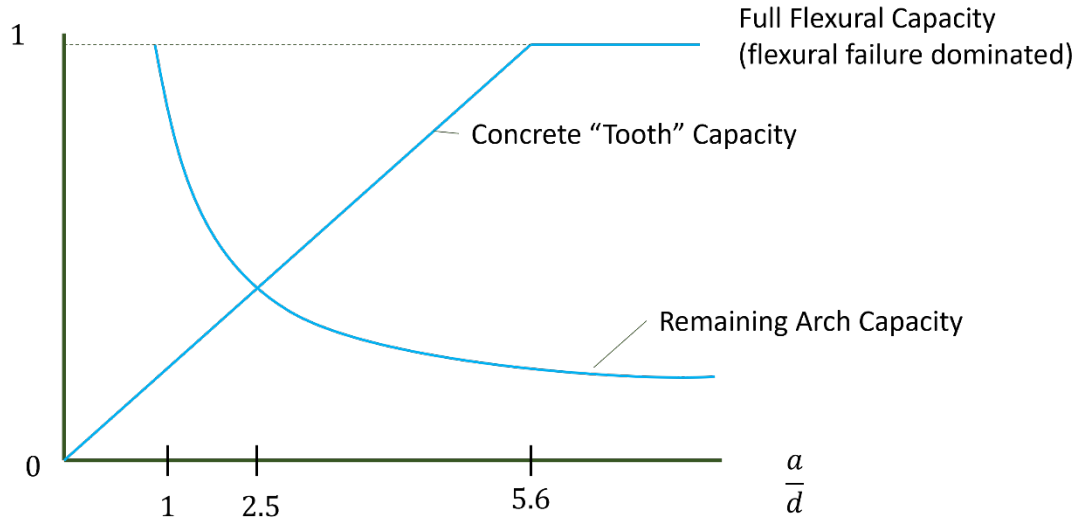


*Figure 2.2: Shear valley explaining variation in shear capacity from beam slenderness (Adapted from (Kani, 1964))*

Finally, the last observation made was of increased shear strength with smooth reinforcement instead of deformed (Leonhardt and Walther, 1961). This reinforces the shear valley mechanic. If there is no deformed reinforcement, there can be no beam action and no tooth failure. The beam

failure is always determined by direct strutting. Of course, using smooth bars decreases moment capacity, so there is a trade-off.

To study the crack shapes that cause failure, how opposite crack faces move relative to each other (crack kinematics), and how inter-crack forces contribute to failure, Campana et al. (2013) tested four simply supported beams. Strains and displacements were measured across the beams using a high-precision distance-measuring device.

No mechanic could be identified that explains the crack shapes that develop near failure, but these tests did observe that crack shapes were consistent in identical beams. All critical cracks (defined by Campana et al. (2013) as cracks that represent the ultimate failure surface) exhibited a shape of a hyperbolic tangent function, as shown in Figure 2.3.

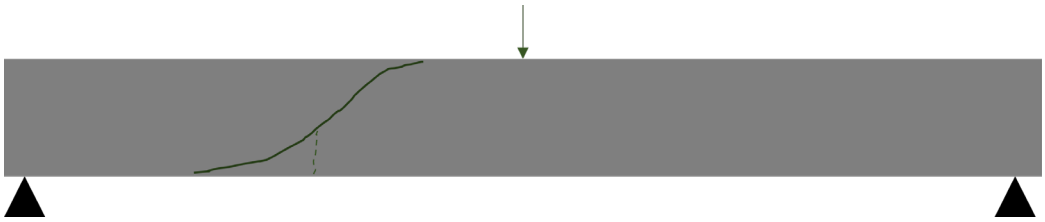

*Figure 2.3: Typical critical crack configuration*

The test results indicated that the crack kinematic mechanics are much more complex than the kinematics proposed by Walraven (1980), Ulaga (2003), and Guidotti (2010), but no mechanics were given in their place. The previous mechanics describe crack opening to occur first and be followed by a combination of opening and sliding. However, test results indicate sliding and opening occur simultaneously. Any mechanism describing crack kinematics must relate loading to crack opening and sliding along the crack's shape. This is usually done by relating the kinematics to strains in the uncracked region, as shown in Figure 2.4 (a).

By analyzing the measured crack shapes and kinematics near failure, the shear resistance contribution of inter-crack and uncracked concrete shear resisting mechanisms were identified. Inter-crack forces include aggregate interlock (Figure 2.4 (b)), doweling action (Figure 2.4 (e)), and residual tensile strength (Figure 2.4 (c)).

- The aggregate interlock mechanism has been studied and modeled extensively (Walraven, 1981; Ulaga, 2003). Jacobsen et al. (2012) conducted a series of push-off tests to determine the force-displacement relationship of the aggregate interlock mechanism. Aggregate interlock is described as the friction forces occurring between crack faces sliding past each other. This force is dependent on aggregate size and concrete strength. Unlike other shear-resisting mechanisms, this has been studied in isolation from concrete beam systems (Huber et al., 2019). Aggregate interlock resistance increases with Mode II fracture and decreases with Mode I fracture.
- The residual tensile strength mechanism describes the softening behavior of concrete when it is loaded past its maximum tensile stress. Once the tensile stress of concrete surpasses its peak stress, the concrete does not fail. Instead, portions rupture partially, creating microcracks and decreasing the resistance capacity of the concrete. This softening behavior continues for increasing strain until microcracks join and combine with the visible crack, the region where the crack can be seen and no residual tensile strength exists (Reinhardt, 1984; Reinhardt et al., 1986; Hordijk 1992; Hillerborg, 1983). Residual tensile strength is dependent on aggregate size and fracture energy and decays significantly as Mode I (opening) fracture increases (Cavagnis et al., 2018).

- Doweling action is activated in the longitudinal reinforcement when opposite crack faces move vertically past each other. The resistance provided by this mechanism can be described by beam theory if some assumptions are made about the reinforcement-concrete interfaces but become much more difficult if factors like slippage or delamination are accounted for.

Residual tensile strength, found in the upper portions of the crack, was found to contribute little to shear resistance because the crack openings were found to be too large in that region. Additionally, the size of the compression zone near failure indicated it would contribute little to the total resistance as well Figure 2.4 (d). From this, the majority of the resistance at failure would be provided by aggregate interlock and doweling action mechanisms.

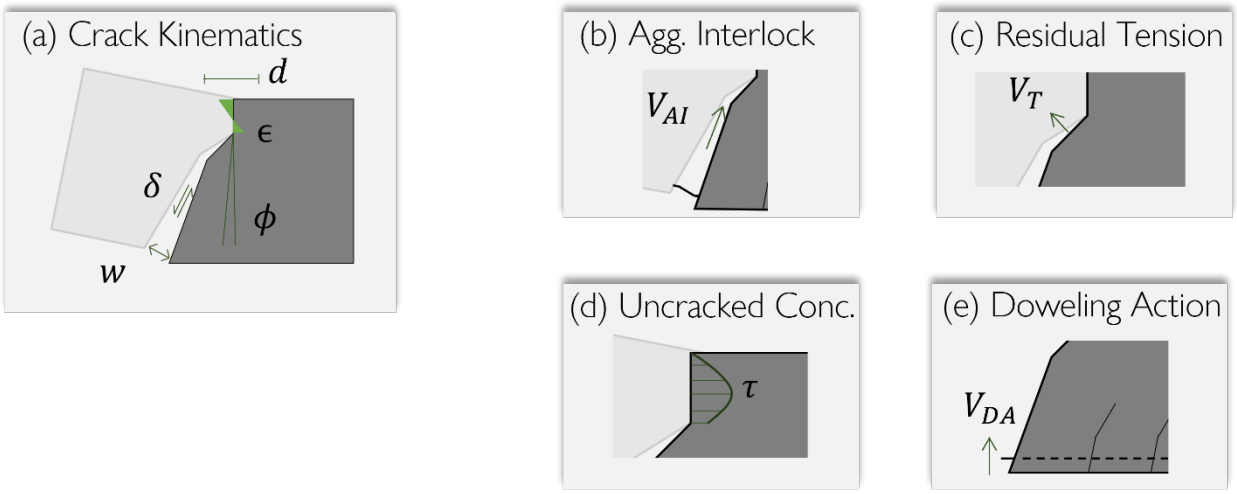


*Figure 2.4: Shear-resisting mechanisms*

Cavagnis et al. (2015) tested a series of 13 beams (two were re-used for a total of 15) to study load-induced cracking mechanisms. These beams varied in geometry and loading conditions, and crack shapes and kinematics were measured using Digital Image Correlation. While no totally inclusive

mechanics were theorized for relating crack shapes at failure to beam properties and loading conditions, mechanics describing the types of cracks that develop and their role in failure were.

Load-induced cracks can be categorized by their shape, position, and the forces that develop them. The most apparent are the primary (type A cracks) and secondary (type B cracks) flexural cracks and the cracks propagating horizontally from the tops of primary cracks (type F cracks). These cracks develop from flexure and cantilever action. Type A & B cracks merging with others are classified as type C cracks, and cracks from delamination are type D cracks. Type D cracks can form early in loading and are the result of doweling action. Type E cracks offshoot from A cracks and are the result of aggregate interlock stresses. Finally, Type G cracks are created from concrete crushing. The typical shape of these cracks is shown in Figure 2.5.

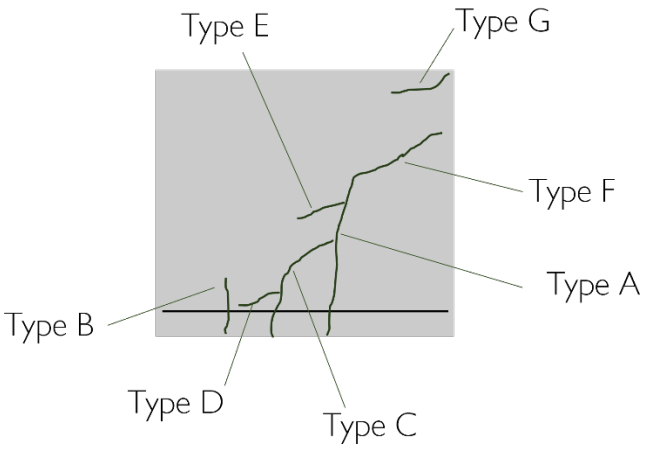


*Figure 2.5: Types of load-induced cracking*

A mechanic was proposed to determine the length of type A cracks, but because it can be difficult to determine where type A cracks end and type F cracks begin, this mechanic is subjective. For example, some cracks appear curved throughout their length, indicating no transition point, and others have multiple segments, indicating too many transition points. A more objective proposed

mechanic was the increase of inclination in an A-type crack when it was in a region with a higher moment-to-shear ratio. This mechanic was implemented mathematically with equation (1).

$$\beta = \operatorname{atan}\left(1 + 1.25 * \frac{M}{V_{vs} * d}\right) \quad (1)$$

Where $\boldsymbol{M}$ is the moment in the virtual section at the crack root, $\boldsymbol{V_{vs}}$ is the shear in that same section, $\boldsymbol{d}$ is the beam depth, and $\boldsymbol{\beta}$ is the crack inclination.

No single combination of crack types describes the critical cracks that develop. However, the proposed *crack development type* mechanic categorizes the types of failure that can occur from load-induced cracking. Type 1 coincides with arching or strutting action where the crack types are relatively insignificant in failure, relating back to the "remaining arch" capacity (Kani, 1964). Type 2 is caused by type C cracks. The joining of secondary or primary cracks causes the kinematics of the crack to change, disengaging an active aggregate interlock mechanism in some portion of the crack. Type 3 is similar to the previous except a type E crack causes disengagement. When stresses from aggregate interlock become too significant, the tensile strength of concrete is reached, and cracks propagate perpendicular to the type A crack where the aggregate interlock is acting. Finally, Type 4 is similar to 2 and 3, but is the result of late-stage type C cracks.

Following the previous study, Cavagnis et al. (2017) tested seven additional specimens under similar conditions, further adding to mechanisms related to load-induced cracking, the contribution of shear resisting mechanism, and crack kinematics.

Crack shapes and kinematics before failure indicate that the critical crack (the crack whose shape and kinematics describe the capacity of the beam) is the same as the merged crack in some

cases, but in many other cases, it is not. No mechanism could be identified for this difference. Because of the way cracks merge to cause failure, it can be difficult to determine which crack should be determined as the critical crack. In some cases, cracks merge and the beam's strength continues to increase. The critical crack for this would be the merged crack. In most cases, however, cracks merge and the beam's strength gradually or rapidly decreases. In this case, the critical crack is defined as the unmerged crack even though its shape and kinematics do not define the beam's capacity.

Observations were made on the crack kinematics that develops, but no mechanics were theorized for these observations. Upper, type F cracks are only characterized by Mode I fracture and do not exhibit sliding. Concrete mostly did not reach the post-peak levels of the stress-strain curve. These experimental observations are portrayed in Figure 2.6.

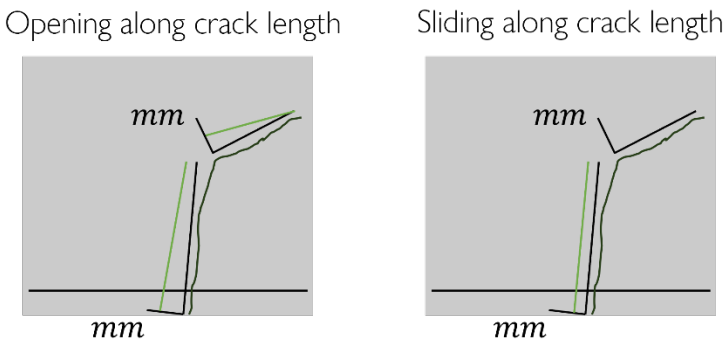


*Figure 2.6: Kinematics of a critical crack*

By using critical crack shape and kinematics and constitutive models, the shear resistance mechanisms were found to depend significantly on the crack shape and kinematics. In deep beams, inter-crack forces in A-F crack types contributed little compared to strutting in the uncracked region while the opposite was true for slender beams. Additionally, critical cracks developed closer to the applied loads for deep beams than for slender beams. From this, a mechanism is proposed that

correlates the location of the crack to the contribution of inter-crack forces to shear resistance. The closer the critical crack develops to the applied load, the less inter-crack forces contribute to shear resistance. Elaborating more on the location of critical cracks, a second, potential critical crack, which developed closer to the applied load, was observed on slender beam SC70. This potential critical crack, however, ultimately did not become a critical crack due to its proximity to the applied load, which allowed its uncracked regions to contribute more to resistance.

## Mechanistic Models

Mechanistic models are those that use mathematics to describe mechanisms. They use mechanisms (e.g. aggregate interlock, cantilever action) as a template to develop equations relating, for example, strains to forces in the uncracked region of the beam. These equations may represent laws of physics, like equilibrium, geometry (strain and displacement relationship), or constitutive relationships. Empirical models are needed because mechanisms are often hard to define accurately. For example, the aggregate interlock mechanism is described as a friction force, which is intuitive from a previous understanding of rough surfaces and friction, but determining the exact relationship between friction forces and displacement based on intuition or physical laws is difficult or impossible.

From this, all mechanistic models need some data-driven portion, in the form of empiric relationships, to relate theorized mechanisms to reality. Due to the inflexibility of empirical models, however, they are not able to fully represent the mechanism. In the following reviewed models, the need for a data-driven portion will be a common theme and will be observed to varying degrees. Some models choose a handful of mechanisms to describe shear capacity and fit available data to that, and others choose many simpler mechanisms and fit each of those. Some shear failure models only

consider one or two inter-crack force mechanisms to be significant while others may consider them all. Most shear failure models are often based on the equilibrium of rigid bodies and focus on one virtual section at a time, as shown in Figure 2.7. The Critical Shear Crack Theory (Muttoni and Ruiz, 2008) epitomizes this single-crack method by only analyzing failure as the degradation of forces in one crack. Other theories also follow this approach, such as the Shear Crack Propagation Theory (Classen 2020).

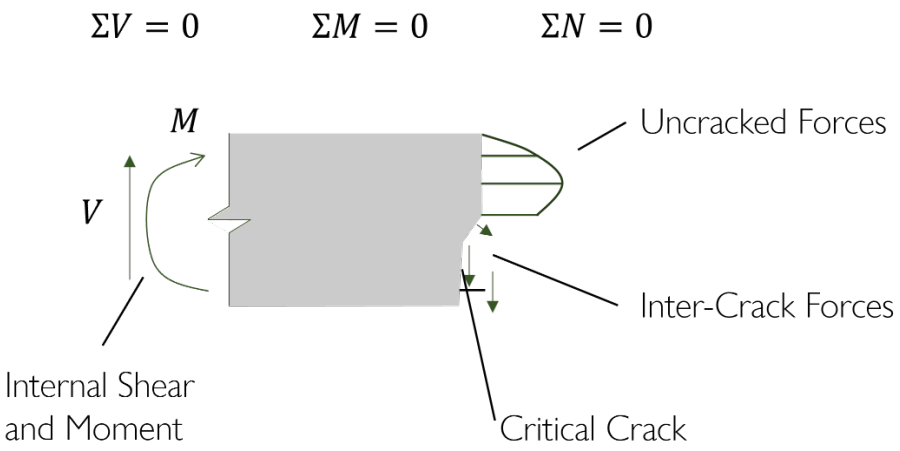


*Figure 2.7: Rigid body equilibrium*

Kani (1964), despite having theorized rather complex mechanics, chose to implement rather simple mechanics in their model. However, this is reasonable given the complexity of shear failure and limited data at the time. As described previously, this work introduces the "shear valley" mechanism. The capacities of the remaining arch and the concrete teeth are the basis for this proposed model: the concrete "teeth" giving way to the arch, and then, the arch collapsing. For deep beams, concrete "teeth" lose their capacity early in loading, but their remaining arch is often sufficient to support shear forces until flexural capacity is reached. For slender beams, the concrete "teeth" have a much greater capacity, but after their failure, the remaining arch's capacity is much less than applied loads, causing a

rapid failure. For the mathematical implementation of this, a simplified version of the concrete "tooth" is used. It is rectangular and has a height and width calibrated from test data. Using this, a simple elastic analysis determines the tensile force that can be supported until the stress in the tooth reaches the concrete tensile strength. This is considered the failure of the tooth. Equation (2) determines the moment that causes the failure of this tooth.

$$M_{CR} = \frac{7}{8} b * \frac{d^2}{6} * f_{ct} * \frac{s_{cr}}{s} * \frac{a}{d} \quad (2)$$

Where $s_{cr}$ is the width of the tooth, and $s$ is the depth of the tooth.

The capacity of the arch can be represented by (3)

$$M_{CR} = M_{FL} * \frac{d}{k * a} \quad (3)$$

Where $k$ needs to be calibrated on test data (taken as 0.9) and $M_{FL}$ is the flexural capacity of the beam.

Using both relationships, the bottom-most point of the "shear valley" can be determined. Based on this point and the two relationships, the moment capacity (and shear capacity) can be determined for the beam. If the shear arm ratio is low enough, the full flexural capacity can be reached, and if the shear arm ratio is high enough, it may also be achieved. However, in the middle is where shear failure dominates.

This model comes from a very fundamental understanding of deep and slender beam failures but is based on a theory that fails to consider inter-crack phenomena, such as aggregate interlock. Additionally, the model omits propagation mechanics in determining the capacity of the remaining arch.

Rieneck (1991) proposed a model for slender beams, as the arching action provided in deep beams is controlled by the failure of a strut and is defined well. The identified slender beam shear resistance components are from aggregate interlock, doweling action, cantilever action, and shear force in the uncracked concrete. A relationship between the inter-crack shear resistance and the uncracked region shear resistance is derived from a stress analysis of the compression zone. Assuming all tensile resistance in the cross section is from reinforcement and the stress distribution in the uncracked region is linear, this analysis shows the compression zone can carry, at most, 30 percent of applied loads near failure. From this, much of the load must be carried in the inter-crack regions of the beam, and constitutive relationships with idealized models of the crack can be used to determine the capacity of a beam. A simple kinematic model for the proposed crack is derived by relating tensile strains to crack openings. These kinematics are then used to evaluate how the inter-crack forces contribute to shear capacity, and a single equation was then produced to describe shear failure at the beginning of the "B-region".

This model considers many important mechanics in its formulation but simplifies and omits many too. Cantilever action is assumed negligible, but if this were true, there would be no beam action, a mechanism on which this model depends. By not including cantilever action, the biaxial stress states in the uncracked region are severely simplified. Additionally, the crack shape is extremely idealized and no residual tensile stresses are considered in the upper portions of the crack.

The mechanistic model proposed by Cavagnis et al. (2018) uses all inter-crack forces and the shear resistance in the uncracked portion to describe concrete beam shear capacity. Aggregate interlock relationships are determined by Walraven (1980) but modified to avoid numerical

integration. Doweling action forces are modeled after Ruiz et al. (2013) but are then simplified to not account for reinforcement spacing. Residual tensile strength is modeled using a fracture softening mechanism proposed by Reinhardt (1984), where the force in the micro-cracked region is inversely proportional to the crack opening. The shear resisted by the uncracked concrete is estimated by considering the stress field from the application of load to the critical shear crack. Assumptions in modeling this stress field are never validated and do not relate to any mechanism. The contribution of the uncracked region is then simplified further to be a portion of the inter-crack contribution, where the location of the critical crack determines the portion. Explicit equations yield the neutral axis depth and crack shape based on the location of the critical crack. The crack kinematics are then iteratively solved through the moment equilibrium of the critical crack section. This process can be repeated for critical cracks occurring at any portion of the beam and the critical shear crack position that results in the lowest shear strength can be assumed as the true position. The validation of these positions is not given for a significant number of these beams, however. Additionally, this model frequently finds the minimum value to occur in the 40% to 60% shear span region, with little variation in shear capacity in this range. From this, assuming the critical shear crack to occur halfway into the midspan will yield reasonable capacities.

This model predicts shear capacity well for slender beams, but is almost entirely empirical and simplifies underlying mechanisms significantly. The proposed aggregate interlock model deviates significantly from push-off tests (Jacobsen, 2012) with the same kinematics. The doweling action model does not include the vertical displacement of crack faces, which is significant in determining its resistance. No explanation is given for the theorized stress field of the uncracked region, and the

model developed becomes invalid for deep beams. The most simplified mechanism, however, is load-induced cracking. In this model, the shape of the crack is determined only by its location (which seems to be constant for all beams), and previously identified failure mechanics are ignored.

Classen (2020), in the most recent attempt to accurately describe shear failure in concrete beams without shear reinforcement, creates a model to not only describe shear failure but also describe the crack propagation process leading to failure. This was not intended to be used in a design scenario, but rather to increase understanding of the system. The model begins by examining a single crack in a pre-determined location. This crack has only propagated to the flexural reinforcement at the beginning of the analysis. At this point, the compression zone depth is decreased (analogous to an increase in load) and the propagation and kinematics of the crack must be solved. A solution for these values is obtained iteratively through inter-crack constitutive models, strain-kinematics relationships, elastic models for stresses in the uncracked section, and the equilibrium of rigid bodies. The compression zone depth continues to decrease until the net shear resistance found through equilibrium starts to decrease. For the analysis of the entire beam, this process must be repeated for new crack locations at intervals of the beam. As this method's goal was to make the most accurate representation of mechanisms, there was little calibration used in this model.

While far better than many other bilinear cracks, the single, multi-segmented crack used in this model still will not represent the crack failure mechanisms presented in Cavagnis (2015). Finally, this implementation makes only a few comparisons to test data to validate itself, so its ability to represent shear capacity accurately is unknown. Additionally, the critical crack this model predicts matches the unmerged crack and not the merged crack that determines the beam's capacity.

These reviewed models simplify or omit many mechanisms from their mathematical representations. These models still predict shear capacity accurately by fitting incorrect relationships for underlying mechanisms, but fitting incorrect relationships limits the model's robustness. Table 2.1 shows a brief summary of some of the omitted and simplified mechanisms for the reviewed models and some additional models that were not described previously.

*Table 2.1: Simplified and omitted mechanisms*

| Model | Mechanism omitted | Mechanism simplified | How they simplified |
|---|---|---|---|
| (Kani, 1964) | Inter-crack forces | "Tooth" geometry | Only considered rectangular tooth. |
| (Reineck, 1991) | Cantilever action | Load-induced cracking | Assumed a single bilinear crack |
| (Cavagnis et al., 2018) | Biaxial stress-strain relationship | Crack kinematic-strain relationship | Assumed crack faces to rotate about the crack tip |
| (Classen, 2020) | Multiple cracks contributing to failure | Delamination crack length | The delamination crack was the length of the primary crack's projection |
| (Ruiz et al., 2015) | Multiple cracks contributing to failure | Load-induced cracking | Assumed a single bilinear crack |
| (Mari et al., 2014) | Change in neutral axis depth from cracking | Shear stress distribution at the crack tip | Shear stress was assumed 0 at the crack tip |

## Machine Learning Models

Machine learning methods are different from mechanistic ones because they do not attempt to use mechanisms as a template, but instead, define relationships entirely from data. While this limits their ability to learn by not providing any structure, it also makes them substantially more flexible by not restraining them to simpler mathematical forms. Machine learning models, like the neural networks

used for image classification, have upwards of billions of trainable parameters. Compared to an empirical relationship, which has three or four data-driven parameters, machine learning models can represent more complex mechanisms. However, machine learning models require large data sets and are largely uninterpretable.

The models reviewed in this section have enough data to learn relationships for shear capacity but are not able to do so interpretably. In some cases, there is not enough data for machine learning to learn a better representation than mechanistic models.

The first model examined in this section is (Zsutty, 1968), which does not employ machine learning as it is known today but rather uses statistical regression (empirical model) and dimensional analysis. These modeling methods resemble machine learning significantly, only differing in the magnitude and complexity of the algorithms used. Additionally, while empirical fitting techniques are often used in mechanistic models, they are done so to fit theorized mechanisms, which distinguishes them from purely empirical models. Because this model does not consider any mechanisms in its derivation, it is considered in this section rather than the *mechanistic models* section. In this work, the initial attempts to make a high-accuracy model were unsuccessful because the simple model proposed was unable to describe the complexity of the two failure states that can emerge: deep and slender beam failure. From this, the data was split and two separate models were made. By only considering beams with a shear arm ratio greater than 2.5, a more accurate model was developed. However, the same was not true for deep beams. Ultimately, the best prediction for deep beam failure was provided by the slender beam model. The difficulty in prediction was attributed to Ferguson's (1956) and Taylor's (1960) explanation of increased strength in deep beams, where they explain that increased

strength is caused by the pressures applied to the top and bottom faces of the beam. In deep beams without these pressures, the slender beam model performed well. While this model achieves reasonable predictions for shear capacity, it can only do so for slender beams and is not able to describe the complex transition from beam failure to strutting failure in deep beams.

Analyzing more contemporary modeling approaches, Mangalathu et al. (2021) use a variety of machine learning models and Shapley Additive exPlanations (SHAP) to predict punching shear capacity in flat slabs and provide interpretability to those predictions, respectively. The key purpose of this work was to provide the accuracy of a machine learning model while remedying some of its interpretability problems. These models were trained with a dataset of 380 slabs. To avoid memorization, data is split into training and testing sets for model creation and evaluation. The extreme gradient boosting model is identified as the best predictor for this problem and is compared to other empirical models. Upon examining the data, it appears the entire dataset, training and testing, was used in this comparison. This invalidates the comparison because performance on training data does not accurately represent the model's "learning". Using the score provided for the testing set, it appears that this machine learning model performs worse than less flexible empirical models. This is likely attributed to the size of the data set. The SHAP analysis is used to provide interpretability to the predictions by indicating which input parameters positively or negatively influence the shear capacity prediction from its average value. This is an insightful analysis because it confirms the machine learning model is respecting some general mechanisms of shear capacity, such as low a/d ratios increasing shear capacity. However, this does not provide the same level of interpretability as mechanistic models, where all modeled mechanics can be observed in mathematics.

In a similar work, Feng (2021) uses ensemble ML models to predict the shear capacity of deep beams with and without transverse reinforcement. Ensemble models are used because they do not require a "best" model to be learned, which can be difficult for a limited dataset. Instead, they combine predictions from several good models. The data set they used for training only had 271 samples. Making a predictive model for this data set would be very difficult because the mechanics of these beams can vary substantially. Depending on the amount of transverse reinforcement, the final failure state could be determined by arching or beam action. This makes the XGBoost's final prediction coefficient of determination of 0.928 significant because this indicates that the model has the flexibility to accurately represent this transition. These results are then compared to empirical models, which the author mistakenly equates with mechanistic models. However, this is an extremely unfair comparison because these models were developed only for deep beams with shear reinforcement, and this dataset contains many other configurations of beams. Even considering the beams these expressions were developed for, the "WVR" beams, the spread is still significantly more than the machine learning model, indicating its superiority in prediction accuracy. It should be noted that there are mechanistic models significantly more accurate than these empirical models shown. Finally, an interpretability aspect of the model is given through the partial dependence of the loss function with respect to the input features. While this does describe the relevance of input features, it does not describe any mechanism of shear failure. The author acknowledges this by stating the two models should be used in conjunction and that mechanistic interpretation is crucial to application.

# CHAPTER III: DESCRIPTION OF THE PROBLEM

Both machine learning and mechanistic models have deficiencies when predicting concrete beams without shear reinforcement's shear capacity. Empirical modeling's flexibility limits the robustness of mechanistic models, and machine learning models need large datasets and lack interpretability. The deficiencies of mechanistic models detailed further are: (1) mechanistic models omit or misrepresent mechanisms known to affect shear failure (2) Even if all relevant mechanisms are included, some are too complex to be accurately represented by empirical models.

Problem (1)'s primary example is all mechanistic models only consider one crack in determining failure when experiments show multiple cracks affect the shear capacity. Simplifying the mechanisms of shear failure must be compensated for by empirical models fitting incorrect relationships for other mechanisms. For example, Cavagnis et al. (2018) proposed a failure model which predicts the shear capacity well (0.95 coefficient of determination) on slender beams, but its prediction of aggregate interlock strength is significantly different from the test results provided by Jacobsen et al. (2012). By relying on empirical models to calibrate mechanistic shear capacity models, the mechanistic models are only sufficient to describe the systems on which they were calibrated. When Cavagnis et al. (2018) model is applied to deep beams, it predicts poorly. Figure 3.1 shows prediction errors for varying slenderness ratios. To robustly predict shear capacity, all mechanisms must be modeled accurately.

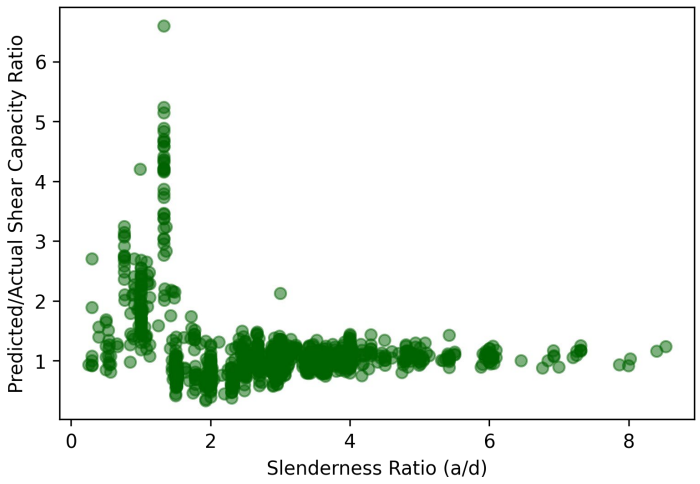


*Figure 3.1: Poor predictions made by mechanistic models for deep beams (a/d<2.5)*

Even if all mechanisms were appropriately considered, some are too complex for empirical models to represent accurately (problem 2). Predicting load-induced cracking is critical to predicting failure because all inter-crack forces are dependent on it. Determining their shape for capacity prediction is seemingly impossible and is, in fact, often described as a "riddle". Many mechanisms have been proposed to explain the cracks angles and types that form but these cannot completely describe load-induced cracking. A mechanism to completely describe load-induced cracking is likely too complex. Empirical fits used in mechanistic models cannot be expected to accurately describe load-induced cracking when its mechanism is this complex. Empirical models are sufficient to model most mechanisms, but the most complex mechanisms, like load-induced cracking, must be modeled with a more flexible method.

If the fitting method's flexibility is considered, machine learning methods have shown a great ability for finding patterns in complex environments (Sun et al., 2020). Regression-based machine learning models have been able to predict many concrete members' shear capacities (Mangalathu et

al., 2021). However, these methods need a large, rich dataset to find the relevant patterns, so while they could theoretically be used in predicting crack shapes consistently, not enough available data on them. If only shear capacity is predicted, issues still arise with mechanistic interpretability and generalization past the dataset. However, because of their flexibility, machine learning methods can generalize better than empirical fitting methods.

# CHAPTER IV: METHODOLOGY

To robustly predict shear capacity in concrete beams without shear reinforcement, the accurate prediction of load-induced cracking is essential. Mechanistic models do not have the flexibility to represent load-induced cracking, and machine learning models do not have enough data to learn load-induced cracking or enough interpretability for their robust shear capacity predictions to be used in practice.

Recently, many new models have been developed that combine machine learning and mechanistic models to make Hybrid Mechanistic Machine Learning models. These have been developed under a variety of names, like "Physics Informed Deep Learning"( Rao et al., 2021), "Knowledge Enhanced Deep Learning" (Wang and Wu, 2020), "Finite Element Network" (Jokar and Semperlotti, 2021), Physics-informed neural networks (PINNs) (Riassi et al., 2019). Hybrid models are most often used to decrease the amount of data required for learning, but can also be used to increase prediction interpretability, and both these qualities are needed to robustly predict shear capacity.

In this thesis, we attempted to create a hybrid model for predicting load-induced cracking, but we were unsuccessful. However, along the way, we made several important discoveries about hybrid modeling and the requirements needed to accurately predict load-induced cracking. We took the following approach to implement hybrid mechanistic-machine learning modeling for the prediction of load-induced cracking in concrete beams without transverse reinforcement:

1. We surveyed various hybrid modeling approaches used in civil engineering and adjacent fields to determine which could be useful in predicting load-induce cracking. As mentioned, many hybrid models have been created, and none have been used to model load-induced cracking

on an entire beam. By surveying and categorizing these modeling approaches by their functionality, we determined which would best predict load-induced cracking. The survey and categorization are presented and discussed in Chapter 5.

2. We determined the appropriate mechanics to include in the hybrid model. Most hybrid models use differential equations as their mechanistic models, but they do not necessarily have to. Our previous hybrid model survey indicated the basic properties the mechanistic model needs, and the mechanistic model should be implemented before hybridization to validate it. The validation of mechanistic models is presented in Chapter 6.
3. We hybridized the previously verified mechanistic model chosen in step two with the hybrid modeling method chosen in step one. By using the flexibility of machine learning, we attempted to obtain an accurate load-induced cracking model can be obtained. The load-induced cracking model would then be used to create a robust model for predicting the shear capacity of concrete beams without shear reinforcement. Because the hybrid methods are relatively new, the best way to hybridize models has not been identified. We created several implementations using the same hybrid method to determine which works best. Implementation details for these hybrid models are discussed in Chapter 7.
4. We assessed the mechanistic consistency of the hybrid model and determined why it could not accurately predict load-induced cracking. Because hybrid models are more interpretable than machine learning models, some explanations for their predictions can be made based on developed mechanisms for shear failure. The analysis of mechanistic consistency is discussed in Chapter 8

5. We assessed additional properties of hybrid modeling that can benefit Structural Engineering. While the hybrid model was not able to achieve our original goal, it and models like it have other uses. The assessment included how efficiently the implementation uses data, how the different implementations created in step 3 affect performance, and how interpretable the model was. This assessment is discussed in Chapter 9
6. We developed a new hybrid model framework that remedies the deficiencies of its predecessor. Deficiencies found in step 4 included not representing multiple cracks, having poorly represented mechanistic models, and not having learning sufficiently constrained. This new framework employs a finite crack approach that uses multiple LSTMs to predict the crack propagations instead of crack shapes. Additionally, it uses mechanistic models that represent underlying mechanics well. This framework is discussed in Chapter 10
7. Finally, we developed an experiment to determine the effect of constraint on hybrid models. Under-constrained models do not have enough mechanistic models to make the machine learning models mechanistically consistent. This experiment varies the number of mechanistic models used when training and adds other forms of constraint besides mechanistic models. The role of constraint and the experiment design are discussed in Chapter 11.

Figure 4.1 shows this approach and its dependencies on previous steps

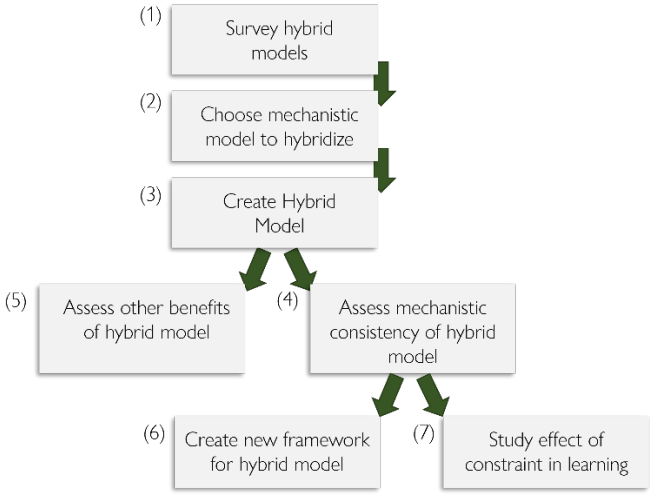


*Figure 4.1: Thesis Methodology and its dependencies*

# CHAPTER V: INVESTIGATION OF HYBRID MODELING METHODS

The survey was conducted by searching for keywords in various engineering journals. From the articles found through this search, additional articles were recognized through cited references. Additionally, articles that were foundational in the field were identified from seminars and, while many of these foundational articles did not apply to structural engineering, they were fundamental to the understanding of the field of hybrid modeling.

Previous attempts have been made to categorize hybrid modeling strategies to various extents. Karniadakis et al. (2021) define hybrid method categories through the biases that can be added to ML models to influence their learning. These biases include observation, inductive, and learning biases. Each bias consists of adding domain knowledge of the system into different aspects of a Machine Learning model. Methods that do not fit in these definitions are labeled as hybrid combinations of the biases, but no explanation is given as to how these other methods are composed of the various biases, limiting the categorization's robustness. Observation and learning biases can apply to any mechanics, but inductive biases are limited to mechanics with symmetry or invariant components and are most directly compared to how Convolutional Neural Networks detect symmetry in images. Furthermore, these methods are limited to describing how machine learning can be enhanced with domain knowledge and leave no definition for how mechanistic methods can be enhanced with ML. Alternatively, He and Chen (2020) categorized hybrid methods more generally as; physical constraints enforced on data-driven models, existing physical models enriched by information learned from data, and applying both models separately to approximate different aspects of the physical system.

Grouping hybrid models into broad categories based on which constituent is dominant is subjective. Any hybrid model is a combination of both mechanistic and machine learning modeling regimes and, depending on your perspective, can be seen as having either modeling regime be dominant. Although a model might be predominantly composed of mechanistic terms, the main predictive component may come from the machine learning model and vice-versa. The perspective of regime dominance can often come from the background of the problem too. If mechanics are being used to improve a machine learning model, the hybrid model is considered machine learning based, and the same is true in the other respect. Additionally, these groupings do not indicate the functionality (how they synergize and their purpose) of the categorized models. The functionality of these two seemingly separate groupings appears to be the same. From this, the best organization of the hybrid methods would be by their functionality instead of any component dominance.

Still, all hybrid methods in the below review will be described from a machine learning background because the main feature of the desired hybrid method is to improve a machine learning method so that it can learn load-induced cracking. In the following paragraphs, the reviewed hybrid modeling methods are grouped into categories based on functionality, and for each category, a general description of the method is given. The hybrid methods' functionalities will also be examined to show how they provide benefits over non-hybrid approaches too. The goal of the categorization is to better define which hybrid methods can be used to predict the load-induced cracking of concrete beams without transverse reinforcement.

When viewing hybrid modeling from a machine learning point of view, mechanics are always providing more information to the model for it to learn from. For mechanics to be used as

information, it can be used as a means of structure or as a means of data. In this thesis, these uses will be termed mechanistic structure (or just structure) and mechanistic data, respectively. These will serve as the main level of hybrid model categorization.

## Mechanics as a means of structure

The methods that use mechanistic structure are mechanistic learning, mechanistic feature engineering, data-driven inclusion, and data-driven tuning. Data-driven inclusion and mechanistic learning are the main methods while mechanistic feature engineering and data-driven tuning are variations of data-driven inclusion but are unique enough to be their own category of methods.

### Mechanistic learning

Machine learning methods learn by evaluating a loss function which measures prediction discrepancies, but if certain properties are desired, then additional relationships can be added to the loss function. The most common example of this is adding a regularization term, as shown in (4).

$$L(Y_{pred}) = \frac{1}{2}(Y_{pred} - Y_{true})^2 + \lambda * R(\theta) \quad (4)$$

Where $R(\,)$ is the regularization function and $\theta$ is some property or prediction of the model.

The most common regularization function in neural networks is the L2 norm (5), which penalizes the model for selecting large weights, $w_p$.

$$R(w_p) = w_p^2 \quad (5)$$

There is no limit to relationships that can be added to constrain learning. From this, additional relationships representing mechanics can be added to the loss function. Mechanistic Learning is often

used to make the machine learning model obey certain laws of physics, but can also be used to satisfy other constraints, like geometric conditions. A general expression for this may look like (6) and (7).

$$Y_{pred} = ML(X) \tag{6}$$

$$L(Y_{pred}) = \frac{1}{2}(Y_{pred} - Y_{true})^2 + \lambda * R(\phi) + Mech(Y_{pred}, X) \tag{7}$$

Where $Mech$ is the constraining mechanism and $X$ are the input features.

A central characteristic of this hybrid method is that the mechanistic relationship is separate from the discrepancy term in the loss function and serves to regulate learning. Furthermore, mechanistic learning can be used without a discrepancy term. In this case, the machine learning model learns entirely from the mechanistic constraints. because the loss function will never reach 0 in training, mechanics imposed in this will only be softly enforced (Rao et al., 2021). This method benefits from mechanistic consistency and improved learning structure, thus it results in a more accurate learned model requiring less data. Finally, this method can also be thought of as semi-supervised learning because learning is being constrained indirectly. This type of hybridization is easy to implement because only the loss function needs to be modified, but finding the appropriate mechanistic term may be difficult.

Wang and Wu (2020) applied this method to modeling structural response from wind loading. To do this, they used a recurrent neural network (RNN) to predict a single degree of freedom structure's displacement, velocity, and acceleration at time step $i$ using the exciting force of the same time step and the predictions from the previous timestep, shown conceptually in (8).

$$u_i, u_i', u_i'' = RNN\left(u_{i-1}, u_{i-1}', u_{i-1}'', F_{e,i}\right) \quad (8)$$

Where $F_{e,i}$ is the exciting force at time step $i$.

Their loss function then includes a term to measure discrepancies in predictions and uses dynamic equilibrium to equate the predictions to the excitation force. However, this is not done directly but rather through wavelet projections, which will be discussed in a later section. The mechanics-based portion of the loss function can be simplified as in (9).

$$mech(\,) = u_i * k + u_i' * c + u_i'' * m - f_i \quad (9)$$

Where $k$ is the stiffness, $c$ is the damping coefficient, and $m$ is the mass of the system.

The results show using mechanistic learning significantly reduces the amount of data required. The mechanistic learning model achieved its minimum error by only considering 3200-time steps while a model that did not use it needed 5600-time steps to achieve the same error. Additionally, mechanistic learning also ensures mechanistic consistency by maintaining equilibrium. When white gaussian noise was added to the responses, the enhanced model was significantly more accurate than the plain machine learning model. Finally, it was able to accurately extrapolate far beyond the training examples of 16s to test samples of 600s. However, this extrapolation was not compared to a plain machine learning model. Therefore, it cannot be concluded definitively that this is a benefit of mechanistic learning, but it is likely given that ensuring mechanistic consistency would prevent drift in later predictions.

Haghithat et al. (2021) implemented a PINNs model to predict solid mechanics state variables from spatiotemporal inputs. This is the common application of PINNs where an automatic

differentiation algorithm is used to find the derivatives of state variables with respect to the inputs. The state variables and their derivatives can then be used in continuum mechanics equilibrium and constitutive equations. In this, the stress and displacement of an elastic plate are predicted and then validated against a synthetic data set and the continuum mechanics equations. By taking the partial derivative of the stresses, the stresses could be validated against the applied loads, and displacements could be compared to strains through their differentiation. Additionally, constitutive parameters for the plate were predicted. These were validated in the constitutive loss term.

This method was also used by Rao et al. (2021) to predict the elastodynamic response of homogenous plates by constraining the loss function with equilibrium equations and explicitly forcing boundary/ initial conditions. This implementation did not use any data and was only constrained by Mechanistic Learning terms. Zhang et al. (2020) predicted the structural kinematics, non-linear restoring force, and hysteresis parameter of a structure by constraining it with equilibrium and hysteresis Mechanistic Learning terms. In a similar work, Zhang et al. (2020) predicted structural kinematics and non-linear restoring force by only using equilibrium constraints. Shukla et al. (2020) constrained a neural network with acoustic wave equations to learn the wave speed and detect cracks in solid surfaces.

### Data-Driven Inclusion

Data-driven inclusion models add structure to learning by incorporating mechanistic expressions in their prediction, which is then used in a loss function to evaluate discrepancy. Often, machine learning and mechanistic models work together to represent different mechanisms of the system. A representation of this can be seen in (10).

$$Y_{pred} = f\big(ML(X), Mech(X)\big) \quad (10)$$

The machine learning and mechanistic model combinations can vary widely. The machine learning model may be a function of the mechanistic model, the mechanistic model a function of the machine learning model, both models may contribute to the same prediction, or any combination may be true. Depending on the configuration of mechanistic and machine learning components, it can appear like the machine learning model is an inclusion in a mechanistic model, giving it its name. Additionally, the number of machine learning models that can be used is not limited; Multiple models may be used to represent different mechanisms. By $Y_{pred}$ being partially predicted by mechanistic models, the machine learning portion has a less complex mechanism to learn, being the one it was assigned. Ideally, this will reduce data requirements or increase prediction accuracy for a given data set. This method also has the benefit of connecting mechanisms which have scarce data to larger datasets through other mechanisms. For example, load-induced cracking can be connected to shear failure through the constitutive relationships of inter-crack forces.

Vianna et al. (2020) use this method to estimate the inadequacy of differential equations predicting aircraft hardware distress. Data on flight characteristics is provided for every flight, but the data relevant to hardware distress, the label in this data set, is only provided during routine inspections, leading to a data imbalance/small data set size. Additionally, the complex failure mechanisms are only partially understood. So, in this problem, the mechanistic models are inadequate because of an incomplete understanding and there is not enough data to make an entirely data-driven model. The inadequacy of the mechanics prevents well-developed PINNs methods, which use differential equations, from being used. The hardware distress models include crack growth from fatigue in

fuselages, crack growth from combined fatigue and corrosion, and bearing fatigue exacerbated by grease degradation. Two methods are proposed to implement a hybrid model:

(1) by introducing a discrepancy "node"

(2) by having a whole mechanism be represented by a data-driven "node".

However, only the second option is ever used. The first method will be discussed in a later section as it is classified as another method. These "nodes" are combined with physics-driven "nodes" (e.g. Paris power law in fracture mechanics) to make the entire model. (11) – (13) represent the relationships used in this model.

$$a_c = a_{c,t-1} + \Delta a_{c,t} \quad (11)$$

$$\Delta a_{c,t} = C\Delta K_t^m \quad (12)$$

$$\Delta K_t = ML(X) \quad (13)$$

Where $X$ are flight characteristics, $\Delta K_t$ is a stress intensity factor, $C$ and $m$ are material properties, and $a$ is the crack length.

Using flight and maintenance session data, the machine learning model is trained with error from the crack size at inspection, that is $a$ at the final timestep. Crack data wasn't available for all predictions, and training had to depend on the few timesteps that there was data for.

Unfortunately, this work does little to compare this method's performance to purely machine learning or purely mechanistic modeling, so no real conclusions can be drawn on its effectiveness. However, these models are one of the few to not implement mechanics through differential

equations, highlighting that differential equations may be just one of many ways to incorporate mechanics.

Wang and Wu (2020) also use this method through their incorporation of the wavelet transform. By doing this, the mechanistic knowledge that some exciting frequencies will not affect the response of the structure is simplifying the relationship that the machine learning model must learn. In this example, the machine learning model is representing multiple mechanics instead of one, but this implementation can still be considered as data-driven inclusion because mechanistic models are used to predict the discrepancy terms.

This method was also used by Eshkevari et al. (2021) to learn the stiffness of a structure given response data. Chakraborty and Adhikari (2021) created a model to predict the time evolution of a structure's mass and stiffness based on the response information

### Mechanistic Feature Engineering

As mentioned previously, this method is a variation of the data-driven inclusion method. This is because it includes all mechanistic expressions as inputs to the machine learning model, as seen in equation (14), while data-driven inclusion might include them at any point in the model. Much like how principal component analysis would be used to engineer features, mechanistic models are combining features based on relevant mechanics.

$$Y_{pred} = ML(Mech(X), X) \tag{14}$$

This allows for the machine learning model to represent a simpler relationship because if the mechanistic expressions were not given, it would have to learn them itself, increasing its complexity. The relationships that are used can be as simple as having dimensionally consistent input features or

combining geometric features like length and width into an area. While it might be common for Data-Driven Inclusion models to represent individual mechanisms with machine learning, Mechanistic Feature Engineering will often represent many mechanisms with one machine learning model. For example, dimensional analysis can be performed on a beam's features to make them relate easier to the predicted variable of beam capacity, one machine learning model would be used to relate loading to stress and relate beam material properties to failure stress, and a Data-Driven Inclusion model would commonly represent only one of these mechanisms with machine learning. However, this categorization does not prevent Data-Driven Inclusion models from representing all these mechanisms with one machine learning model.

Gunaratnam and Gero (1994) use dimensional analysis to improve the performance of a neural network predicting a variety of phenomena in structural engineering. In one application, the neural network was used to predict the loading on a beam given moments along its length. The dimensionless variables $\frac{M}{P\delta}$ and $\frac{x}{L}$ were used, where $M$ was the moment in the beam $\delta$ was the location of that moment, $P$ was the load that caused the moment, $x$ was the location of that load, and $L$ was the length. Despite overlapping training and testing data in their evaluation, the model with dimensionless Input achieved more accurate predictions than a normal neural network. This effect was observed in the predicting moment capacity of concrete beams and maximum bending moments in rectangular plates as well.

Other works use a similar method for the prediction of failure in concrete members (Perez, 2014) (Gondia, 2020). However, instead of using dimensional analysis, components from existing equations are used with genetic algorithms to essentially optimize them. The basis for these models'

classification as hybrid is in question, though, and depends entirely on the equations used. Most equations in design codes, like ACI 318-19 (2019) bear little relation to the mechanisms they are describing and are almost entirely empirical, so if these are the basis for prediction, then the model should not be considered hybrid. Instead, it may be considered as some refinement process as one empirical model is being replaced with a better empirical model, which was likely developed using the same data. However, there are also design code equations, like those for strut and tie models, which significantly relate to the underlying mechanics. In this case, these can be considered hybrid.

Xu et al. (2021) were able to use "combined parameters" like slenderness ratios and tensile to yield strength ratios to achieve more accurate predictions of cold-formed stainless-steel tubular columns.

### Data-Driven Tuning

Just as in mechanistic feature engineering, this method is also a variation of data-driven inclusion. Instead of the machine learning model representing mechanisms of the system, it represents a modification of mechanistic expressions, whether that be an amplification, reduction, or discrepancy prediction of the mechanism. A possible type of modification can be seen in (15)

$$Y_{pred} = ML(X) * Mech(X) \quad (15)$$

Often mechanistic expressions do not accurately represent underlying mechanisms because of simplifications or assumptions made and because of the limited flexibility of empirical models, so this method accounts for those simplifications with a machine learning model. When discussing the work presented by Vianna et al. (2020), their method of adding a discrepancy "node" was not considered a data-driven inclusion method because it belongs in this category. This method is great

for increasing prediction accuracy because the machine learning models have a much simpler relationship to learn compared to the other hybrid methods presented. If the mechanistic expressions are at least somewhat accurate, then most of the system's complexity is already being described, and the machine learning model often only needs to describe relatively simple relationships. However, this is the least interpretable hybrid implementation, as there are no mechanics to relate the machine learning predictions to. For example, if load-induced cracking is predicted using Data-Driven Inclusion, where the whole model is predicting shear capacity, then the predictions can be related to crack inclination mechanisms (Cavagnis et al., 2015), but if Data-Driven Tuning is used, it will only correct mechanistic predictions for shear capacity and not represent any underlying mechanisms.

Zhang and Sun (2020) applied this method to damage localization. Understanding that finite element model updating is prone to errors from simplification and that there also isn't enough data to make a machine learning model outright, they used this method to make a neural network that corrects the finite element predictions based on data of a real damaged structure. This method is never compared to finite element updating or neural networks directly but was shown to only predict well for cases similar to training data (small damage states were predicted well because they were well represented in training data). However, in a later comparison, this method combined with another hybrid method (mechanistic data) shows increased performance over finite element updating

This method was applied by Guan et al. (2021) to amplify the linear response history of a structure under seismic excitation to non-linear response histories.

## Mechanics as a means of data

Mechanistic models can also be used to generate data about a system rather than using those mechanics to provide structure to learning. This may be the most straightforward approach to hybrid modeling, as data only needs to be generated from another simulation.

The methods that use mechanistic data can be distinguished by those that use *entirely simulated data* and those that only use *simulated data as a supplement*. Typically, the former is very useful in metamodeling, reduced-order modeling, or solving inverse problems, and the latter has only been used to help with generalization (increase accuracy).

Metamodeling and reduced order modeling use a similar process to achieve the same goal: describe a system with different mathematics than the one used to create data for it. Solving inverse problems has a similar purpose as metamodeling or reduced-order modeling except, as the name suggests, the inputs and outputs are swapped in the machine learning model from how they were used in the mechanistic one.

Methods that use *entirely simulated data* are always used to improve computational efficiency. There are significantly fewer computations required in executing the layers of a neural network than inversing stiffness matrices in finite element formulations, and regression in inverse problems can speed up and automate the process of finding the inputs that produced a given output. Using *simulated data as a supplement* to help with generalization can hurt the predictive model by providing inaccurate information but is beneficial to learning in the absence of sufficient data.

Napolitano and Glisic (2020) use this method to solve the inverse problem of predicting the damage events (loading or displacements that caused damage) that caused a structure's current health

state. Typically in a finite element simulation, the damage event would be applied to the structure and the damage state could be predicted using mechanistic models. Given that a structure's current health state could be caused by any combination of damage events, it is difficult to provide an inverted model with mechanics. Instead, a database of many damage events' effects on a structure is made and a Gaussian Process Regression is used to find the likely damage event that caused a structure's current state. Without this procedure, simulation outputs would have to be manually compared to the damaged structure to determine the events that led to the structure's current health state.

Additionally, using an algorithm to update the simulation's parameters to more closely predict the damaged structure, as is done in finite element updating, would be time-consuming because simulations would have to be done online. However, using machine learning in inverse problems, all simulations can be performed offline and a computationally efficient model can then be used when needed.

Sofi and Steelman (2021) used neural networks to make a metamodel of bridge finite element simulations, providing a tool for rapid retrofit decisions. Jokar and Semperlotti (2021) created metamodels for finite elements, reducing the computational expense associated with the finite element method. Kim et al. (2021) created more computationally efficient models for predicting the strength of circular hollow section x-joints using support vector machines and neural networks trained on high-fidelity finite element models. Similarly, Zhang et al. (2021) created a model to efficiently predict the flexural capacity of RC structures based on their extent of corrosion-induced cracking. These models were trained on finite element models that included the effect of corrosion. Based on finite element simulations, Esteghamati and Flint (2021) created a support vector machine model to

predict the seismic vulnerability and environmental impacts of buildings based on their early design parameters and location.

Methods that use *simulated data as a supplement* do so to help with generalizability. As presented earlier, Zhang and Sun (2020) use data-driven tuning to increase the accuracy of finite element updating strategies for damage localization. Their predictions were very inaccurate for large damage intensities, a scenario that was relatively absent in their data. However, including finite element updating labels for large damage intensities helped the model generalize even though the labels were relatively inaccurate.

## Parameter-Free Data-Driven Modeling

A method that was studied but not considered hybrid was Parameter-Free Data-Driven Modeling. It is both data-driven and incorporates mechanics, but it does not include any learned model. Instead, predictions are made directly from a database. This method was still included in the survey because of its adjacency to the methods of interest.

Kirchdoerfer & Oritz (2016) identify that the main issue with modeling a system accurately is the constitutive models that relate physical laws to each other. Often, constitutive models include too many simplifications and assumptions, so rather than making a model for constitutive relationships, data on the relationships will be used directly in prediction. The basic formulation of Parameter-Free Data-Driven Modeling finds an observed material property that is the closest to satisfying the governing physical laws. Therefore, with a perfectly accurate observation, a perfectly accurate simulation can be found. This method was originally applied to the static analysis of a 3D truss.

He & Chen (2020) and Kirchdoerfer & Oritz (2017) both realize that the accuracy of this method is then entirely dependent on the accuracy of the dataset. If significant noise is present in the dataset, the noise will detract from the method's accuracy. From this, an alternative formulation was made that finds a material relationship, interpolated between observed states, that exactly satisfies mechanistic laws.

Kirchdoerfer & Oritz (2018) then used this method to model the dynamics of structures too.

## Discussion

Several discussions about the preceding methods are provided in the following sections. To better define the categorization and compare it to others, the relationship between proposed methods and their relationship to other categorizations (Karniadakis et al, 2021) are discussed. Next, to better understand the relationship between mechanistic models and hybrid models, the relationship between machine learning and empirical modeling is discussed. Then, the concept of interpretability is better defined because improvements in accuracy and computation efficiency are easy to determine, but improvements in interpretability are subjective and have not been evaluated well in the past. Finally, many investigated hybrid models have used neural networks for their machine learning portions, so we investigate the reason for their popularity.

### The Relationship Between Proposed Methods and PIML biases

Figure 5.1 shows a decision tree to classify a hybrid model. This decision tree helps to clarify the differences in hybrid modeling methods.

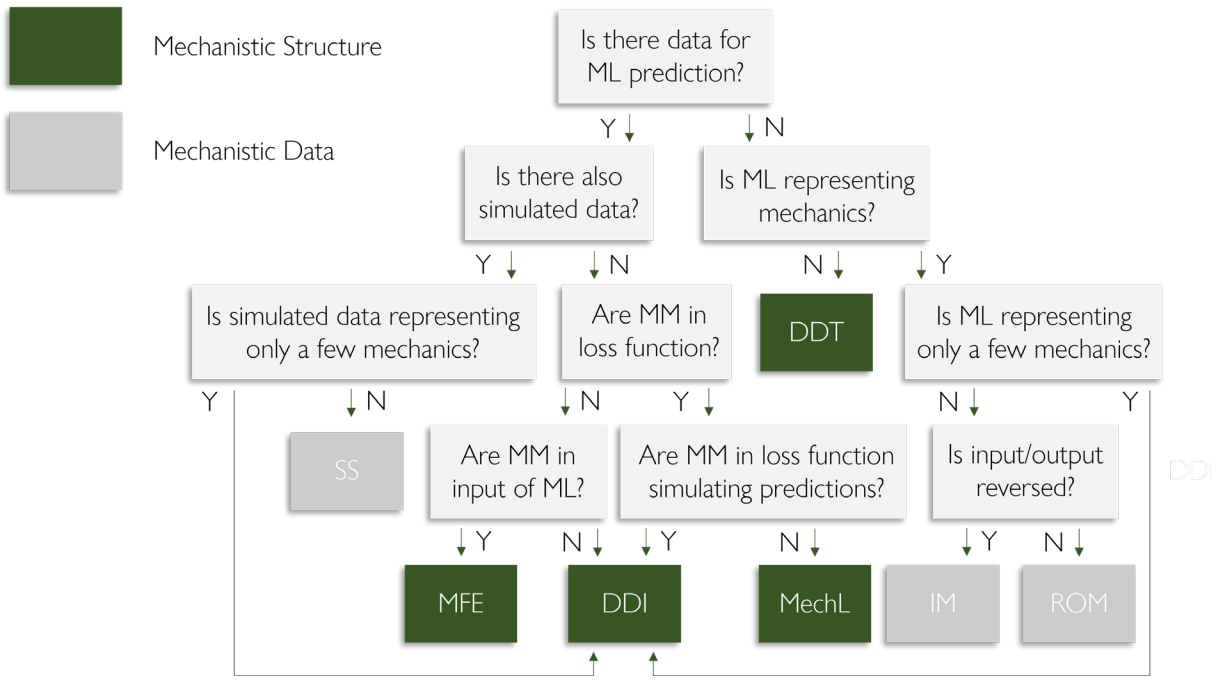


*Figure 5.1: A decision tree to help clarify the difference in hybrid modeling methods. DDT is Data-Driven Tuning, SS is Simulated data as a supplement, MFE is Mechanistic Feature Engineering, DDI is Data-Driven Inclusion, MechL is Mechanistic Learning, IM is Inverse Modeling, ROM is Reduced-Order Modeling or Metamodeling, MM is mechanistic model, and ML is machine learning model.*

Additionally, the typical uses for these methods are shown in Figure 5.2. This figure shows that Mechanistic Data methods are often used to increase computational efficiency and Mechanistic Structure Methods are often used to increase prediction accuracy.

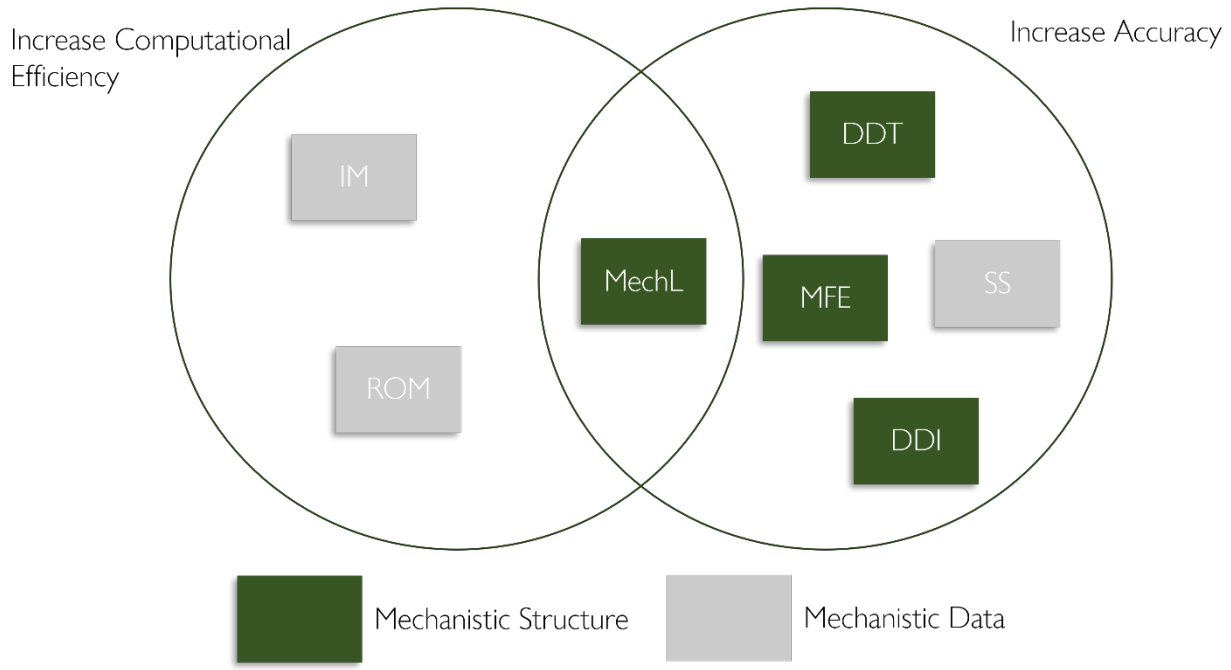


*Figure 5.2: Method Purpose, where the acronyms are the same as in Figure 5.1.*

The methods proposed previously are all fundamentally similar and only differ by the location in the learning process that mechanistic models provide information. Mechanistic Learning includes mechanistic models in the loss function, Data-Driven Inclusion, Mechanistic Feature Engineering, and Data-Driven Tuning all include mechanics in the prediction of the target variable (the variable whose discrepancy is evaluated in the loss function), and all mechanistic data methods use data simulated from mechanistic models.

Mechanistic Learning and Data-Driven-Inclusion-like methods have the biggest distinction. Although, they can appear similar. In Mechanistic Learning, the mechanistic relationships are included in the loss function and regulate learning. The Data-Driven Inclusion method potentially includes mechanistic relationships before and after the machine learning prediction. However, if the mechanistic terms following the machine learning are algebraically reorganized to be included in the

loss function, it can appear as if the modeling method used was Mechanistic Learning or even as if data was being simulated for the predicted variable. Upon closer examination, however, the Data-Driven Inclusion method is using these mechanics as a "bridge" from the machine learning predictions to the dataset, and Mechanistic Learning methods only every use mechanistic relationships separate from discrepancy loss terms. This relationship carries for Data-Driven tuning but not necessarily for Mechanistic Feature Engineering. Because Mechanistic Feature Engineering's mechanics are included before the machine learning predictions, the mechanics will never be in the loss function. In short, Data-Driven Inclusion-like methods' machine learning models will be connected to the data set through mechanics and Mechanistic learning's machine learning models will either have data for their predictions or not use data at all.

As mentioned, the Physics Informed Machine Learning categorization (Karniadakis et al, 2021) differentiates methods by the type of bias that is included in the machine learning model. These biases can be related to the developed methods to show that they provide a more robust method of categorization.

Observation bias is explicitly the information available from data, real or simulated. This bias has a significant overlap with the bias in standard machine learning and does little to effectively add information from mechanics. Only through simulated data is additional information given to a learned model, and using simulated data corresponds directly to the Mechanistic Data methods. Additionally, no distinction is made between models that solely use simulated data and those that use it as a supplement.

Inductive bias affects learning through specially designed neural architectures. This bias is best exemplified by how convolutional neural networks are efficient with spatial data. Inductive bias could be related to Data-Driven-Inclusion-like methods (Data-Driven Inclusion, Mechanistic Feature Engineering, Data-Driven Tuning) because the incorporated mechanics could be considered a special form of architecture, but this analogy ultimately does not work because (1) Data-Driven Inclusion applies to more machine learning methods than neural networks and (2) Inductive bias is explicitly referencing neural structures that respect symmetry, translation, rotation.

Finally, learning bias is defined as softly imposing constraints through the loss function, and it includes PINNs as a representative method using this bias. PINNs are similar to both Data-Driven Inclusion and Mechanistic Learning because PINNs are only defined as having some mathematical operators in the loss function, and, as mentioned before, both Data-Driven Inclusion and Mechanistic learning can be represented in this way. PINNs do not distinguish between these even though they affect learning differently. Additionally, PINNs are exclusively used to represent constraints from differential equations and show little utility in how these can be used with other mathematical representations of mechanisms. They also have a special format in which spatiotemporal information is used as an input and state variables are the output. Because of this, the derivatives of the predictions can be computed easily using the automatic differentiation algorithm and thus making PINNs suited toward differential equations. However, many applications in civil engineering exist where differential equations are not suitable to represent underlying mechanisms. For example, the equilibrium of large rigid bodies, as is often used for modeling shear failure in cracked concrete beams, is more amenable to the vector sums of forces and moments on its boundary. To make the shear failure system

amenable to being constrained by differential equations, a finite element discretization would need to be implemented.

The Physics Informed Machine Learning organization (Karniadakis et al., 2021) does not include many methods or explanations for how mechanics can be used as a structure for learning even though they included models (Racauckas, 2020) that exemplify this behavior. Instead of creating a categorization for these methods, they were designated as hybrid combinations of biases without any explanation for how they hybridized biases.

For this reason and those considered above, the proposed categorization is more general and applicable to Civil Engineering than those provided in Karniadakis (2021).

### Relationship between machine learning and empirical modeling

At first glance, you might think mechanistic and hybrid models are very different, but they actually have many similarities. This can be seen through the relationship between empirical and machine learning models, the data-driven portion of mechanistic and hybrid models, respectively.

Empirical modeling is widely used and trusted for making predictive models. Empirical modeling shares many characteristics with machine learning because both are entirely data-driven. The only substantial difference between the two is that machine learning models are vastly more complex than empirical ones, which may only have one parameter being calibrated. However, aside from this complexity, both are still attempting to find patterns in data. In this sense, it is logical to say that machine learning models are empirical models too, and many of the same principles carried for empirical models may be shared with machine learning ones. As stated by Charalampakis and Papanikolaou (2021) "It is worth noting that ML, as a field of study, did not appear abruptly in the

scientific scene; a simple regression analysis on experimental data, used for decades across all fields of engineering, can be considered as a primitive ML application." Considering that all mechanistic models have some empirical contribution, the distance between mechanistic and hybrid models is smaller you might consider. However, one difference between mechanistic and hybrid models is machine learning models are more prone to overfitting and memorization than empirical ones. This can have a potentially harmful effect in terms of robustness. This is because the memorization capacity of the handful of parameters used in simple regressions (empirical models) is negligible, but when machine learning models, like neural networks having millions of parameters, are fit, they can easily memorize the entire data set. This is not a substantial issue, though, because separating training and testing data have become standard to avoid memorization and prove machine learning actually learns. Finally, one interesting consequence of the memorization ability of each fitting method is empirical models have more data available to them for fitting because there is no need to separate data into training and testing. From this, hybrid and mechanistic modeling are equivalent besides the complexity of fitting techniques and the need to separate training and testing data.

### On the interpretability of models

All new models aim to be more accurate, computationally efficient, or interpretable than previous ones. Understanding how accuracy or computational efficiency increases is quantitative and objective, but assessing interpretability is qualitative and subjective. In general, machine learning models are always described as uninterpretable, mechanistic models are interpretable, and hybrid models seem to have improved interpretability compared to machine learning models. By investigating these models, we can determine a common factor that affects interpretability.

When discussing machine learning models, we always say they are uninterpretable because of a "black box" effect, meaning inputs go into the model, then come out without any indication of what transformations occurred (Gondia et al., 2020). It is not that the mathematics between inputs and outputs are unknown, it is just there are too many of them to make sense. On the other hand, mechanistic models are often much simpler, and we can see how inputs to the model affect the output just by examining its mathematical expressions.

We might consider this to be the basis of interpretability (seeing how inputs transform into outputs), but it ultimately does not fit because sometimes mechanistic models are too complex to determine input and output relationships. For example, in finite element modeling, it can be difficult to determine how complex loading will translate to stress states. What both the finite element models and simple mechanistic model both have in common is their mathematical forms represent underlying mechanics. For example, when looking at the ACI 318-19 (2019) equation for concrete shear capacity, we see that shear strength increases with an increase in depth.

$$V = 2 * \lambda * \sqrt{f_c'} * b * d \tag{16}$$

Where $\lambda$ is a factor to account for lightweight concrete.

This correlates to previous mechanics observed in experiments. We can see that the ACI equation is observing this, and by inspecting the basic components of a finite element model, we can see that it follows equilibrium and constitutive mechanisms.

We can't tell if a machine learning model is representing mechanics just by looking at its weights and biases, but this isn't the only way of verifying mechanism representation. We can tell if it is representing mechanics by testing the sensitivity of its predictions. This makes two ways to

determine interpretability: one by looking at the mathematical form of the model and one by analyzing its predictions.

Using this definition, the interpretability of a machine learning model can be more robust than the interpretability of mechanistic models. Often, mechanistic models aren't able to fully model the complexity of underlying mechanics, and thus, lead to inaccurate predictions for cases they weren't validated on. However, your interpretation of a machine learning's prediction is more likely to be accurate because they have the flexibility to accurately describe complex mechanics. In fact, relying solely on the familiarity of the model's mathematical form for interpretability often lead to misinterpretations of predictions. Back to the ACI example, this model doesn't account for aggregate interlock, delamination cracks, or failure caused by crack merging, so when concrete strength is too high and aggregate is cracked along with the concrete matrix, this relationship will misinterpret underlying mechanisms (Huber et al., 2016).

This definition is also a better explanation of machine learning's lack of interpretability than the "black box" effect because at the base of the "black box" effect argument lies the fact that the underlying mechanics cannot be seen in the machine learning model's mathematical form. Often when machine learning is used for prediction, outputs are generated but there is no validation of them with underlying mechanics, so the prediction is uninterpretable. Validating all the mechanisms for a system as complex as shear failure in concrete beams would be impossible by only examining predictions. Changing the depth, for example, in machine learning predictions could cause any number of underlying mechanisms to behave differently. The beam could transition into a deep beam state and cause an increase in capacity or beam capacity could increase simply because there is more cross-

sectional area to act on. Without knowing how a change in depth is altering capacity predictions, there is no way to know if it is respecting underlying mechanisms. Additionally, there would be no point in trying to modify the machine learning algorithm so that its mathematical form could be analyzed because then it would be as restricted as empirical models and would thus lack the flexibility to *accurately* represent underlying mechanisms. From this, the only type of interpretability that should be used with machine learning should be correlating its predictions with underlying mechanisms.

This last point directly transitions into why hybrid modeling is more interpretable than machine learning. In Mechanistic Learning, constraints are added on the loss function that explicitly satisfies underlying mechanisms, so by sufficiently training the machine learning model, predictions will not have to be analyzed for respecting underlying mechanisms. They will explicitly be respected. Data-Driven-Inclusion-like models provide interpretability in another way. By incorporating many more mechanistic models into prediction, the machine learning only has to represent a few mechanisms, then their predictions can be effectively evaluated for respecting those mechanisms. For example, when predicting load-induced cracking, predictions for a critical crack should show the crack extending most of the way up the beam and should be closer to the application of loading than the support. These mechanisms could be verified by analyzing predictions.

### The prevalence of neural networks

Hybrid methods typically use Artificial Neural Networks or one of their derivatives (RNN, CNN, etc.) as their machine learning model, and the use of SVM, Gaussian process regression, or decision trees is much less common. Several factors may contribute to the neural network's popularity,

and these factors must be considered to decide if neural networks provide some advantage over other machine learning methods.

The first factor contributing to the neural network's popularity is its somewhat loose relationship to the human brain (Sofi and Steelman, 2021). This may provide an initial allure when relatively new users are looking for a method to use. Still, experience in regression identifies that neural networks are the same as any other regressor, so this is not enough evidence alone.

Another reason may be their continuous development and success in other fields. Deep learning has shown promise in many fields with abundant data, and new variations of neural networks are always being developed. RNNs and CNNs have found popularity for their ability to recognize sequence-dependent mechanics, which can be useful for time-series analyses (Eshkevari et al., 2021). However, similar spatiotemporal structures can be made in other algorithms, and boosting and bagging methods have shown much promise for small datasets, which is a common case in engineering domains.

Neural networks are also popular because of the automatic differentiation (Baydin et al., 2018) training algorithm they use. With a suitable automatic differentiation library, any number of mathematical operations may be used to create a unique learning structure, making them very modular and most amenable to hybridization. Of course, other methods can use gradient-based training, but, as in the case of the support vector machine's ability, gradient-based training may defeat the other methods' purpose. A support vector machine employing gradient-based training effectively turns into a more restricted neural network. The main advantage of SVM is that the kernel trick can be used to significantly reduce the complexity of the model, allowing for more accurate predictions

with fewer data. From this, most machine learning methods are restricted to incorporating mechanics in their loss functions or their input features. Additionally, the automatic differentiation procedure is key to the operation of most PINNs models because they use automatic differentiation implicitly to use the derivatives of outputs in the loss function. While this may not be the main reason for their popularity, it is a substantial reason why they should be preferred in hybrid modeling. There are drawbacks to neural networks, however. Mainly, they typically require large amounts of data because neural networks have a large parameter space. This is partially reconciled in hybrid modeling.

## Hybrid Learning

A central feature of hybrid models is that they decrease data requirements for learning by adding more information from mechanistic models. This is usually explained vaguely by simulations adding more data or mechanistic models decreasing the complexity the machine learning models must describe, but this increase in data efficiency can be described concretely through the bias-variance tradeoff. We use Hybrid Learning to term this theory for increased data efficiency.

We will describe learning more thoroughly first to set up the definition of Hybrid Learning. Learning (or fitting) is often described as updating parameters in a parameterized model for the model better to better suit a dataset. However, learning can alternatively be described as selecting a model from a set of possible models all having different parameters, where the selected model has the desired parameters. These two descriptions are equivalent because selecting one model over another is like updating parameters in the former definition.

This set of possible models is the model space. The complexity of this space depends on the number of unique combinations of learnable parameters, and the model space's flexibility to describe

complex mechanics correlates to its complexity. Then, the goal of fitting or learning is to use in-sample data as an "image" of underlying mechanics to determine or "learn" the model in this space that best describes the mechanics. To determine how well it describes the mechanics, it is tested against an out-of-sample data set, which contains an independent "image" of the underlying mechanics. If there is low error, it can be said the mechanics have been learned well. (Yaser et al., 2012). The advantage of viewing learning like this is that effect of the model space size (or the number of trainable parameters) can be more easily seen. The more models in the space (more parameters), the more difficult it will be to select the best one (best combination of parameters).

Before learning begins, the bias-variance trade-off can use the complexity of the model space ($\boldsymbol{n_m}$), the complexity of underlying mechanics ($\boldsymbol{C}$), and the size of the data set ($\boldsymbol{D}$) to explain how the machine learning model will perform. The trade-off has many similarities to the mathematical proof of error linked to the VC dimension for classification models (Vapnik and Chervoneskis, 2015), and describes the out-of-sample error as being composed of two components, one from bias and one from variance. Error from variance increases when there is not enough in-sample data to adequately choose a model from a space that is too complex, and error from bias increases when the model space complexity cannot represent the complexity of the mechanics. This trade-off is shown conceptually in (17) and (18).

$$E_{bias} \propto \frac{C}{n_m} \tag{17}$$

$$E_{var} \propto \frac{n_m}{D} \tag{18}$$

The "trade-off" between these two errors occurs when increasing the complexity of space; the error from bias decreases and the error from variance increases.

To illustrate this relationship, consider the problem of fitting data generated from a 10th-order polynomial with random coefficients. If a 10th-order polynomial is used to fit the data with only 4 points generated from the original polynomial, any number of compatible relationships could be learned, generating substantial error on out-of-sample predictions. Alternatively, if a 2nd-order polynomial is used with the same points, dramatic errors from overfitting can be avoided, but this will never be able to approximate the true relationship. These examples are shown in Figure 5.3.

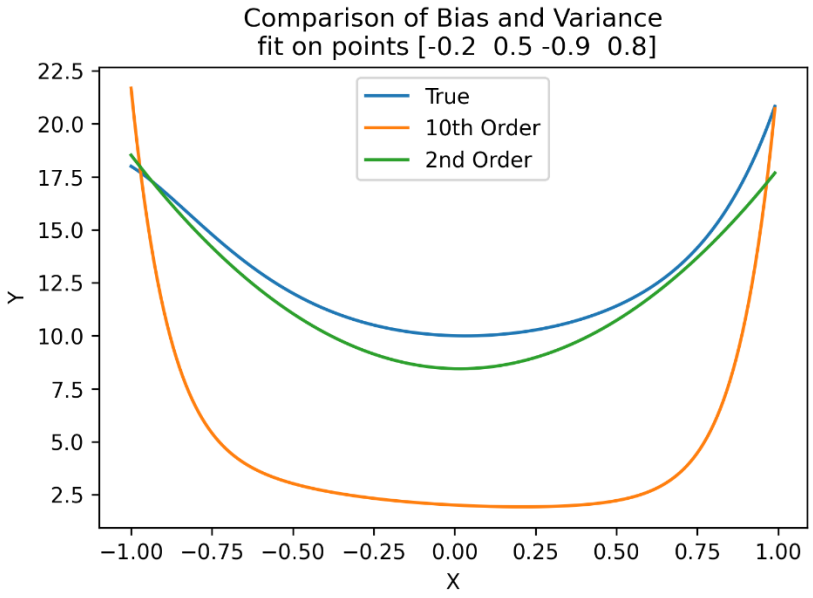


*Figure 5.3: Comparison of error from Bias and Variance*

Setting up this definition for learning makes understanding Hybrid Learning simple, as it is just a small extension of this definition. However, hybrid methods affect the bias-variance trade-off differently. In Data-Driven-Inclusion-like methods, additional mechanistic relationships are used to describe some of the underlying mechanisms, essentially reducing the complexity ($\boldsymbol{C}$) the machine learning model must represent. This decreases the machine learning model's error from bias. **Figure 5.4** shows the model space for standard and hybrid learning. Mechanistic data provides extra data ($\boldsymbol{D}$) from mechanistic simulation, decreasing the error from variance. Mechanistic Learning also provides extra data ($\boldsymbol{D}$), although, not directly. By providing constraints in the loss function, Mechanistic Learning is providing extra data for predictions in the form of constraint equations.

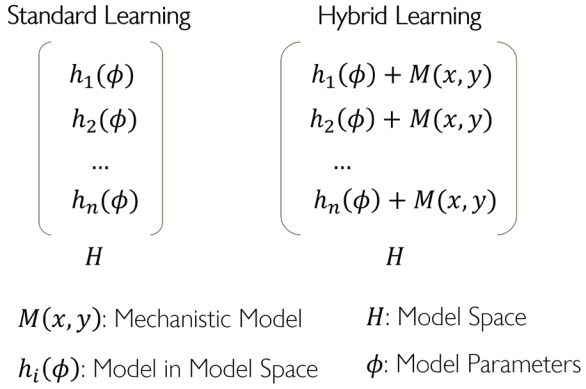


*Figure 5.4: Model Space Changes for Data-Driven-Inclusion-Like Methods*

To extend the polynomial analogy, the mechanistic models could represent the 2nd-order to 10th-order terms in a 10th-order polynomial while the data-driven portion must only learn a linear and constant term.

As every model is wrong (Box, 1979), however, any error in mechanistic relationships will contribute additional error to the out-of-sample predictions of the machine learning model. In Data-

Driven-Inclusion-like models, the machine learning model receives all its information from the mechanistic relationships. To reduce the in-sample error, the machine learning model will learn its mechanisms as well as correct the error from mechanistic relationships. Thus, the machine learning model will not be representing its own mechanisms. Similar conclusions can be easily extended for the other hybrid methods. When flawed mechanistic relationships are used to generate data, the data will be partially erroneous, giving bad information to the machine learning model. From this, the out-of-sample error of the machine learning models is composed of parts from bias, variance, and mechanistic error, which we will term mechanistic bias in this thesis.

Throughout this thesis, we will use Hybrid Learning to explain both the data efficiency and mechanistic inconsistency of our models.

## Application to Shear Failure

The purpose of studying the reviewed models and defining the proposed hybrid method categories was to determine the best hybrid approach to predict load-induced cracking in concrete beams without shear reinforcement. Given that there is scarce data relating crack shapes to loading, a method is needed that reduces the amount of data required for learning or provides an increase in data. While any method could potentially be implemented for this, the Data-Driven Inclusion method is used because it connects mechanisms with relatively little data (load-induced cracking) with larger datasets (shear capacity data sets). From this choice, the Data-Driven Inclusion method will be defined more thoroughly now. Through this definition, we can better select the mechanistic model used in hybridization and determine any other implementation details that must be considered. Additionally,

this does not have to be the only hybrid modeling method used; many reviewed hybrid models incorporate multiple methods to great effect.

We will thoroughly define this method through an example. To begin using this method on a system, the mechanistic models of the system must be organized by how well they represent underlying mechanics. The ones that represent poorly will be replaced by a machine learning model. Consider the mechanistic models, $f_1$, $f_2$, and $f_3$, of the example system shown in Figure 5.5 (equations (19)-(21)). These models represent their underlying mechanics well except for $f_2$, which is the source of most of the error in the end prediction. Predictions for $f_1$ and $f_2$ depend only on input features (observable characteristics of the studied system), $X$, and $f_3$ depends on $X$ and the predictions of $f_1$ and $f_2$, which are labeled $\alpha_1$ and $\alpha_2$, respectively. $f_3$'s prediction is the end prediction of the model, $Y$.

$$\alpha_1 = f_1(X) \tag{19}$$

$$\alpha_2 = f_2(X) \tag{20}$$

$$Y = f_3(\alpha_1, \alpha_2, X) \tag{21}$$

Because $f_1$ and $f_3$ have acceptable/low error associated with their predictions, they will continue to be described by mechanistic models.

Mechanistic and Data-Driven Inclusion models differ in how they handle $f_2$. The typical procedure for implementing $f_2$ in a mechanistic framework would be to study $f_2$'s mechanism, then identify the parameters that affect it most significantly, and then create some fitted relationship for it using some power-law or polynomials, using idealizations and assumptions wherever necessary to

reduce the fitted relationship's complexity. Instead of this, $f_2$ will simply be replaced with a machine learning model, which is known for its flexibility in finding complex relationships (Rackauckas, 2020). Through this, the mechanism doesn't need to be simplified and its full relationship can be learned

To train this model, however, information on $\alpha_2$ will be needed, but data on $\alpha_2$ will not be available. Otherwise, a normal machine learning model could be used. Ultimately, $\alpha_2$ is only needed to obtain error from predictions, so finding alternative methods for predicting error will be sufficient to train the machine learning model. This error can be obtained in two ways: (1) The value of $\alpha_2$ can be solved in terms of the data on $Y$ and the $f_3$ mechanism and the error can be computed directly (equations 24 and 25). (2) If the machine learning architecture is amenable to gradient-based training, the prediction error from $\alpha_2$ can be computed simply using the automatic differentiation algorithm. For example, if the loss from $Y$ is (22)

$$L(Y_{pred}) = \frac{1}{2} * (Y_{true} - Y_{pred})^2 \quad (22)$$

The change in error occurring from $\alpha_2$'s model parameters is (23).

$$\frac{\partial L}{\partial \Phi} = \frac{\partial L}{\partial Y_{pred}} * \frac{\partial Y_{pred}}{\partial f_3} * \frac{\partial f_3}{\partial \alpha_2} * \frac{\partial \alpha_2}{\partial \Phi} \quad (23)$$

Where $\Phi$ are the trainable parameters of the machine learning model for $\alpha_2$.

Examining equations (23) and (25), the final trained model will depend largely on the accuracy of the $f_3$ mechanics in either option. The loss function for option 1 is shown in (24).

The solutions for the machine learning model's output ($\alpha_{2,mech}$, shown in (25)) using option 1 may not be explicit, especially if multiple mechanisms are being represented by machine learning. In this case, iterative or other numerical solutions may be used to pre-generate many solutions in a

somewhat "synthetic" dataset. This shows this method's relationship to Mechanistic Data Methods. However, the key functionality difference between these is that Data-Driven Inclusion methods are only representing a few mechanisms and Mechanistic Data Methods usually gather data from finite element simulations, which represent many more mechanisms. Additionally, option 1 can appear to resemble PINN's and Mechanistic Learning method, where the physics is incorporated entirely in the loss function, but, as discussed earlier, Mechanistic learning differs in that its mechanics are incorporated separately from the discrepancy term.

$$L(\alpha_{2,pred}) = \frac{1}{2} * (\alpha_{2,mech} - \alpha_{2,pred})^2 \quad (24)$$

$$\alpha_{2,mech} = f_3^{-1}(Y_{true}, \alpha_1, X) \quad (25)$$

Option 2 will pass the same information to the machine learning model as option 1, only without having to solve for $\alpha_2$.

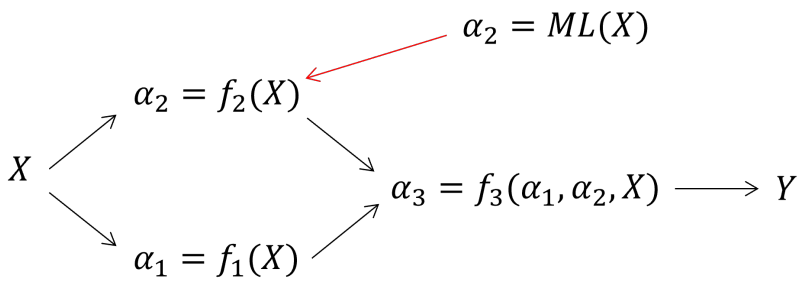


*Figure 5.5: Data-Driven Inclusion Model Layout*

If option 2 is used in training, additional constraints must be added to $f_1$ and $f_3$.

1. The predicted values from $f_1$ and $f_3$ must always exist for any expected value of $\alpha_2$. For example, if some term in the $f_3$ were to be divided by $\alpha_2$, $\alpha_2$ should never be 0.

2. $f_3$ must always be a function of $\alpha_2$. If this is not true, the gradient information will never reach the machine learning model and training cannot occur.
3. $f_1$ and $f_3$ must be amenable to the automatic differentiation algorithm. This is largely important in the software implementation and is handled well by most machine learning packages (TensorFlow, PyTorch, or Sci-Kit Learn).

By fully defining the Data-Driven Inclusion method, we are now able to search for a mechanistic model to hybridize. The mechanistic model can include any type of mathematical form and does not have to be restricted to differential equations. Also, the mechanistic model must have some mechanics that are not well represented and some that are. The mechanics that are not well represented will then be replaced with machine learning.

# CHAPTER VI: RECREATING MECHANISTIC SHEAR MODELS

To use the Data-Driven Inclusion method to predict shear failure, a base mechanistic model will be needed. Based on our definition of the Data-Driven Inclusion method, the mechanistic model must represent multiple mechanisms, some of which are defined more accurately than others, and does not need to have any specifical mathematical form, like a differential equation. Ideally for our purpose, all mechanisms should be well represented except load-induced cracking. This way, we can use machine learning to predict that complex mechanism. The model that represented shear capacity mechanics most accurately was the Shear Crack Propagation Theory, so it will be investigated as a candidate for hybridization. However, this model does not attempt to predict load-induced cracking directly but instead predicts *crack propagation*.

The main goals in recreating this mechanistic model are: (1) to verify its mathematical representation of mechanisms can be accurately reproduced and (2) to provide a basis for comparison for the hybrid model.

## Shear Crack Propagation Theory

As mentioned before, this model attempts to express not only the failure state of the beam but also the entire failure process starting from the initial flexural cracks. This model was chosen because it represents crack propagation, strain-crack opening, and tension stiffening mechanisms in addition to the common mechanisms used in other mechanistic models. However, the Shear Crack Propagation Theory does not consider multiple cracks, limiting its ability to robustly predict shear failure.

The evaluation process of this model can be described as follows. First, a loading is chosen just past the initial flexural cracking such that the crack would propagate further. From this, four parameters must be assumed: the propagated crack height and angle, vertical stress from cantilever action, and section rotation. Given the propagated crack geometry and constitutive models, these assumed parameters are updated to satisfy the equilibrium of a rigid cracked section. Once equilibrium is found, this sequence of crack propagation is complete and another can begin based on an additional increase in load. Once the cracked concrete section is no longer able to support the increased loading, failure is assumed, and the capacity of the beam can be recorded. The appropriate choice for critical crack location is implied in this. If no location is known or assumed, all locations on the beam can be attempted, and the location with the lowest capacity governs.

The process of re-creating the Shear Crack Propagation Theory began by reproducing its mechanistic models. They consist of models to:

1. Describe the spacing of primary cracks;
2. Relate delamination cracks to primary cracks;
3. Relate strains in the uncracked region of the beam to crack openings;
4. Describe principal stresses at the fictitious macro-crack tip;
5. Describe the failure state of the crack tip as a result ;
6. Represent residual tensile strength in the fictitious macro-crack;
7. Represent aggregate interlock friction in the cracked region;
8. Represent shear resistance from doweling action;

9. Describe the stress-strain relationship in the tensile reinforcement, including the effects of tension stiffening and delamination; and,
10. Describe the stresses imposed on the uncracked concrete from cantilever action.

Many of these are empirical but some are based purely on mechanics, such as the identification of principle stresses and their planes.

Then, a framework for propagating the crack was needed, as the Shear Crack Propagation Theory generally describes a multi-segmented framework but then only explains sufficiently the implementation of a much simpler bilinear framework. A more detailed implementation is now given. First, the initial flexural crack is created (26)-(27).

$$y_0 = 0 \tag{26}$$

$$\beta_0 = 90° \tag{27}$$

Where $y_0$ represents the tip height of the flexural crack and $\beta_0$ represents the crack's angle.

The origin for describing crack tip locations is located at the flexural reinforcement, which is common for many models like the Shear Crack Propagation Theory. Then, the unknown parameters must be estimated (29)-(32) and an increase in load must be imposed. However, the increase in loading can be represented in many, similar ways, such as by decreasing the depth of the compression zone or increasing cracked section rotation. The former is chosen in the Shear Crack Propagation Theory's implementation. The location of the neutral axis, $x_0$, can be assumed just above the midpoint of the depth for initial propagation (28).

$$x_0 = d * 0.55 \quad (28)$$

$$\delta y = 10\ mm \quad (29)$$

$$\beta_{est} = 80° \quad (30)$$

$$\sigma_{z0} = 0\ MPa \quad (31)$$

$$\phi = 0.0002\ rad \quad (3216)$$

These are appropriate starting estimates for initial propagation. Next, geometric relationships are used to compute the sliding and opening of crack segments, and a delamination crack is assumed based on the shape of the primary crack (model 2). Proposed geometric relationships were overly complex and limited to bilinear cracks, so new relationships were developed based on two triangles, $abc$ and $def$, that can always be found for any crack segment, as shown in Figure 6.1.

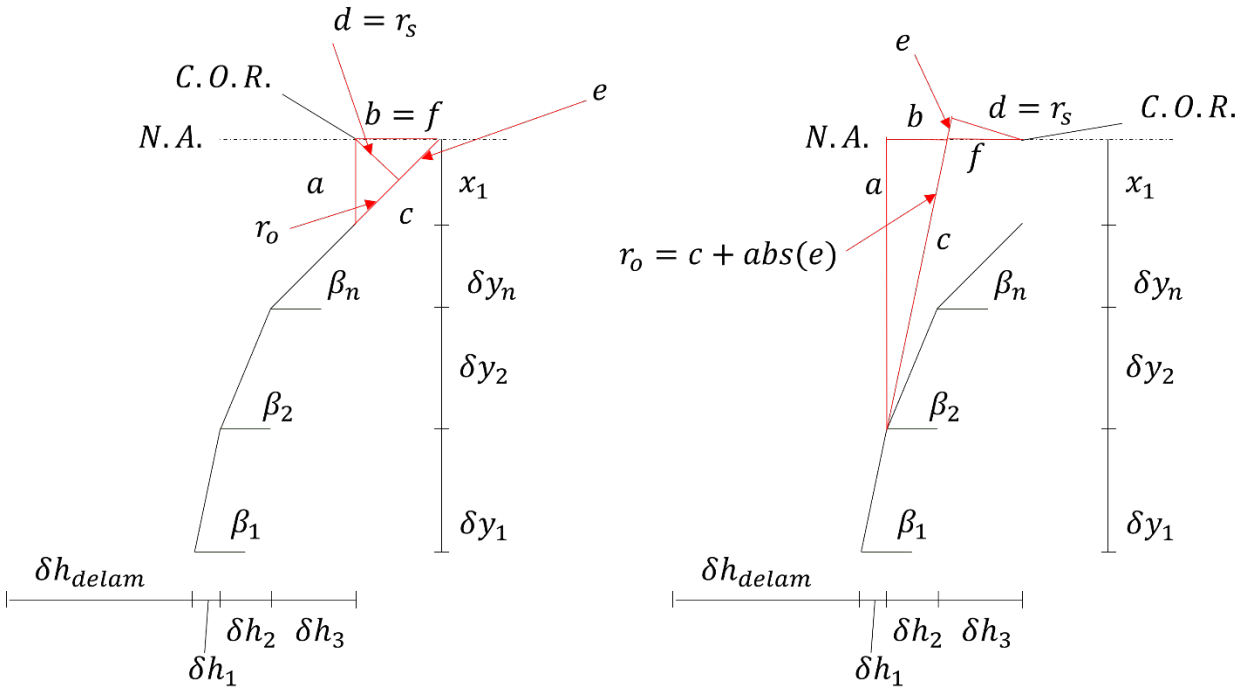


*Figure 6.1: New Crack Geometry Model*

If each crack segment is labeled $\mathbf{1}$ to $\boldsymbol{n}$ starting with 1 at the first propagated crack, then the relationships for the shapes of these triangles are (33)-(40)

$$a_i = \sum_{k=i}^{n} \delta y_k + x_1 \tag{33}$$

$$b_i = \frac{a_i}{\tan(\beta_i)} = f_i \tag{34}$$

$$c_i = \frac{b_i}{\cos(\beta_i)} \tag{35}$$

$$h_i = \frac{\delta y_i}{\tan(\beta_i)} \quad (36)$$

$$h_i = \sum_{k=i}^{n} h_k \quad (37)$$

$$f_i = b_i - h_i \quad (38)$$

$$d_i = \sin(\beta_i) * f_i \quad (39)$$

$$e_i = \cos(\beta_i) * f_i \quad (40)$$

The first triangle is simply the projection of the crack to the neutral axis, and the second is for finding the opening and sliding radii to multiply by the crack rotation, as represented in (41) and (42). When $f_i$ is negative, the crack's projection intersects the neutral axis before the center of rotation. This geometric relationship holds even if later crack angles become steeper or if cracks propagate into the compression zone. It also accurately describes the reverse shear friction effect that would occur from that sliding.

$$r_{o,i} = abs(c_i - e_i) \quad (41)$$

$$r_{s,i} = abs(d_i) \quad (42)$$

Where $r_{o,i}$ is the opening radius and $r_{s,i}$ is the sliding radius for crack $i$.

These radii explain sliding and opening at the tip of crack $i$ (assuming crack faces rotate about the neutral axis (model 3), but the crack opening can be found on any portion of the segment as well by simply adding the distance along the crack from the tip to the location of interest as in (43).

$$r_o = r_{o,i} + l \tag{43}$$

The sliding radius is the same for any location on a crack segment. From the above relationships, the sliding and opening values can be obtained at any point on the crack with equations (44)-(46).

$$l_i = \frac{\delta y_i}{\sin(\beta_i)} \tag{44}$$

$$w_{i,\xi} = \left(r_{o,i} + \xi * l_i\right) * \phi \tag{45}$$

$$\delta = r_{s,i} * \phi \tag{46}$$

Where $\xi$ is between 0 and 1, representing the tip and base of the crack, respectively.

In the Shear Crack Propagation Theory, however, the uppermost crack is assumed to have no sliding or opening at the tip (model 3), but its bottom fully respects the kinematics imposed from the above rotation, as represented in (47)-(49).

$$w_{n,0} = 0 \tag{47}$$

$$\delta_n = 0 \tag{48}$$

$$w_{n,1} = \left(r_{o,n} + l_{c,n}\right) * \phi \tag{49}$$

The delamination crack length is then assumed to be the length of the primary crack's horizontal projection. This can be represented through (50)

$$h_d = \sum_{k=1}^{n} h_k \tag{50}$$

Using the above kinematic values for each crack segment, the constitutive relationships may then be computed with a few modifications to fit the more complex framework.

First, the forces in the uncracked region will be described (model 10), as they are the most complex. The computation of these forces begins by relating section rotation to strains in the uncracked region with equations (51)-(53).

$$\epsilon_{cr} = \frac{\phi}{s_{cr}} * x_1 \tag{51}$$

$$\epsilon_{top} = \frac{\phi}{s_{cr}} * -x_0 \tag{52}$$

$$\epsilon_s = \frac{\phi}{s_{cr}} * (d - x_0) \tag{53}$$

(51)-(53) are acceptable only when realizing the assumptions made in them. First, the control section is assumed to be a rigid body, so no deflection from cantilever action would skew the relationship between opening and strain. Additionally, it is assumed the strain of the control section is representative of the strains $s_{cr}$ distance (model 1) around the crack tip. Multiplication of this strain by the distance allows for relation to crack openings and is valid when strain increases linearly along the beam's length. While linear strain distribution is typical for prismatic elastic beams, the distribution for cracked concrete beams has not been reported extensively. A linear strain distribution is also assumed across the depth of the uncracked region. Finally, the above equations assume that all strains in the surrounding area contribute to the primary crack, which is an acceptable assumption for a critical crack implementation but is not realistic.

After determining strains in the uncracked section, a crack propagation criterion can be implemented (model 5). This is done by realizing a biaxial failure criterion and analyzing principal stresses at the crack tip. The factors that affect this stress state are crack tip location (in compression zone or not) and cantilever action contribution. The principle of stress orientation is assumed to be in line with the crack angle since cracking is caused by a tensile failure in the concrete (model 4). The principal stresses can be computed from horizontal, vertical, and shear stresses with equations (54) and (55)

$$\sigma_1 = \tau_0 * \tan(\beta_n) + \sigma_{z0} \quad (54)$$

$$\sigma_2 = -\frac{\tau_0}{\tan(\beta_n)} + \sigma_{z0} \quad (55)$$

Assuming that the crack tip is near a state of failure, the Kupfer failure criterion (Kupfer and Gerstel, 1973) can be employed and stresses $\tau_0$ and $\sigma_{x0}$ can be solved explicitly. These stresses are then related to strains through an elastic modulus. This assumes the relation between stress and strain is linear. The stresses can then be integrated along the uncracked section and produce forces to be used in equilibration. The final equations (56)-(58) depend on stresses at the crack tip, distance from the crack tip to the neutral axis, and the neutral axis depth.

$$V_{conc} = \frac{2}{3} * b * \tau_0 \left( (x_0 + x_1) + \frac{1}{2} \left( \frac{x_1^2 + x_0 * x_1}{x_0 - x_1} \right) \right) \quad (56)$$

$$F_{ct} = \frac{1}{2} * b * \sigma_{x0} * x_1 \quad (57)$$

$$F_{cc} = \frac{1}{2} * b * \epsilon_{top} * E_c * x_0 \quad (58)$$

It is interesting to note that $F_{cc}$ and $F_{ct}$ are not directly coupled, so instances in which they do not share a strain distribution could arise.

The remaining shear-resisting mechanisms are those from residual tensile strength (model 6), aggregate interlock (model 7), and doweling action (model 8), and all these are represented by empirically derived models. More complex mechanistic models are available(Walraven, 1981; Hordijk, 1992), but their computations were too complex to implement. Fracture process zone strength is represented through an exponential decay in (59)-(61).

$$\sigma_{fpz}(w) = f_{ct} * \exp\left(-\frac{w}{w_1}\right) \quad (59)$$

$$w_1 = \frac{G_f}{f_{ct}} \quad (60)$$

$$G_f = 0.028 * f_c'^{0.18} * d_{ag}^{0.32} \quad (61)$$

Where $d_{ag}$ is the maximum aggregate size and $w$ is the width of the crack.

The stress from these relationships can be integrated along all cracks and its vertical and horizontal components can be computed. The process for computing the aggregate interlock stress is similar. However, the Shear Crack Propagation Theory provides an explicit equation for the integration of fracture process zone stresses but does not for aggregate interlock. This is because fracture process zone stresses typically only occur in the uppermost crack segment, and aggregate

interlock stresses occur through many crack segments. To account for the aggregate interlock's widespread distribution across crack segments, a numerical integration scheme was implemented to find the vertical and horizontal forces due to the aggregate interlock stresses, which were based on the following constitutive relationships (62) and (63).

$$\tau_{ai} = -\frac{f_c}{30} + (1.8 * w^{-0.8} + (0.234 * w^{-0.707} - 0.2) * f_c) * \delta \quad (62)$$

$$\sigma_{ai} = -\frac{f_c}{20} + (1.35 * w^{-0.63} + (0.191 * w^{-0.552} - 0.15) * f_c) * \delta \quad (63)$$

Finally, the vertical force provided by doweling action can be computed with (64)-(66).

$$V_{da,0} = 1.64 * b_n * d_s * {f_c}^{0.33} \quad (64)$$

$$b_n = b - d_s * n_s \quad (65)$$

$$V_{dowel} = \begin{cases} v_a \leq 0.05mm: V_{da,0} * \frac{v_a}{0.05} * \left(2 - \frac{v_a}{0.05}\right) \\ v_a > 0.05mm: V_{da,0} * \frac{2.55 - v_a}{2.5} \end{cases} \quad (66)$$

Where $v_a$ is the vertical displacement of the crack at the origin.

While not a shear-resisting mechanism, the force in the tensile reinforcement will need to be determined to find equilibrium. This force can be determined by considering tension stiffening and delamination effects (model 9). First, the average strain, $\epsilon_s$, computed from section rotations, must be related to strain in delaminated portions of the beam and strains that still are affected by tension stiffening, as represented in (67)

$$\epsilon_s = \frac{\epsilon_{ts} * (s_{cr} - h_d) + \epsilon_d * h_d}{s_{cr}} \quad (67)$$

Then, the constitutive relationships (68)-(72) for each can be used to solve for the stress in reinforcement.

$$\sigma_s = \epsilon_{ts} * E_s + \frac{f_{ct}}{1 + \sqrt{3.6 * M * \epsilon_{ts}}} \quad (17)$$

$$M = \frac{A_c}{\Sigma d_s * \pi} \quad (69)$$

$$A_c = h_{c,eff} * b_w \quad (70)$$

$$h_{c,eff} = \min\left(2.5 * d_s, \frac{d - x_0}{3}\right) \quad (71)$$

$$\sigma_s = \epsilon_d * E_s \quad (72)$$

No explanation is given for the values in computing $M$, but from Bentz (2005), $d_s$ is the diameter of the reinforcement and $b_w$ is the width of the beam. Additionally, the relationship for $h_{c,eff}$ is the portion of the beam in tension.

Considering all the forces present on the beam and in the control section, equilibrium can be taken about two rigid bodies. The first rigid body includes the control section and applied loading. The equilibrium of this body provides 3 constraint equations. The second rigid body includes two identical control sections separated $s_{cr}$ distance from each other. The moment equilibrium of this body allows for the computation of $\sigma_{z0}$ and provides the final equation to match the four unknowns and assumed variables.

The process of solving for these variables should be converging, but attempts to implement the Shear Crack Propagation Theory update process lead to diverging updates. The proposed process

begins with assumed values and computes all internal forces except for the steel tensile force, which is then computed based on the equilibrium of horizontal forces and moments. From this steel force, an updated section rotation can be computed from the average tensile strain in the reinforcement. Then, the vertical stress at the crack tip can be computed by the moment equilibrium of the concrete tooth using only the previously computed internal forces and a delta steel force (73) and (74), which is computed using the steel force derived from equilibrium.

$$\Delta F_s = F_s * \frac{n+1}{n} \tag{73}$$

$$n = \frac{a_{crit}}{s_{cr}} \tag{74}$$

Where $a_{crit}$ is the location of the crack along the beam.

The propagated crack angle can then be computed through the vertical and moment equilibrium of the first rigid body, and finally, the propagated crack height is computed using section rotation and vertical tip stress. In a typical solution-finding procedure, the computed values of unknown parameters should be closer to the solution than those originally assumed, but this updating process quickly becomes unstable. A related effect can be illustrated in Figure 6.2, which shows how varying propagated crack angle and section rotation on an initial crack effects vertical force equilibrium. Since vertical tip stress is not significant for beginning cracks and the crack height only depends on the crack angle and section rotation, they do not need to be varied. As the estimated parameters come closer to equilibrium (the minimum on the plot), the gradient of the error with respect to $\phi$ and $\beta$ explodes. When using gradient-based updating methods, a solution was unobtainable even when

updating step sizes. The inability to find a solution could be from the modifications made to the presented implementation.

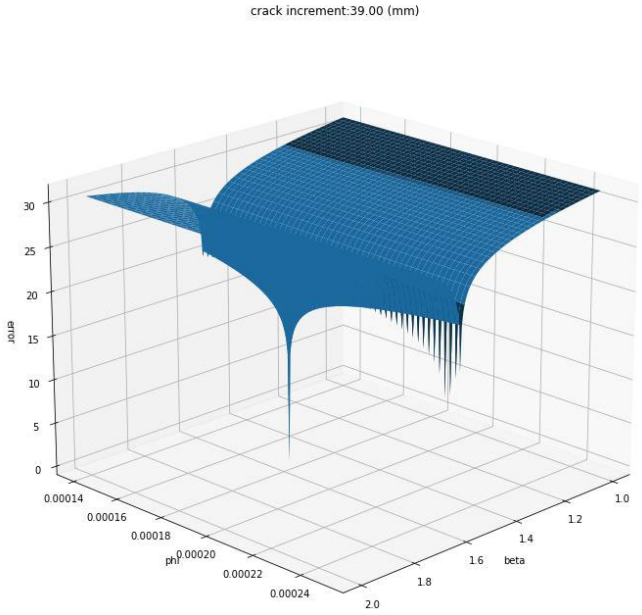


*Figure 6.2: Sensitivity plot of vertical equilibrium*

While this model claims to be able to accurately reproduce crack shapes given the crack location, the crack shapes were not able to be confirmed here. As such, the model proposed by Cavagnis et al. (2018) will be investigated.

## Cavagnis et al. (2018) Critical Shear Crack Theory

This model provides a simpler framework for predicting shear capacity in concrete beams without transverse reinforcement at the cost of misrepresenting some mechanisms. This model considers all shear-resisting mechanisms to contribute to capacity but heavily modifies their empirical

relationships. A simple, explicit relationship is given for load-induced cracking even though there are no easily identifiable mechanisms for it. Furthermore, this model only considers a single crack to contribute to failure. So while the Critical Shear Crack Theory will be easier to implement, its mechanistic models will be much less accurate.

More information on the mathematical form of this model can be found in later sections, and only information on replication will be presented here. Accurate replication was difficult to confirm. Computation results for individual beams were not presented with the description of the Critical Shear Crack Theory; only aggregated results were presented numerically. Thus, it is not possible to validate its implementation directly. However, results were presented graphically for individual beams (Cavagnis et al, 2020), so this was chosen as a basis for validation. Figure 6.3 shows the shear resistance distribution of six simply supported beams with a point load at midspan. The dark blue portion represents resistance from aggregate interlock, the light blue from residual tensile strength, the orange from doweling action, and the red from inclined compression chord (uncracked concrete shear resistance). These distributions are identical to those provided by Cavagnis et al.(2020), showing that the model was accurately reproduced and that a hybrid version of it can be accurately compared.

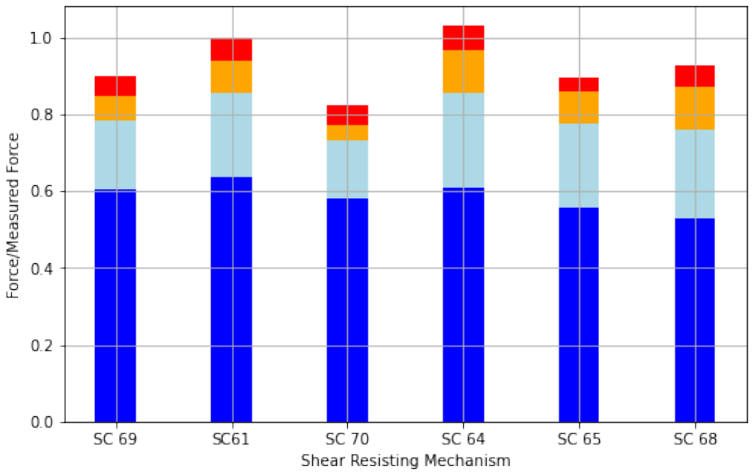


*Figure 6.3: Validation of the Critical Shear Crack Theory Model*

# CHAPTER VII: IMPLEMENTATION OF THE DATA-DRIVEN INCLUSION METHOD

For our implementation of the Data-Driven Inclusion method, we used the Critical Shear Crack Theory as our mechanistic model and found the crack position, crack geometry, crack kinematics, and aggregate interlock models need to be replaced with machine learning models. While replacing these portions of the mechanistic model decreases mechanistic bias, there still is one significant source of mechanistic bias inherent to this formulation, being that shear failure occurs due to one critical, bilinear crack. To describe more complex cracking patterns, the hybrid model must be further modified. The crack shape and aggregate interlock model are replaced because they do not represent the test values found in (Cavagnis et al., 2015), and the crack kinematics and location are replaced because they are dependent on assumptions of the previous model and may not accurately represent the shear failure mechanisms.

Other models in the Critical Shear Crack Theory still do not represent underlying mechanisms well, such as the force from the inclined compression zone. However, this component has been shown to contribute little to the shear capacity of slender members, and to avoid increasing the complexity represented by the machine learning portions, the mechanistic model provided in the Critical Shear Crack Theory will remain in the hybrid model.

The implemented hybrid model can be described as follows: The model begins by predicting the crack location ($\alpha_{crit}$), angles ($\beta_{AB}, \beta_{BF}$) and lengths ($l_A, l_F$) of the bilinear crack, and the horizontal opening of the crack at the height of the longitudinal reinforcement ($u_a$) in (75).

$$\alpha_{crit}, \beta_{AB}, \beta_{BF}, L_{AB}, L_{BF}, u_a = ML(X) \quad (75)$$

Where $X$ is determined in Table 7.1 for each model, depending on the configuration. These machine-learning predictions can then be used with simple geometric expressions (equations (76)-(81)) to yield the inputs required for the constitutive models of cracked and uncracked concrete.

$$l_b = l_A * \sin(\beta_{AB}) \quad (76)$$

$$d_F = l_b + \sin(\beta_{BF}) * l_F \quad (77)$$

$$l_1 = l_F * \cos(\beta_{AB} - \beta_{BF}) \quad (78)$$

$$l_2 = l_1 + l_A \quad (79)$$

$$r_F = a - a_{crit} - l_A * \cos(\beta_{AB}) - l_F * \cos(\beta_{BF}) \quad (80)$$

$$h_F = d - d_F \quad (81)$$

These geometric quantities are represented in Figure 7.1. Using the crack opening, $u_a$, the Mode I displacements of the crack can be obtained with equations (82)-(84).

$$\phi = \frac{u_a}{d_F} \quad (82)$$

$$w_{BF} = \phi * l_F \quad (83)$$

$$w_A = \phi * l_2 \quad (84)$$

The sliding quantities needed for predicting aggregate interlock will simply be predicted in the machine learning model as a result of automatic feature engineering. The shear force from aggregate interlock is predicted with equation (85).

$$V_{agg} = ML(X) \tag{85}$$

The contribution from residual tensile strength can be computed with expressions (86)-(90).

$$f_{ct} = f_c^{\frac{2}{3}} * 0.3 \tag{86}$$

$$w_C = 0.073 * \frac{{f_c}^{0.18}}{f_{ct}} * \frac{1.31}{0.31} \tag{87}$$

$$l_3 = \max\left(min\left(l_2, \frac{w_c}{w_A} * l_2\right), l_1\right) \tag{88}$$

$$l_{F1} = \min\left(l_F, \frac{w_c}{w_{BF}} * l_F\right) \tag{89}$$

$$V_{res} = f_{ct} * b * \cos(\beta_{BF}) * l_{F1} * \left(1 - \left(\frac{1}{1.31} * \left(\frac{u_a * l_{F1}}{d_F * w_c}\right)^{0.31}\right)\right) + \cos(\beta_{AB})$$

$$* \left(l_3 * \left(1 - \left(\frac{1}{1.31} * \left(\frac{u_a * l_3}{d_F * w_c}\right)^{0.31}\right)\right) - l_1\right. \tag{90}$$

$$\left. * \left(1 - \left(\frac{1}{1.31} * \left(\frac{u_a * l_1}{d_F * w_c}\right)^{0.31}\right)\right)\right) * \frac{f_{ct}}{\sqrt{f_c}}$$

Where $w_c$ is a property of concrete fracture mechanics, and $l_3$ and $l_{F1}$ are the lengths where residual tensile strength is active on the vertical and horizontal crack segments, respectively.

The presented formulation above varies from (Cavagnis et al., 2018) because its second term was originally included in the aggregate interlock constitutive model. However, because the second term describes the residual tensile strength, it will be included in this quantity. The doweling action can be computed through equations (91) and (92).

$$k_b = \min\left(0.063 * \left(\frac{l_b}{u_a}\right)^{\frac{1}{4}}\right) \quad (91)$$

$$V_{dowel} = 5 * k_b * f_{ct} * \rho * b * d \quad (92)$$

Finally, the shear resistance contribution from the uncracked concrete can be computed (93) and used with the other shear resisting forces to predict the shear capacity (94).

$$V_{conc} = \frac{V_{agg} + V_{res} + V_{dowel}}{1 - 0.5 * \frac{h_F}{r_F}} - (V_{agg} + V_{res} + V_{dowel}) \quad (93)$$

$$V = V_{conc} + V_{agg} + V_{res} + V_{dowel} \quad (94)$$

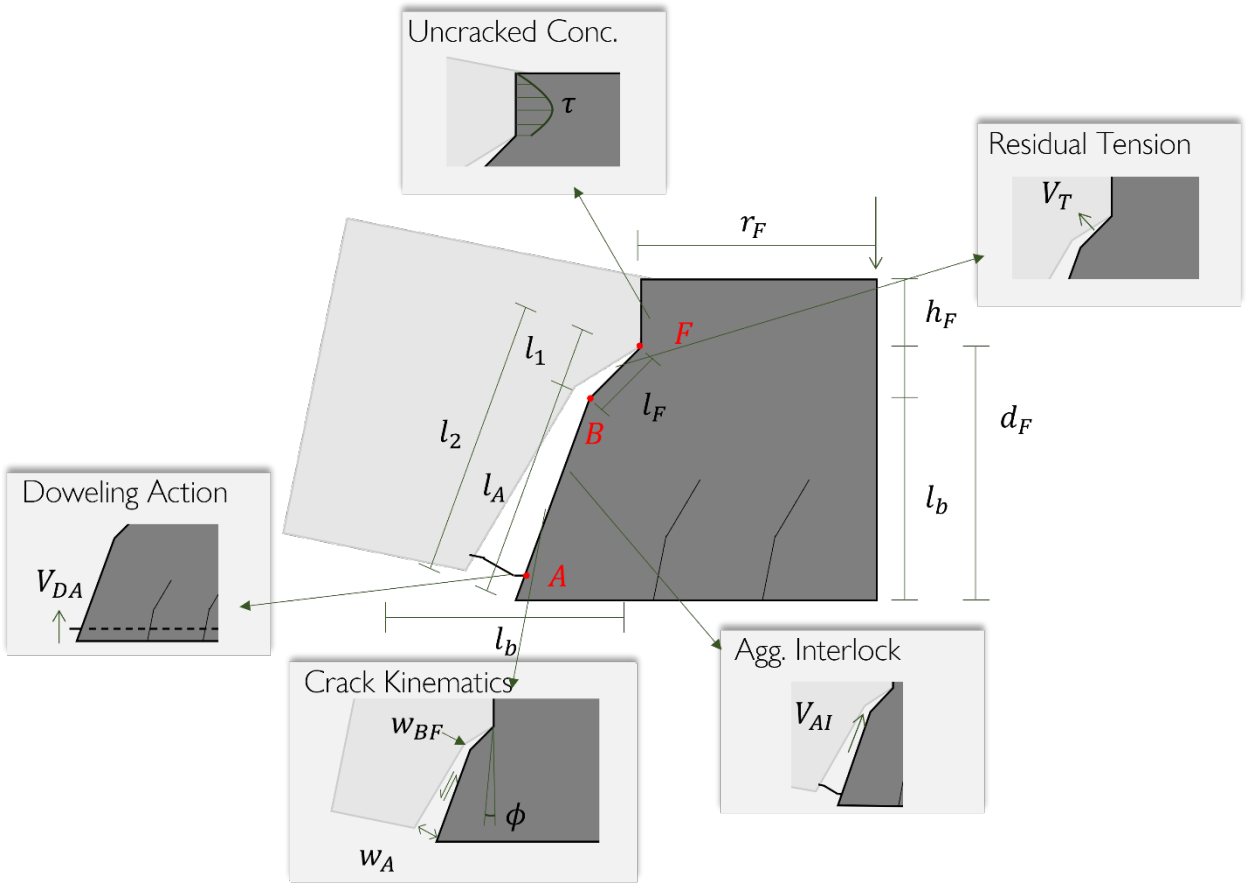


*Figure 7.1: Shear Mechanics of Concrete Beam*

*Table 7.1: Input Parameters used to Predict Shear Mechanics Quantities*

| Output Parameter | $a_{crit}$ | $\beta$ | $l$ | $u_a$ | $V_{agg}$ |
|---|---|---|---|---|---|
| Input Parameter | | | | | |
| Shear span $(a)$ | X | X | X | X | |
| Beam Height $(h)$ | X | X | X | X | |
| Reinforcement Ratio $(\rho)$ | X | X | X | X | |
| Reinforcement Yield Strength $(\sigma_Y)$ | X | X | X | X | |
| Beam Width $(b)$ | X | X | X | X | X |
| Beam Depth $(d)$ | X | X | X | X | X |
| Maximum Aggregate Size $(d_{agg})$ | X | X | X | X | X |
| Concrete Compressive Strength $(f_c)$ | X | X | X | X | X |
| $a_{crit}$ | | X | X | X | X |
| $\beta$ | | | | X | X |
| $l$ | | | | X | X |
| $u_a$ | | | | | X |

A neural network architecture was chosen for the machine learning models in this hybrid framework so that gradient-based training could be used. However, the optimal layout of this neural architecture is not clear because multiple parameters are predicted (critical crack location, crack opening), and one parameter may depend on the value of previous ones (e.g. aggregate interlock depends on crack opening).

Several implementations can be chosen. They will all be considered to determine their potential effects on learning. The first to consider would be having every parameter be predicted by one neural network, not accounting for this dependency. This layout can be called "connected". Next, a layout having crack quantities (kinematics, angles, and lengths) and aggregate interlock quantities predicted by different networks, one feeding into the other, can be considered. This layout can be

called “unconnected”. Finally, as an extreme case, we can consider a model where each mechanism has its own neural network, each receiving separate inputs and feeding information sequentially from one network to the next. This layout can be called “spread”.

From Haghighat et al. (2020), the spread model would be expected to perform the best. Additionally, because neural architectures have a difficult time learning an identity mapping between layers (He et al., 2016), it will be difficult for the input parameters used in the beginning layers of the model to be unaltered in later layers. From understanding this difficulty, instead of considering the architectures as having varying numbers of networks (spread vs. connected), they can be considered as having varying degrees of residual connectivity. This means neural networks that use more individual networks will have more residual connections than ones using a single network. It is important to note that the residual connections described previously are significantly different than those used in image recognition. They are used in image recognition to create deeper networks because of the same difficulty in learning identity layers.

The connected, unconnected, and spread networks are shown schematically in Figure 7.2. Based on underlying mechanics, the best inputs to use for each model can be determined in Table 7.1.

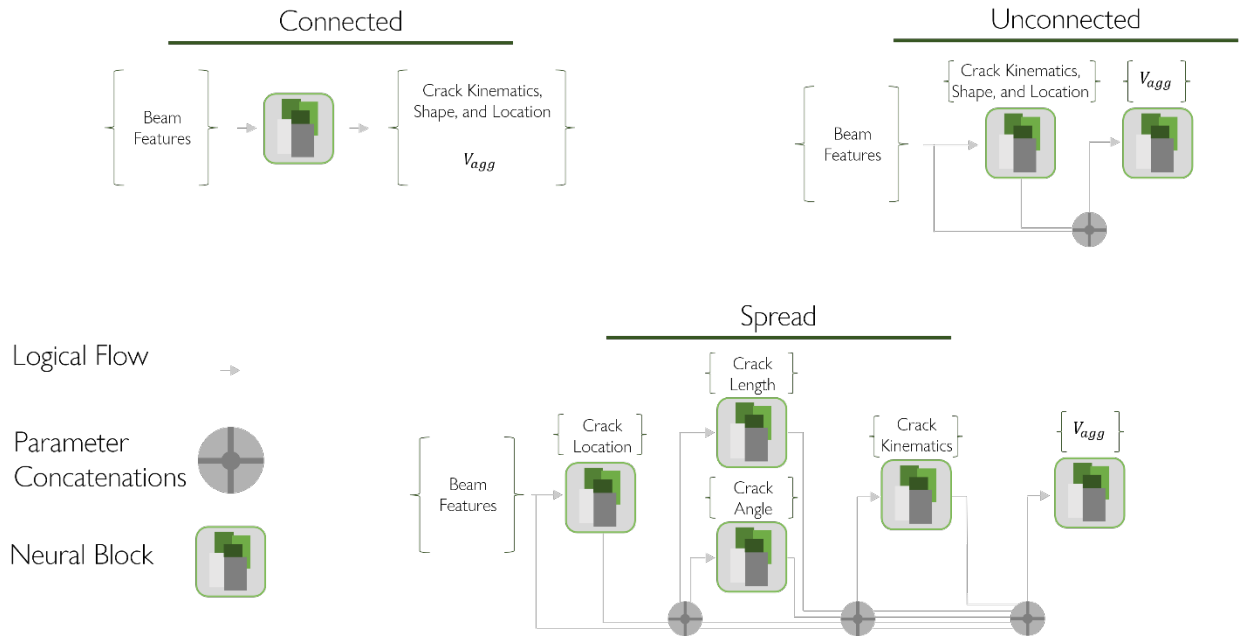


*Figure 7.2: Model Layouts*

There are some quantities predicted from the networks in which a-priori knowledge of their expected values is available; the knowledge mostly comes from geometric constraints of crack prediction. For example, the angle of the crack's inclination is expected to be between 0 and 90 degrees. While predictions between 360 and 450 degrees would result in the same trigonometric relationships, constraining these predictions between the two expected bounds simplifies learning. We term this kind of bounding "two-sided bounding" Additionally, aggregate interlock shear resistance and crack lengths should only be positive. These can be bound similarly, termed "one-sided bounding". However, when bounding these outputs, satisfying the second condition posed earlier is crucial (the new output is still a function of the trainable parameters of the network); if the condition is not satisfied, the network will not receive gradient information. The best method to achieve this and satisfy the second condition is to use activation functions. Two-sided and one-sided bounding uses the sigmoid and ReLU or ELU functions, respectively, as shown in Figure 7.3. It is important to note that

the ELU function can be very useful in predicting small values if its response is shifted 1 unit upward, essentially allowing the function to translate a wide range of negative input values to decimal outputs.

This mechanistic bounding may cause this type of hybridization to appear like Data-Driven Tuning because a machine learning prediction is amplifying a pre-determined value, but this hybridization is actually more similar to, and perhaps a modification of, Data-Driven Inclusion. This similarity is because most of the mechanics are still being represented by the machine learning model, so the pre-determined value is doing the tuning.

Explicit bounds are not known for some quantities, but Mechanistic learning can further bound aggregations of predictions. In this model, Mechanistic Learning is used to limit the neural network from predicting a crack shape that is out of the beam's bounds, as shown in (95) and (96):

$$L_1 = relu(-r_F)^2 \tag{95}$$

$$L_2 = relu(d_F - d)^2 \tag{96}$$

All geometric constraints could be represented this way, but it is best to represent as many prediction bounds as possible through the one-sided and two-sided bounding because Mechanistic Learning only enforces soft constraints and the mechanistic boundings impose hard constraints, which is important if their predictions are to be used in later mechanistic relationships. If a neural network were to predict a value outside of its expected range, that value could break the first condition posed earlier (mechanistic models must exist for all machine learning predictions) and cause numerical instabilities in the mechanistic relationships. The expressions used to bound predictions in this hybrid implementation are shown in Table 7.2.

*Table 7.2: Bounding Expressions uses, where CB is a crack-bound value determined by the user*

| Predicted Quantity | Bounding Type | Expression |
|---|---|---|
| $a_{crit}$ | Two-Sided | $a_{crit} = \sigma\big(NN(X)\big) * a + 1$ |
| $\beta$ | Two-Sided | $\beta = \sigma\big(NN(X)\big) * \left(\frac{\pi}{2} - \frac{\pi}{18}\right) + \frac{\pi}{36}$ |
| $l$ | Two-Sided | $l = \big(\sigma\big(NN(X)\big) * \big(CB_{upper} - CB_{lower}\big) + CB_{lower}\big) * d$ |
| $u_a$ | One-Sided, Soft | $u_a = elu\big(NN(X)\big) + 1.01$ |
| $V_{agg}$ | One-Sided, Soft | $V_{agg} = elu\big(NN(X)\big) + 1$ |

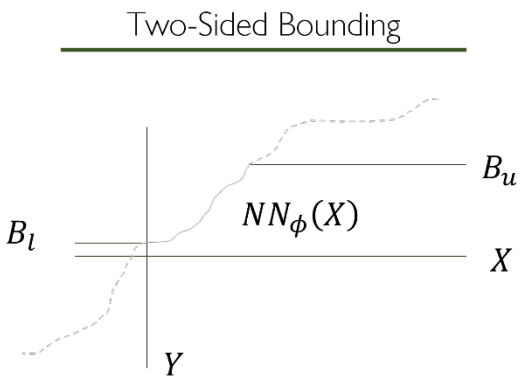


11a: Two-Sided Bounding

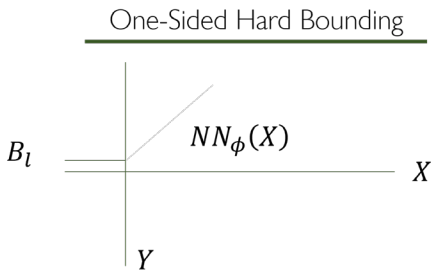


11b: One-Sided Hard Bounding

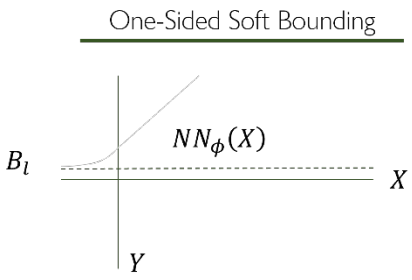


11c: One-Sided Hard Bounding

*Figure 7.3: Mechanistic Bounding Expressions*

Each neural network contains a batch normalization layer at the beginning, followed by the remaining layers to produce the predicted value, which is then bounded if necessary. Once the neural networks are defined, they are used with the remaining mechanistic relationships to produce the final

prediction: the shear capacity of the beam. A schematic of these neural blocks' and mechanistic relationships' configurations in the layout of the entire hybrid model is shown in Figure 7.4. The entire model is trained based on a loss function containing the mean squared error of the beam shear capacity predictions, the L2 regularization norm, and any additional Mechanistic Learning terms. Gradient-based training is implemented with the Nadam optimizer, and a learning rate is determined via hyperparameter optimization.

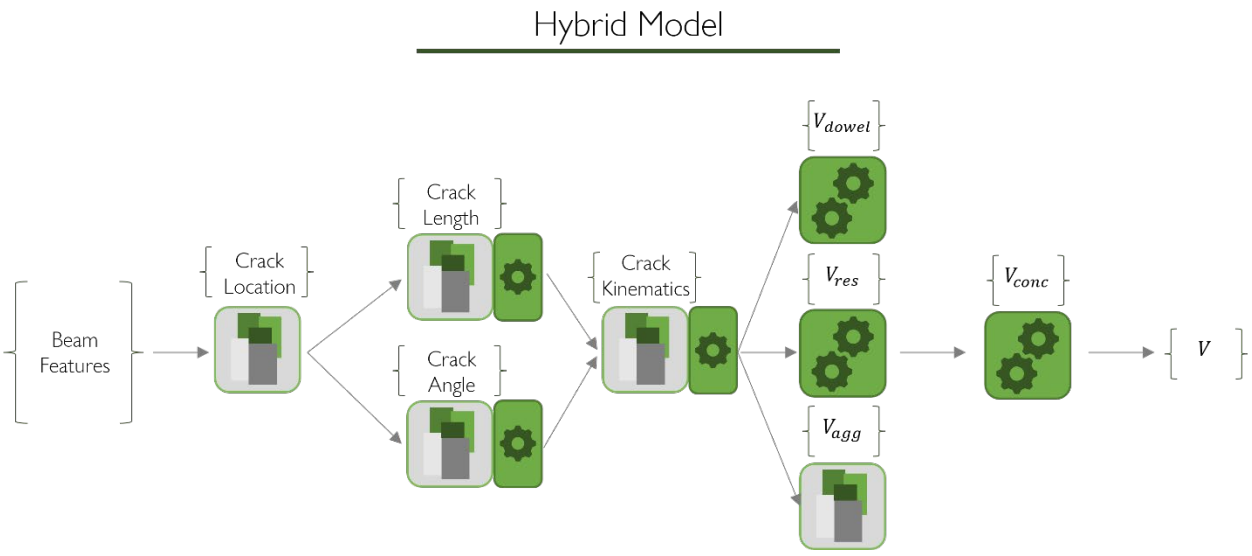


*Figure 7.4: Data-Driven Inclusion Model*

Each of the above-mentioned models has its number of layers, number of nodes, and L2 regularization parameters optimized using a Random Search optimization tuner over 300 trials. The search parameters used are given in Table 7.3. Each trial performs 10 attempts at training and the training run that achieves the lowest coefficient of determination for the validation set is used as the representation for those hyperparameters. Using multiple attempts helps to avoid local minima. Optimal hyperparameters for each layout are shown in Table 7.3.

*Table 7.3: Hyper Parameter Search*

| Connected | | | | |
|---|---|---|---|---|
| Hyper Parameter | Min | Max | Sampling Strategy | Optimal |
| Nodes | 10 | 150 | Random Integer | 100 |
| Layers | 1 | 6 | Random Integer | 5 |
| Regularization Coefficient | 1e-5 | 1e-2 | Random Logarithm | 0.03 |
| Learning Rate | 1e-6 | 1e-2 | Random Logarithm | 0.001 |
| Unconnected | | | | |
| Hyper Parameter | Min | Max | Sampling Strategy | Optimal |
| Nodes_1 | 10 | 150 | Random Integer | 19 |
| Nodes_2 | 10 | 150 | Random Integer | 98 |
| Layers_1 | 1 | 6 | Random Integer | 1 |
| Layers_2 | 1 | 6 | Random Integer | 6 |
| Regularization Coefficient_1 | 1e-5 | 1e-2 | Random Logarithm | 0.0013 |
| Regularization Coefficient_2 | 1e-5 | 1e-2 | Random Logarithm | 4.7e-5 |
| Learning Rate | 1e-6 | 1e-2 | Random Logarithm | 0.0047 |
| Spread Model | | | | |
| Hyper Parameter | Min | Max | Sampling Strategy | Optimal |
| Nodes_1 | 10 | 50 | Random Integer | 33 |
| Nodes_2 | 10 | 50 | Random Integer | 32 |
| Nodes_3 | 10 | 50 | Random Integer | 34 |
| Nodes_4 | 10 | 50 | Random Integer | 30 |
| Nodes_5 | 10 | 50 | Random Integer | 28 |
| Layers_1 | 1 | 3 | Random Integer | 2 |
| Layers_2 | 1 | 3 | Random Integer | 2 |
| Layers_3 | 1 | 3 | Random Integer | 2 |
| Layers_4 | 1 | 3 | Random Integer | 2 |
| Layers_5 | 1 | 3 | Random Integer | 1 |
| Regularization Coefficient_1 | 1e-5 | 1e-2 | Random Logarithm | 0.006 |
| Regularization Coefficient_2 | 1e-5 | 1e-2 | Random Logarithm | 0.0012 |
| Regularization Coefficient_3 | 1e-5 | 1e-2 | Random Logarithm | 0.0007 |
| Regularization Coefficient_4 | 1e-5 | 1e-2 | Random Logarithm | 0.0008 |
| Regularization Coefficient_5 | 1e-5 | 1e-2 | Random Logarithm | 0.004 |
| Learning Rate | 1e-6 | 1e-2 | Random Logarithm | 0.0048 |

The dataset used for training, validation, and testing is composed entirely of specimens with $\frac{a}{d}$ ratios of 2.5 or greater, that failed in shear, and are loaded with point loads at midspan. While the

dataset is composed mainly of beams $\left(\frac{b}{d} < 4\right)$ , it also includes slab-like specimens. This is not significant because the shear failure mechanisms should be similar considering St. Venant's principle (Saint-Venant, 1855). The total data set includes 750 specimens which are always split into 0.55, 0.25, and 0.20 portions for training, validation, and testing data for hyper tuning and 0.72, 0.08, and 0.20 during 10-fold validation when the model is being trained for evaluation.

# CHAPTER VIII: ANALYSIS OF CRACK PREDICTIONS

The primary objective of this thesis is to accurately predict load-induced cracking in concrete beams without shear reinforcement. Even though the hybrid model was developed for this objective, it was not able to accomplish it.

Overall, the connected hybrid model makes very accurate predictions for shear failure on slender beams, as shown in **Figure 8.1.**

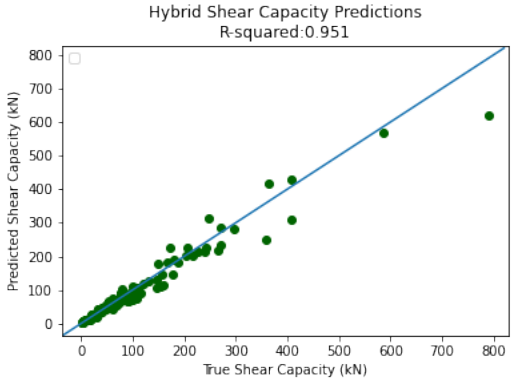


*Figure 8.1: Connected hybrid model prediction accuracy*

No mechanistic consistency (a term we will use to describe how well machine learning predictions match underlying mechanics) can be found in the machine learning predictions, however. Upon examining the predicted crack shapes in **Figure 8.2**, no resemblance can be found between the predicted shapes and the true shape. Additionally, the crack openings at the level of tensile reinforcement ($u_a$), shown in **Figure 8.2**, are much smaller than indicated in the test results (Cavagnis et al., 2017). Test results show openings near 1mm while the hybrid model predictions are nearer to 0.05mm.

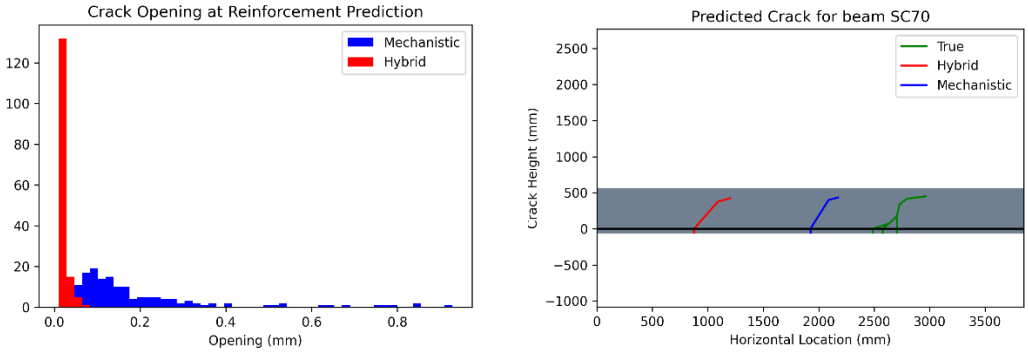


*Figure 8.2: Demonstration of erroneous machine learning predictions*

The remainder of this section will investigate the cause of this mechanistic inconsistency and propose solutions to fix them.

First, The Critical Shear Crack Theory misrepresents many mechanisms in its implementation. Consequently, the machine-learning-based portion of the hybrid model must also misrepresent its mechanisms. This effect is best illustrated by considering the mechanisms used from the Critical Shear Crack Theory and data used in training. Because the machine learning model gets its information from data through the mechanistic models, the mechanistic bias in them will cause the machine learning model to misrepresent its mechanisms in accounting for the mechanistic bias. The machine learning model's goal to minimize the error in the shear capacity predictions will make it learn any mechanism, even incorrect ones. From this, the mechanistic bias will be attributed to the machine learning predictions, as originally theorized in the Hybrid Learning Theory. An example of this can be seen in the crack shape, crack opening, and aggregate interlock predictions. Crack openings are experimentally observed to be near 1mm at failure (Cavagnis et al., 2017), but the mechanistic model utilizes openings between 0.1 and 0.5 mm with 1mm as an extreme case, highlighting the discrepancies in supporting

mechanisms. As a result, the hybrid's machine learning predictions will prefer crack openings closer to 0 mm, misrepresenting the true mechanism. Predictions of crack openings are shown in Figure 8.2.

Second, there is a lack of constraint between crack shape and opening predictions. For the crack opening at the base to be realistically near 0mm, the crack must be sufficiently small. Left unconstrained from this mechanism, the machine-learning model will find any suitable representation that predicts shear capacity accurately. As a result of this, machine learning models often predict low aggregate interlock strength predictions, large crack shapes, and small crack openings.

While these predictions do not make sense in terms of mechanics, as aggregate interlock strength is often dominating in slender beams, they do make sense in the given framework. These predictions are allowed because the aggregate interlock machine learning model is not constrained by crack shape or opening and, as mentioned previously, the opening is not constrained by the crack shape.

To show this, the crack opening can be constrained to its shape (Figure 8.3), and shear resistance components can be graphed for a variety of crack openings, where the residual tensile strength resistance is allowed to act on the full crack shape (Figure 8.4). We constrained the crack opening to crack shape by segmenting the mechanistically predicted crack into $n$ segments. To find the size of the segments, the residual tensile strength model will be used to relate crack shape and size to crack opening, assuming some crack length on which the residual tensile strengths act. An appropriate assumption may be 0.1*d length at the beginning of cracking with a linear decay until failure. The decay in length is appropriate, as this translates directly to an increase in section rotation under the given framework. To keep this exploration focused on the effects of constraining opening

to crack shape, the center of rotation will remain at the crack tip. A fracture criterion to relate openings to crack shape would better represent underlying mechanics, but one could not be implemented because the Critical Shear Crack Theory does not include tensile stresses in the uncracked concrete. This relationship is fairly inaccurate for beginning segments but aligns with the Critical Shear Crack Theory for later segments. The following expression (97) can be made to relate crack propagation to section rotation.

$$\phi_i = \frac{w_c}{0.1 * d - \left(0.1 * d - \frac{d_F * w_c}{u_{a,max}}\right) * \frac{i}{n}} \quad (97)$$

Where $i$ is the current step and $n$ is the total amount of steps. $u_{a,max}$ determines the crack width at failure.

1mm will be used for $u_{a,max}$ to agree with the testing information. The dot in Figure 8.3 represents a typical value of crack shape and opening that would be obtained from the Critical Shear Crack Theory. Because the crack shape is not constrained to the opening in the hybrid model, the residual tensile strength is overrepresented in the final model. If the residual tensile strength is allowed to act on a fully developed crack with a small opening, it can account for most of the shear resistance mechanism of the beam. Additionally, the aggregate interlock capacity is not constrained to shapes or openings in the hybrid model, so it can account for the remaining capacity prediction, even when they should not exist. Figure 8.4 shows that the aggregate interlock should not exist at low crack openings. This is because no sliding has developed in the crack yet. If the aggregate interlock predictions were constrained by crack shape or opening and the opening was constrained by the crack shape, mechanistically inconsistent predictions would not be possible.

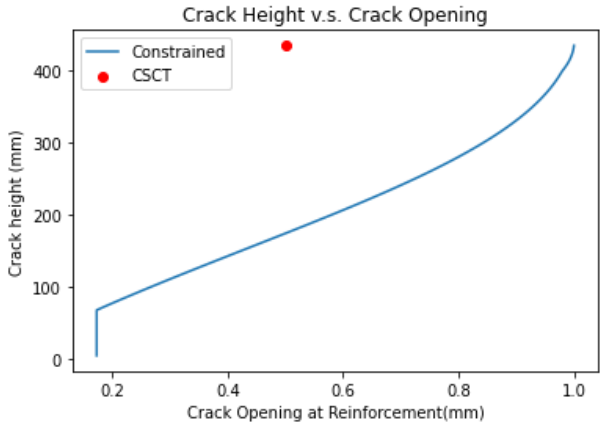


*Figure 8.3: Crack opening constrained by crack shape and typical Critical Shear Crack Theory values*

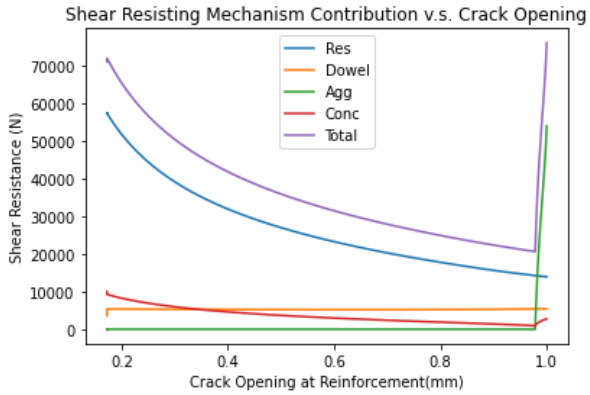


*Figure 8.4: Contribution of shear-resisting components over crack openings*

All factors caused by a lack of constraint are summarized now:

- Small crack openings are predicted because the crack shape is not constrained to the crack opening, resulting in significant contributions from residual tensile strength;
- Aggregate interlock is not a significant contributor because most of the capacity is already provided by residual tensile strength; and,
- Crack shape predictions are chosen to accommodate the above relationships and thus will never represent the true crack shape.

Third and lastly, even considering if the mechanistic bias was removed in the constitutive models and the predictions were sufficiently constrained, the hybrid model will still be limited as it does not consider multiple cracks. To accurately model the cracks that develop and predict the failure state in a mechanistically consistent manner, multiple cracks must be considered.

The above-mentioned factors can be attributed to two deficiencies of the hybrid model: (1) lack of sufficient mechanistic constraint; and (2) misrepresentation of underlying mechanisms (significant mechanistic bias). There is still much that is unknown about the contribution of these deficiencies to inaccuracies of intermediate predictions. An accurate representation of supporting mechanisms (decreasing mechanistic bias) may not be sufficient to constrain the solution space and could result in still incorrect intermediate predictions. Likewise, adding constraints without accurate mechanistic models may lead to inaccurate failure capacity prediction.

To remedy both issues, Chapter 10 will develop a framework for decreasing mechanistic bias, and Chapter 11 will investigate how to incorporate sufficient constrain. Remedying these issues will allow for the creation of a model capable of accurately predicting crack shapes.

# CHAPTER IX: INVESTIGATING DIFFERENCES IN MODEL PERFORMANCE

While this implementation was not able to predict load-induced cracking accurately, it still may be useful in other scenarios. The Data-Driven Inclusion method's usefulness has been investigated by other authors, but many other benefits have not yet been mentioned. (Vianna et al., 2020) was reviewed in a previous section and uses Data-Driven Inclusion to predict aircraft hardware distress by having neural networks predict hard-to-determine mechanisms. Rackauckas et al. (2020) applied Data-Driven Inclusion to differential-equation-mechanistic models across many scientific disciplines. Rackauckas implemented this method similarly to Vianna, adding "universal approximators" (neural networks) into differential equations to estimate entire mechanisms or closure terms, while the rest of the modeled system would be defined by well-established mechanistic relationships. This is explained as giving "structure" to the learned model, which reduces the data needed in training.

These works usually emphasize how accurate relationships can be learned for mechanisms without a lot of data. What these works do not address are the following:

- What is the best way to integrate machine learning and mechanistic models? This is a relatively new field of machine learning, and past works do not explore the possible combinations of these models. From this, it is unclear how to best implement them.
- *How* do mechanistic relationships reduce required data? Incorporation of domain knowledge has been reported many times to reduce the amount of data required for generalization (Rackauckas et al. 2020; Schaeffer et al., 2018; Tipireddy et al., 2019), but an explanation for this phenomenon is not given. Often vague analogies are given like mechanistic models give

more "structure". A better explanation for this data efficiency is given through the Hybrid Learning theory, but this theory has not been tested yet.

- Is this method applicable to structural engineering? This is a question about the utility of hybrid modeling. This method uses machine learning to represent a mechanism, but traditionally, empirical methods have been used for a similar effect. Are hybrid methods more useful in structural engineering than mechanistic methods? This should investigate both shear capacity accuracy and interpretability. Interpretability plays a significant role in the usability of any developed model. In the previous studies, no discussion was provided on this topic. Will replacing these empiric methods that are considered interpretable with machine learning significantly affect the overall model's interpretability?

To investigate all these unconsidered questions, our hybrid implementations will be compared to the performance of the mechanistic and machine learning methods in predicting shear failure capacity in concrete beams without transverse reinforcement. The mechanistic model will be one proposed by (Cavagnis et al., 2018), employing the Critical Shear Crack Theory, and the data-driven model will be a neural network. Comparing our various implementations of the hybrid model will help to identify the best way to combine mechanistic and machine learning models. Comparing hybrid model performance with machine learning performance verifies the Hybrid Learning Theory and explains *how* incorporating mechanics increases data efficiency. Finally, comparing hybrid and mechanistic performance will determine if hybrid modeling is feasible for use in Structural Engineering.

The data-driven model uses a neural network architecture with a hyper-optimized structure. The network's architecture information is provided in Table 9.1. The architecture was selected using a random search algorithm. Inputs are normalized before being used in the network. Each layer has a ReLU activation function, including the output layer since the output should be strictly positive. The Nadam training algorithm is used for its ability to avoid local minima. The loss function is composed of a simple mean squared error (MSE) function and an L2 regularization function. The network is trained using 10-fold cross-validation, keeping the model that achieves the lowest MSE on the validation set. Using 10-fold cross-validation ensures the resulting model is not at a local minimum.

*Table 9.1: Plain Neural Network Configuration*

| Layers | Nodes | Regularization Coefficient | Learning Rate |
|---|---|---|---|
| 4 | 140 | 0.00029 | 0.0044 |

The prediction accuracy of "connected", "unconnected", and "spread" hybrid models, the neural network, and the mechanistic model are compared on a test data set in Figure 9.1.

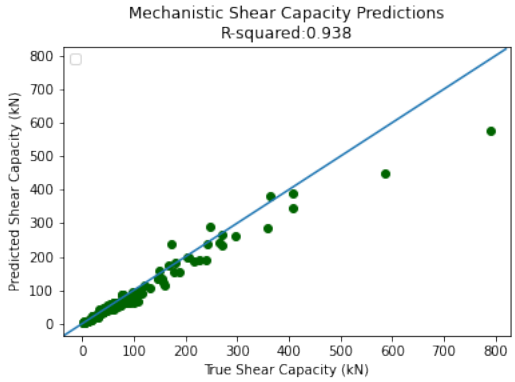


9.1(a): Mechanistic prediction results

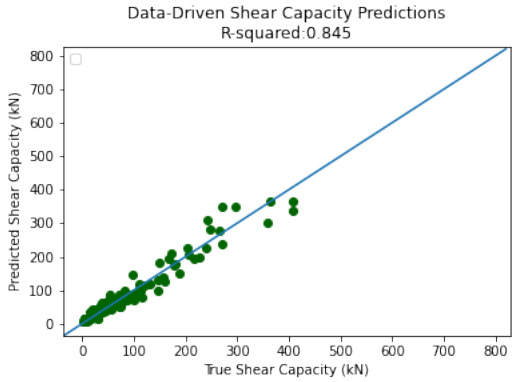


9.1(b): Machine Learning prediction results

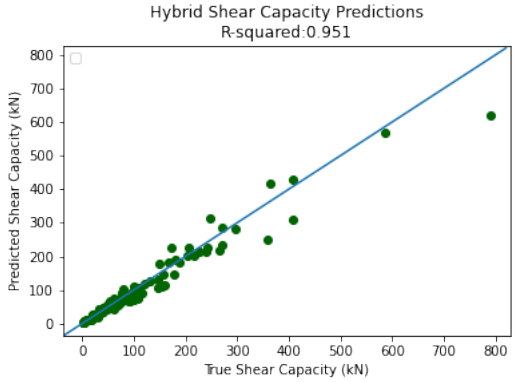


9.1(c): Connected prediction results

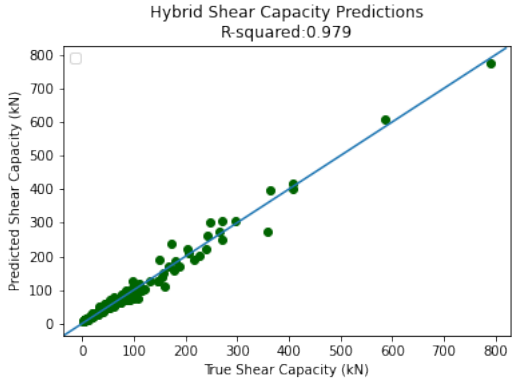


9.1(d): Unconnected prediction results

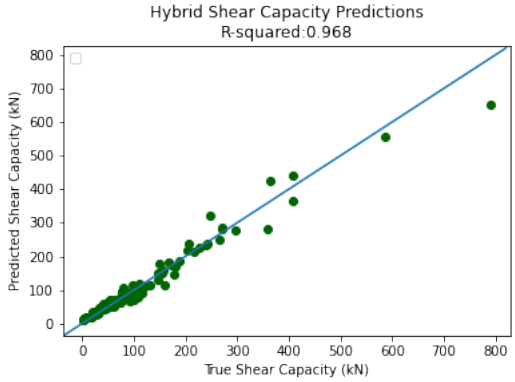


9.1(e): Spread prediction results

*Figure 9.1: Prediction Results*

The number of trainable parameters used in each model is given in Table 9.2. While not an exact representation, the number of trainable parameters in a neural network is a great indicator of its model space complexity.

*Table 9.2: Trainable parameters*

| Mechanism | Crack Location | Crack Length | Crack Angle | Crack Opening | Aggregate Interlock | Shear Capacity | Total |
|---|---|---|---|---|---|---|---|
| Neural Network | 60653 | | | | | | 60653 |
| Connected | 42663 | | | | | | 42663 |
| Unconnected | 461 | | | | 51665 | | 52040 |
| Spread | 1707 | 1694 | 1864 | 1841 | 985 | | 8091 |

## Optimal Model Configuration

Upon examining the differences in hybrid model configurations, we can observe how to best combine mechanistic and machine learning models

The Unconnected model performs the best. However, the spread model makes similarly accurate predictions with significantly fewer trainable parameters, indicating it may be a more efficient architecture. If all models are constrained to have equivalent numbers of trainable parameters to represent each mechanism (same model complexity), it can be seen that adding more residual connections results in a more efficient machine learning approach. The performance of an Unconnected model when it has the same number of parameters as the Spread model can be seen in Figure 9.2 It is important to note that while these constrained models have similar trainable parameters, the comparison could be skewed because the constrained models have not had their hyperparameters re-optimized. As such, the optimal layers-to-node ratio has not been determined.

However, because of the significant difference in prediction accuracy, hyperparameter tuning would likely not change this conclusion. Finally, a better spread model could be obtained by increasing its complexity. A more complex and more accurate model may have not been discovered due to the limited search range during hyperparameter tuning.

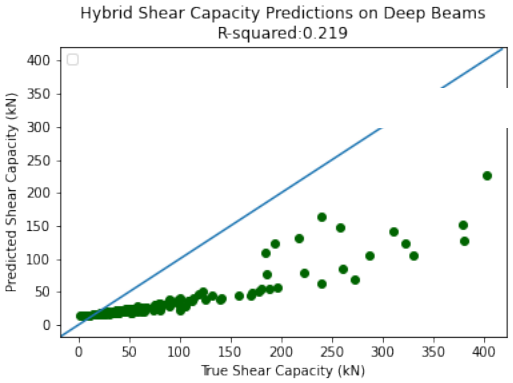


*Figure 9.2: Model Architecture Comparison with Equivalent Trainable Parameters*

## Validation of Hybrid Learning Theory

The hybrid models outperform the neural network by a larger margin for reasons explained in the hybrid learning theory. Because the neural network must represent a more complex system with the same amount of data, it will have greater error from variance. To validate the concept of data efficiency explained by the hybrid learning theory, the neural network's performance is compared to the spread model's while having similar model space complexity (number of trainable parameters). This will better highlight how the error from variance changes with data set size. By being limited, the neural network will not be able to represent its system adequately (having greater bias) but should have low error from variance due to the low number of trainable parameters. Figure 9.3 shows the comparison for varying sizes of training sets. Performance is still comparable between the models for

large data set sizes, but as the size decreases, the performance of the neural network reduces significantly.


*Figure 9.3: Data Efficiency of Data-Driven Inclusion*

The mechanistic bias can play a significant role in the effectiveness of mechanistic knowledge to reduce a learned model's complexity, and in some cases, can even reverse this relationship if any mechanistic error is significant. For example, the Critical Shear Crack Theory is unable to predict arching action for deep beams because of the constitutive relationship it uses for the shear strength in uncracked concrete, which is the dominating component in deep beams. In this case, adding this mechanism for predictions on deep beams will actually increase the complexity of the model space. Figure 9.4 shows this a hybrid model's predictions when deep beams are included in training and testing data.

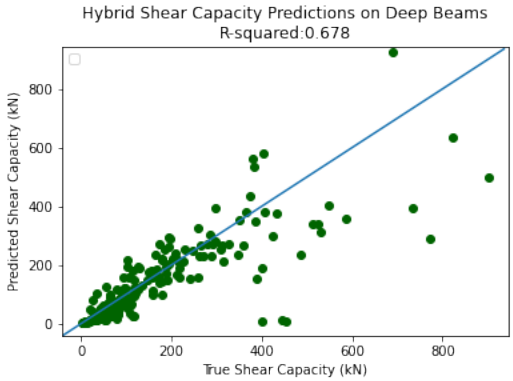


*Figure 9.4: Adverse effects of mechanistic bias*

From these observations, we can verify the Hybrid Learning theory and also identify an extra property of it: when mechanistic bias is too significant, the data efficiency effect is actually reversed. The Hybrid Learning theory provides a simple explanation for the data efficiency that mechanistic relationships provide. The data efficiency is best described as "targeted" learning on shear capacity mechanisms. Instead of machine learning needing to learn all the mechanisms of shear failure, it only "targets" the few it was assigned to. This decreases the hybrid model's out-of-sample prediction error from variance while keeping the error from bias constant. Hybrid models can produce marginally higher accuracy for larger data sets, or significantly higher accuracy for small data sets.

## Use in Structural Engineering

The accuracy and interpretability of the hybrid model will be compared to the mechanistic model to determine hybrid model usability in Structural Engineering.

The hybrid model outperforms the mechanistic model, showing that machine learning is more able to represent the complexities of shear capacity predictions. Given the already-high accuracy of the mechanistic model, this represents a substantial increase in modeling flexibility from using hybrid methods.

Another benefit of hybrid models, as illustrated in Chapter 8, is they have interpretability. Through this interpretability, we were able to realize that the machine learning models were not respecting underlying mechanisms. Even though not accurately representing the mechanisms of shear failure is a problem for the current model's use in Structural Engineering, its interpretability does show promise for the method in future applications when the problems identified in Chapter 8 are resolved. In this case, the interpretability of the hybrid model will be more robust than that of mechanistic models, where the mathematical form of mechanistic models can often lead to the misinterpretation of underlying mechanisms. Using hybrid methods also fixes the interpretability problems of machine learning while providing the flexibility associated with machine learning.

This method can be useful in Structural Engineering in terms of increasing accuracy and robustness of interpretability. The hybrid model makes more accurate predictions than the mechanistic and machine learning model. Additionally, the hybrid model is more interpretable than machine learning models and has more robust interpretability than mechanistic models.

# CHAPTER X: THE BASIS OF MODEL IMPROVEMENT

To predict load-induced cracking in concrete beams without transverse reinforcement, modifications will need to be made to previously used mechanistic and machine learning models. In previous implementations, the failure (or critical shear crack) surface was represented by a bilinear crack. From the reviewed experimental programs, however, it is evident that multiple cracks, not just one bilinear crack, must be considered to adequately predict cracked surfaces and the failure surface. In the analysis of the previous hybrid model's predictions, the mechanistic bias decreased the accuracy of the crack shape, crack kinematics, and aggregate interlock predictions, and insufficient constraint allowed for multiple solutions to satisfy the failure capacity of the concrete beam. For accurate prediction of load-induced cracking, multiple cracks, accurate constitutive models, and proper constraint on learning will be needed. This section will develop a framework: (1) that predicts load-induced cracking for multiple cracks and (2) that has mechanistic models with low bias. We will save the investigation of sufficient constrain for Chapter 11, as it is a more complex topic.

## Consideration of multiple cracks

Multiple cracks must be considered to accurately determine the failure state of concrete beams without shear reinforcement for two reasons:

1. Slender beams always fail after adjacent cracks merge and disrupt each other's kinematics (Cavagnis et al. 2015).
2. Strains in uncracked portions cannot be related to crack openings unless multiple cracks and multiple strain states are considered (Cavagnis et al. 2018).

To better define how crack merging causes failure, we will define two types of cracks, the critical crack and the failure crack. The critical crack is one whose degradation of internal shear-resisting mechanisms causes failure, while the failure crack is where the beam ultimately separates during failure. Sometimes these cracks are the same, and sometimes there is no critical crack, and the reason why models solely using a critical crack approach misrepresents the underlying mechanisms of failure is that there isn't always a critical crack. Sometimes cracks merge early during loading, and what was once considered the critical crack must be re-defined to consider the crack that merged with it. Loading then continues until the merged crack's internal force degrades and the beam fails. When adjacent cracks merge, the beam either continues to resist shear capacity, creating a new critical crack to analyze, or the beam begins to fail. The Critical Shear Crack Theory or any model that employs a single crack with simple geometry should then represent this crack to accurately represent underlying mechanisms. However, when cracks merge later in failure, failure occurs rapidly and there is no degradation of internal forces. In this case, there is no critical crack, and the merged crack only represents a failure crack (Cavagnis et al., 2017). In this case, a single crack is not sufficient to accurately describe underlying mechanisms. Because of this, a multi-crack approach must be used.

Additionally, the main reason the Critical Shear Crack Theory, or other models like it (Reineck, 1991), cannot robustly represent failure is that they were never meant to accurately represent the cracking occurring in a failing beam (Classen, 2020). Rather, they are models that were developed to apply the well-known constitutive models (e.g. Aggregate Interlock, Tension Softening), developed independently from beam analysis, and provide a reasonable mechanistic interpretation of the problem (Reineck, 1991).

Considering multiple cracks is also important for relating strains in the uncracked region to crack openings in the cracked region. To relate strains in the uncracked region to crack openings in the cracked region of the beam, the strains must be applied to a distance along the beam's length, and if that distance covers other cracks along the beam's length, the calculated displacement must be attributed to all crack openings for affected cracks. Cavagnis et al. (2018) illustrate this by saying the crack opening only increases linearly with depth when considering all the crack openings in a tributary area. The strains across an arbitrary length of the beam will be distributed to the cracks in that same portion, so without knowledge of the surrounding cracks, this distribution would be difficult to determine. Additionally, considering that the crack's kinematics will determine the capacity of the beam, determining this distribution is crucial. Figure 10.1 shows the benefits of predicting multiple cracks.

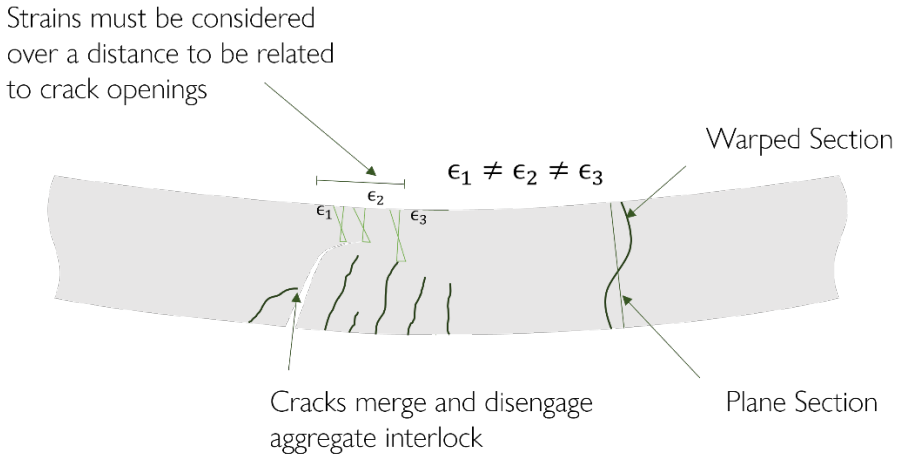


*Figure 10.1: The effect of predicting multiple cracks and warping caused by shear stresses.*

## Model framework

An adequate framework will need to be developed to coordinate the predictions of multiple cracks and apply constitutive models appropriately. The single cracked-section analysis used in the Critical Shear Crack Theory and Shear Crack Propagation Theory will not be suitable when predicting multiple cracks, especially considering the delamination and aggregate interlock cracks that nucleate from primary cracks. A very generalizable framework for automatically analyzing the states of an entire beam is the finite element method.

The prediction of load-induced cracking would benefit from the finite element method but would bring significant challenges in hybridizing the model too. A highly discretized method of analysis would allow for multiple cracks to be considered and for a more refined application of constitutive models, but the finite element implementation would have to be re-programmed to be amenable to automatic differentiation and the other constraints of the TensorFlow library. Even in the case the implementation works, the computational expense may be substantial.

While it may be difficult to use a finite element framework, a similar framework might be implemented that still takes advantage of the discretization used in the finite element framework.

Making larger, simple elements, a finite "tooth" method can be developed, where the teeth are defined by the cracks that develop on either side of it. This would be like Kani's (1964) model for predicting tooth failure but would include all teeth developed along the beam. The tooth geometry would be more complex as well. In the finite element method, elements are deformable bodies. These bodies are equilibrated to form the constraints of the element's deformation, then compatible deformations are solved (Reddy, 2019). A similar approach can be taken with each tooth and the

uncracked portion above them being the elements. The elements do not need to be too complex, as the deformations occurring in the actual beam only consist of cantilever action bending teeth and beam action in the uncracked portion. However, the beam action in the uncracked portions may be more complex than initially assumed, as discussed in a later section. This significantly-less-flexible implementation of the finite element method would allow for its hybridization. A finite teeth method provides an adequate framework for evaluating the states of each tooth and uncracked region. Upon evaluating these states, the elements can be updated to acknowledge crack propagation. However, their need for simple, uniform crack distribution would limit its accuracy for modeling the true cracking behavior. The cracks idealized in many proposed models (Reineck 1991; Cavagnis et al. 2018; Kani, 1964) would suit this framework, but these cracks do not include delamination cracks, secondary cracks, or aggregate interlock cracks. Additionally, many failure cracks represent S shapes, as a combination of secondary and delamination cracks (Cavagnis et al., 2015). S-shaped cracks would not be suitable for this framework.

Alternatively, a finite crack method might be developed to better account for the complexities of crack development while still allowing for discretized application of constitutive models. This approach would improve the Shear Crack Propagation Theory to include multiple cracks and the cracks that branch from the primary cracks. Ensuring forces in the crack are in equilibrium and accounting for the deformation of concrete "teeth" would be much more difficult in this approach, however, because of the complex geometry that results.

Figure 10.2 compares the frameworks, showing that delamination and aggregate interlock cracks would be difficult to model for the finite tooth framework and computing equilibrium would be difficult for the finite crack framework.

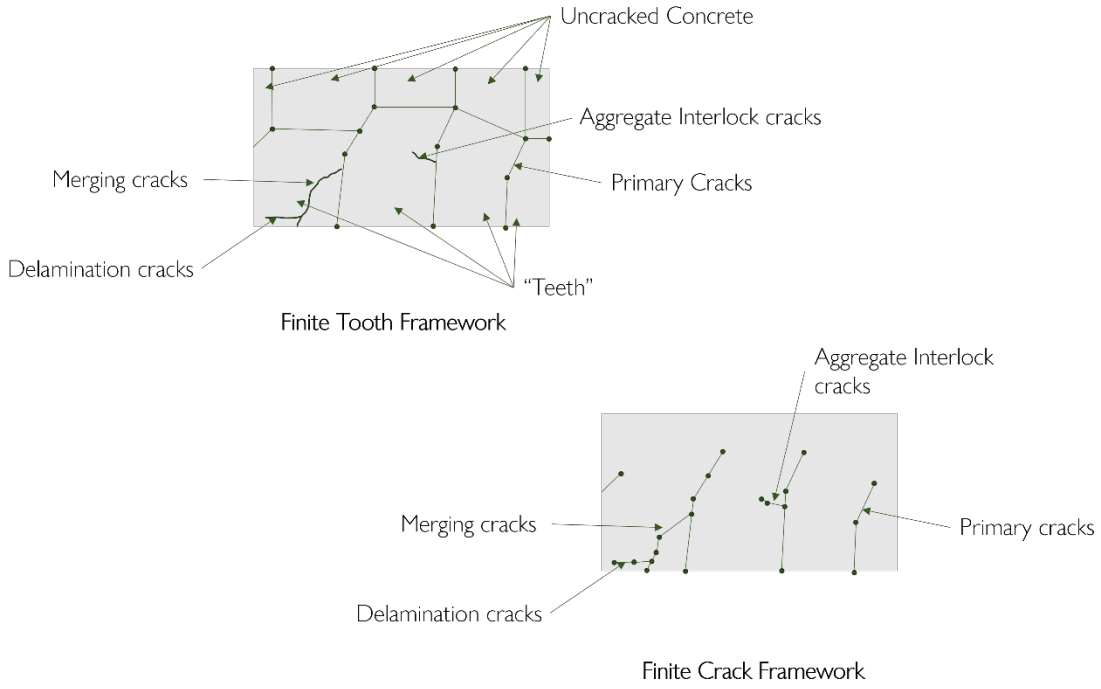


*Figure 10.2: Crack analysis frameworks*

## Machine Learning Prediction of Crack Shapes

Assuming the constitutive models used in this new implementation contain low mechanistic bias, only load-induced cracking should be predicted by machine learning. This will keep the relationships learned by data simpler than if constitutive models needed to be learned too. How the machine learning model predicts cracking must be considered, however, as there are many strategies.

Any new implementation must predict multiple cracks as opposed to our previous implementation which predicted one crack with two segments. The best approach for this is to model a *crack propagation* mechanism instead of a load-induced cracking mechanism. By doing this, the

machine learning model can predict the propagation of cracks at each load step instead of predicting all the crack segments that will develop at once.

It would be unfeasible for us to predict a finite amount of crack segments because the outputs of a neural network are fixed and the number of cracks occurring in the beam is unknown. Constraining the number of crack segments predicted to a fixed number would add significant bias. Additionally, hundreds of crack segments develop during loading. Predicting all of these would result in an extremely complex model.

By predicting *crack propagation*, Long Short Term Memory (LSTM) models can be used instead of neural networks, which can predict as many *crack propagations* as there are load steps. This makes the LSTM able to predict all the segments of a crack. Certainly, multiple cracks would need to propagate at once, and the number of cracks that need to propagate cannot be determined in advance. This leaves us with the same issue we previously had: an unknown number of machine learning models are needed. However, this problem can be solved by only using one LSTM and using very small load increments. By making the load increment steps very small, you could account for more crack propagations being needed that are set to predict from the LSTM. For example, if the LSTM is set to predict the propagation of one crack and a load increment causes the need for two propagations, the first prediction can handle one propagation. Then on the next load step, the next prediction from the LSTM will predict the other required propagation, this works assuming no other propagations need to occur in the second load step. Hence, this approach crucially depends on the small load increments.

This method can be extended by considering different types of cracks that will propagate under different criteria. Doweling action causes delamination cracks whereas increased moment and cantilever action causes the propagation of primary cracks. From this, it would be beneficial to have separate LSTMs for each crack type instead of one LSTM predicting all types of crack propagation so that each LSTM can specialize on its own propagation criterion.

Having one or a few LSTM cells predicting multiple cracks on a beam would require the following additional constraints on their implementation:

- They must be able to not predict crack propagations if it is not necessary and;
- They must predict crack segments that are spatially oriented to one another and associated with the crack proceeding them.

Having the LSTM cell predict no cracks for a load step is especially important at the beginning of loading, where the loading is still elastic and no propagation has occurred but would also be relevant for specialized LSTM cells whose cracks only develop later in loading. The LSTM would need to halt a prediction such that no propagation is added to the cracked state of the beam. This can be achieved by predicting a signal along with the propagation information. This signal can be an arbitrary value, such as one or zero, indicating propagation or not, but to provide a physical sense of the signal, it could be the length of the crack. If the length is positive, then propagation occurs, and if it is negative, it doesn't.

We must also determine a system for identifying which existing cracks LSTM propagation predictions should be attributed to. Additionally, once that problem is solved, how will we determine the spatial orientation of existing cracks (which is closer to the application of load and which cracks

have merged)? Spatial orientation will be crucial for determining cantilever action effects and predicting failure. One simple method is to predict a crack id along with the coordinates and length, and the propagated crack gets matched to the crack with the closest id. Matching cracks can be grouped in mutable objects, and once grouped, can be ordered in another mutable object. Additionally, we can add a condition to check for intersecting propagations, and the two crack objects can be merged.

Figure 10.3 shows this prediction framework, equilibrium is solved after every propagation.

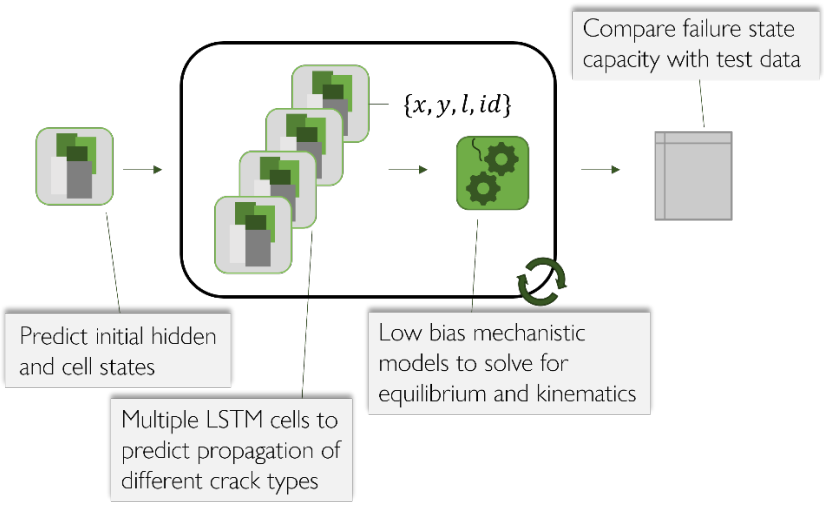


Figure 10.3: Crack prediction framework

## Low Bias Mechanistic Models

To have a low mechanistic bias in machine learning predictions, the mechanistic models used in the Data-Driven Inclusion method need to accurately represent underlying mechanisms. Many mechanisms have been identified to contribute to shear failure, like aggregate interlock and residual tensile strength, but many others have not been identified throughout, such as how cantilever action affects the strain states in the uncracked region of the beam. For these less studied mechanisms, this section will rationalize how to best represent them, and for well-defined mechanisms, models will be

identified that represent test data well. First, we will discuss how to represent strains in the uncracked region and how they relate to crack openings. Then, we will discuss how to consider the microcracked region and propagation criterion. Finally, we will identify mechanistic models that represent underlying mechanisms well.

## Kinematic Hypothesis

The kinematic hypothesis (strain distribution) is the most difficult portion to select, as the strains occurring in the uncracked region are not apparent, as the stress distributions from the cracked and toothed region will likely affect it significantly. Determining this hypothesis is crucial to representing the stresses in this region and relating the strains in the uncracked region to crack openings in the cracked region.

We will use elementary beam theory to begin our analysis of an appropriate kinematic hypothesis. From beam theory (Beer et al., 2015), the cross-section of an elastic beam warps due to applied shear force to look like an "s" shape. In the section analysis, the extent of warping must be determined if the strains in the cross-section are to be accurately related to the crack openings. This warping for an elastic beam is shown in Figure 10.1.

Euler Bernoulli beam theory and Timoshenko beam theory handle shear deformation differently (Beer et al., 2015).

Euler Bernoulli beam theory (Beer et al., 2015) considers the plane section to remain plane, and section rotation is only affected by the moment that is applied, so shear stress doesn't cause any additional warping strain. This theory can be used without significant error because, in slender beams, the displacement and strain from cross-section warping are much less significant than the strain from

bending. This can be easily realized in the force-moment relationship of beam equilibrium. If the force is applied very far away from the section of the analysis, then the moment will be high compared to internal shear forces. This is the case for a midspan section of a simply supported beam loaded with a point load at its midspan. However, at the support of this beam, shear strains and warping account for most of the strain in the cross-section since the moment is negligible in these sections.

In Timoshenko beam theory (Timoshenko, 1921), an additional rotation is applied to account for the warping of shear stresses, but they do not use a warped "s" shape to represent this. Instead, a plane is still used, but the plane is oriented to match the warped section sufficiently.

However, these considerations do not account for the non-linearity in concrete stress-strain relationships or the additional forces applied to the uncracked region from the cracked region. Concrete softens as it nears its peak capacity, especially when considering biaxial loading (Kupfer and Gerstle, 1973). If loads cause stress to enter the non-linear region, the strain distribution of the uncracked section would become non-linear, altering the kinematics in the crack portion of the beam.

If the uncracked region is considered to be a separate beam then forces from the cracked region can just be applied as if it were an external force. To further illustrate this behavior, the concrete teeth can be considered shear connectors, making a composite section between the reinforcement and uncracked section. This indicates how the cracked sections affect the uncracked sections, as the presence of the teeth will alter the uncracked section's strain distribution based on the shear transferred from the teeth to the uncracked section.

Still many models consider strains to vary linearly through the depth of the cross-section and do not consider effects from warping, potentially affecting the kinematic model imposed on the crack

opening. As the depth of the uncracked region decreases, however, it becomes more slender, thus the shear deformation can be considered negligible to the flexural deformation. So, a linear strain distribution should not introduce significant error. Still, the forces from the uncracked region should be considered when determining strain distributions. To do this, Classen (2020) makes the shear stresses non-zero at the crack tip.

Without an in-depth study on the strain distribution present in cracked beams, a simple linear strain distribution and linear uni-axial stress-strain response must be assumed. Additionally, a non-zero shear stress on the bottom of the uncracked region should be assumed.

The relationship between the crack kinematics and strains in the uncracked region depends on determining a center of rotation compatible with both. If the center of rotation for the crack is assumed to be the neutral axis of the beam, which aligns with the kinematics of the uncracked region, then sliding will occur in the uppermost portions of the crack, which is not consistent with experimental results. Instead of obeying this relationship caused by the center of rotation, mechanistic models often set the sliding values for the uppermost cracks to zero, causing a discontinuity in the kinematic relationships. If the center of rotation is placed at the crack tip, then no sliding occurs in the upper regions of the crack, but the kinematics of the uncracked region are inconsistent. These discontinuities could be avoided by choosing a center of rotation that causes no sliding in the upper cracks and obeys the kinematics of the uncracked region, but no mechanism has been identified to explain a center of rotation like this.

## Propagation Model and Residual Tensile Strength

Fracture mechanics are crucial because they will ultimately determine the crack shapes, which ultimately determine beam capacity. Fracture mechanics will also determine the decay of internal forces along the crack (residual tensile strength).

Concrete's force-displacement relationship can be considered linear-brittle on very large scales (the scale of a building) or on very small scales (smaller than aggregate size), and linear-brittle relationships do not need to consider fracture mechanics much. However, on an intermediate scale, the scale of structural members, the relationship is much different due to the development of microcracks (Reinhardt et al., 1986).

Discrete crack and crack band approaches are used to model the force-displacement relationship of the micro-cracked region.

To understand the difference in these approaches, the distinction between visible cracks and microcracks must be understood. Visible cracks are, of course, visible and make one continuous segment, and microcracks are dispersed chaotically above the visible crack, not making a continuous segment, that is, until propagation increases further and the micro-cracks connect. This distinction is shown in Figure 10.4.

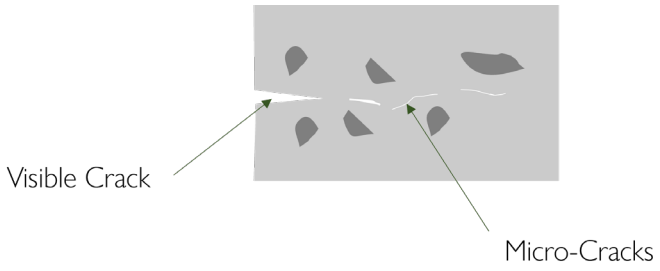


*Figure 10.4: Distinction between visible cracks and micro-cracks*

The discrete crack simplifies these visible and micro-cracks with one fictitious crack. Since the micro-cracks have a deteriorating force-displacement relationship, meaning they are allowing more displacement per force applied, the micro-cracked region can be summarized as a crack with a small opening but still retaining some resistance.

To increase the computational efficiency of the discrete crack models in finite element analysis and remove the dependency on element size, Bazant and Gambarova (1980) developed the crack band approach. Instead of considering any visible cracks, cracked regions are replaced with elements having micro-cracks distributed throughout. The aggregation of cracked elements is the crack band.

The discrete-crack approach is common among the mechanistic models currently considered, while the crack band approach is common in finite-element modeling. However, the crack band approach only considers Mode I fracture. This is fine for initial fracture, but in later stages of cracking, Mode II must be considered. The discrete crack approach allows for the kinematics to be represented easier, as the micro-cracked region is represented with crack openings instead of strain. However, this approach makes relating strains in the uncracked region to openings in the cracked region more difficult. In a more realistic model, the micro-cracked region serves as a transition between these types of displacements (crack openings and strain). The discrete-crack approach should be used in future implementations because of its representation of crack kinematics.

The Kupfer fracture criterion should be used to determine crack propagation because it considers biaxial effects, and uniaxial fracture process zone models can be used without significant error (Kupfer and Gerstle, 1973). Realistically, the contribution from residual tensile strength would be less in biaxial loading than in uniaxial loading because the stiffness of concrete decays much faster

when tensile and compressive forces are applied biaxially. Using a uni-axial relationship instead will cause residual tensile strengths to be over-estimated, but since these forces only account for a small portion of the overall resistance, this simplification should not cause significant mechanistic bias. The tensile stress-strain relationship for tensile loading has a much different shape when compressive forces are applied in the other direction.

### Inter-Crack Constitutive Models

Appropriate inter-crack resistance models are readily available, as many of their mechanisms have been studied in isolated experiments (e.g. aggregate interlock, doweling action, tension stiffening) (El-Arris, 2007).

Cantilever action is best represented by an elastic, non-prismatic cantilever beam since the concrete "tooth's" failure is determined by the tensile strength of the concrete and there is a very small plastic region for tensile stress (Reinhardt et al., 1986). While the elasticity of the analysis simplifies finding the cantilever action stress at the crack tip, the non-prismatic shape makes finding deformations of a tooth difficult, especially since the bounds of the tooth can change in an instant. For simple crack geometries, Classen's (2020) approach can accurately account for the stresses occurring from cantilever action, but not the deformations.

Many models (Ugala, 2003; Walraven, 1979; Walraven and Reinhart, 1981; Guidotti, 2010; Bazant and Gambarova, 1980; Cavagnis et al. 2018; Tirassa et al. 2020) have been developed for predicting aggregate interlock stresses (Koscak, 2022). By applying these models on experimentally obtained crack kinematics, Koscak (2022) identifies Walraven's (1979) to be the most consistent. However, this model has a poor consideration of crack kinematics (Koscak, 2022; Cladera et al., 2013).

Ulaga's (2003) model was derived from Walraven's while considering sliding and opening to occur at the same time, so this model can be implemented to have the least mechanistic bias.

Tension stiffening, which was not considered in the Critical Shear Crack Theory, can be accurately represented with the model proposed by Bentz (2005). Bentz studied this effect for varying levels of bond, and the models they produced can be used in this.

We can use the model proposed by (El-Ariss, 2007) for dowling action because it is derived from many mechanistic principles and corresponds well with test data on concrete beams without shear reinforcement.

This model was made by incorporating several smaller models. The first was replicated from Friberg's (1940) model to describe the deflection and slope of dowels in concrete pavement. Deflection in this model was very dependent on the stiffness of the concrete cover. The stiffness of this was estimated with Soroushian's (1987) model. The relationship between deflection and strength decay was provided by Millard and Johnson (1984). Finally, a model for ultimate strength was used from (Dulacska, 1972). This model contains less mechanistic bias than the others because it considers deflections in the bonded region as well as in the cracked region. Taking into account all these factors makes for mechanistic consistency. This model also accurately represents the ductility present in the later stages of loading.

# CHAPTER XI: CONSTRAINT EFFECTS

In the previous implementation, erroneous machine learning predictions were caused by the crack shape not being constrained to the crack opening. This allowed the fracture process zone to contribute greater to the resistance than it actually should have, and as a result, the aggregate interlock contributed less than it should have. To have mechanistically consistent predictions from the machine learning models, they must be sufficiently constrained. In this section, we will illustrate the effect of constraint on learning.

In hybrid modeling, sufficient constraint means a unique solution can be obtained for the predicted variables in terms of the mechanistic models and the data set. In linear algebra, the number of independent constraints must match the number of unknown variables for a unique solution to occur. If there are more constraints than variables, some of the constraints must be linearly dependent on the others for there to be a solution, and if there are too few constraints, then multiple solutions can occur. However, the relationships used in hybrid modeling are not linear. They are very non-linear, so these rules do not apply. Given an equal amount of constraints and unknowns, there could be many possible solutions, no solutions, or a unique solution. For example, consider the system of equations of a second and first-order polynomial shown in Figure 11.1. Depending on the equations, there could be one solution, two solutions, or no solutions even though there are 2 equations and two unknown variables, x and y.

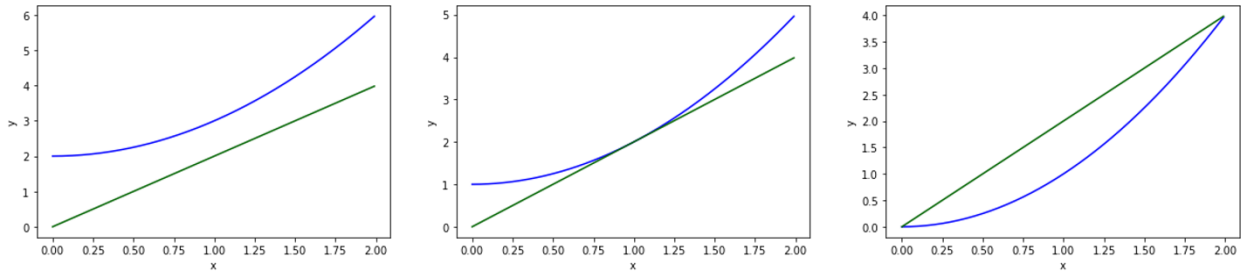


*Figure 11.1: Solutions to non-linear systems of equations*

This hypothesis explains the phenomena observed in the previous hybrid implementation. In the mechanistic model proposed by Cavagnis et al. (2018) (the model the previous hybrid implementation was based on) the model used did not need to constrain predictions from their aggregate interlock and crack shape models because they were defined explicitly in terms of characteristics of the beam. These explicit relationships were developed outside of their model (crack shape was determined from images of cracked beams and the aggregate interlock model was modified from previous experiments), so you could say they were defined by external data. They did, however, need to constrain their kinematics. To do this, they solved for the crack opening (thus the crack kinematics) by iteratively computing the moment equilibrium of an elastic section, updating an assumed value; to extend the system of equation analogy, there was one unknown and one equation. By replacing the relationships for crack shape, crack kinematics, and aggregate interlock in the hybrid models with machine learning relationships, the explicit relationships and constraints used to solve for crack kinematics were taken away, leaving a system of equations with many more variables than constraints. This is fine if accurately representing the mechanics of the predicted variables is

unimportant, but if you want the separate machine learning predictions to observe some mechanistic principle you must constrain them sufficiently.

When unconstrained, machine learning models can make infinitely many predictions that will result in the correct shear capacity, and only one of them will be mechanistically consistent. We cannot use the data to find that constraint relationship itself. Data and mechanics play different roles in constraining hybrid models. Data is used to constrain the learning algorithm, and mechanistic models constrain what is given to the learning algorithm. If multiple unknowns are being predicted their values must be constrained to each other so that the information from data can be appropriately allotted to each prediction. To accurately predict the cracks that develop due to loading, there must be a unique solution for them given the mechanics. For example, the crack opening, crack shape, and aggregate interlock were predicted in the previous implementation. The crack opening, crack shape, and aggregate interlock were tied to each other in that they must all be used to predict the total capacity of the beam. This means they were all constrained by the data. However, the crack shape, crack opening, and aggregate interlock were not constrained to each other. This allowed for multiple possible combinations of crack opening, crack shape, and aggregate interlock that would have satisfied the data constraint, so the machine learning model could not discover the mechanistically consistent crack shape.

Finally, one way to prove the necessity of a unique solution is by considering the mechanistic models as being used to generate a synthetic data set instead of constraining the machine learning predictions. By generating a synthetic data set, the machine learning models can be trained directly as if they were ordinary machine learning models. The accuracy of this synthetic data set, however,

would depend on the mechanistic models that generated them. If multiple solutions are possible when generating the data set, then the information given for learning will not be consistent.

One way to improve the previous implementation would be to re-introduce the constitutive models for aggregate interlock so that it is explicitly predicted, fix the location of the critical crack to the midpoint of the shear span, as is done in the mechanistic model, and determine crack opening from equilibrium. While these changes would add significant bias, they would further constrain the crack shape machine learning predictions. However, there are still four unknown variables, the lengths and angles of the two crack segments. Thus, there would still be variability in the crack shapes and angles. To provide a unique solution without any further constraints, the machine learning model would have to only predict one crack length or angle. This highlights further difficulties in predicting load-induced cracking instead of crack propagations. For crack propagations, a unique solution can be found for every load step, as there are significantly fewer unknowns.

## Testing the Effect of Constraint

We now define an experiment to further explore the role of constraint in hybrid modeling and test our hypothesis on the requirements of unique solutions. This experiment will vary the amount of constraint to study its effects on mechanistic consistency, and will also implement other sources of looser constraint to study their effect. The Shear Crack Propagation Theory's constraints will be used for this experiment because its mechanistic models predict crack propagation instead of crack shape at failure, so there will be fewer unknowns associated with the crack prediction. However, a solution could never be found in our implementation of the model, so solutions may only be possible when removing some constraints.

The level of constraint can be altered by adding or removing mechanistic constraints, but it can also be increased by adding less strict constraints like the Mechanistic Learning terms introduced in the previous implementation. If predictions are not sufficiently constrained, more constraints can be added even if they have a significant mechanistic bias or other, less strict constraints can be added to encourage a mechanistically consistent prediction. The less strict constraints are similar to how crack shapes were constrained within the boundaries of the beam in the previous hybrid implementation. If too many constraints are present so that no solution exists, constraints can be removed.

To begin designing this experiment, the constraint of the Shear Crack Propagation Theory must be examined. In Classen (2020) the variables and constraints are presented plainly: four unknowns, being vertical tip stress, propagation angle, propagation height, and section rotation and three constraints, being derived from various equilibriums. However, the propagation height can be explicitly solved in terms of the other variables, reducing the number of variables to be equal to the constraints. Considering the number of solutions is unknown for a system of nonlinear constraints, any number of solutions or no solutions could result. So, unique solutions cannot be guaranteed just based on this information.

Because the Shear Crack Propagation Theory is likely over-constrained, an extra unknown variable will be added in the control case for this experiment. In the original mechanistic model, beta is used to describe the angle of the previously propagated crack and to describe the principle stress plane at the tip of the crack. We can add an extra free variable by making the angle of the principle stress plane different from the previously propagated crack, essentially removing the constraint that

these two angles are the same. This is a realistic modification since the principle stress orientation will determine the angle of the next crack, which should not always be in the same direction as the previous crack. In this way, there will be four variables and three constraint equations. The four variables will be the vertical stress at the tip, the orientation of the principle stress plane at the crack tip, and the x and y position of the crack. Figure 11.2 shows the sources of constraint. Equilibrium constraints are from the moment equilibrium of a concrete tooth and the moment, shear, and horizontal equilibrium of a cracked section. The moment and shear equilibrium of a cracked section must be considered as the same constraint because applied shear forces are not considered explicitly in the Shear Crack Propagation Theory.

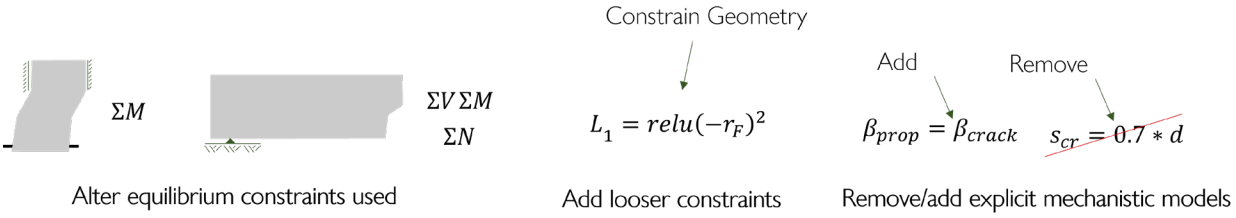


*Figure 11.2: Source of constraint for experiment*

We can first experiment with the equilibrium constraints, trying different combinations of them or only one of them at a time. If no constraints are considered, then the variables would essentially be random values.

Additionally, three extra constraints can be added to loosely constrain the prediction of the cracks. The first two constraints make sure the crack stays within the bounds of the beam, and the third makes the angle of the crack decrease with every propagation. This is not realistic but simplifies the kinematics significantly. These constraints are shown in equations (98-100)

$$0 = relu(-r_f) \tag{98}$$

$$0 = relu(h_{crack} - d) \tag{99}$$

$$0 = relu(\beta_i - \beta_{i-1}) \tag{100}$$

Additionally, the cracks in this experiment will always propagate positively because the LSTM is restricted to positive predictions and it predicts crack increments instead of crack locations. This is another loose constraint, but instead of being applied through Mechanistic learning, it is applied explicitly in prediction. These constraints limit the number of solutions that can be found in an underconstrained system, but without mechanistic constraints, multiple solutions are still possible.

Finally, other constraints besides equilibrium can be added or removed. First, we can reinstate the constraint on the principle angle by equating it to the previous crack's angle. Then, other variables can be added by removing their constraints or explicit relationship. For example, stresses from cantilever action depend on the spacing of major cracks. In the shear crack propagation theory, the crack space is assumed empirically to be 70 percent of the beam depth. Instead of using this explicit relationship. The spacing between critical cracks can be added as an unknown variable.

In Table 11.1. we show all the combinations of effects applied in this experiment. According to Classen (2020), Case 12 should be sufficiently constrained, but due to our implementation of the model, likely, case 12 is over-constrained, and the control case or case 8 would provide a sufficient constraint.

*Table 11.1: Experiment setup for testing the effect of constraint*

| Case | Equilibrium | | | Loose Constraints | | | Mechanistic Models | |
|---|---|---|---|---|---|---|---|---|
| | $\Sigma M$ | $\Sigma M \Sigma V$ | $\Sigma N$ | (98) | (99) | (100) | $\beta_{prop}$ | $s_{cr}$ |
| Control | X | X | X | X | X | X | X | |
| 1 | | | | X | X | X | | |
| 2 | | | | | | | | |
| 3 | X | | | | | | X | |
| 4 | X | X | | | | | X | |
| 5 | X | X | X | | | | X | |
| 6 | | | | X | X | X | X | |
| 7 | X | X | X | X | X | X | X | X |
| 8 | X | X | X | X | X | X | | X |
| 9 | X | X | X | X | X | X | | |
| 10 | X | X | X | | | | X | X |
| 11 | | | | | | | X | X |
| 12 | X | X | X | | | | | |

# CHAPTER XII: CONCLUSIONS AND FUTURE WORK

Currently, there is no agreement on a model to predict shear failure in concrete beams. This is primarily because mechanistic models simplify and misrepresent failure mechanics to accurately predict shear capacity, and this compromises prediction robustness. Namely, the mechanics severely simplified in mechanistic models is load-induced cracking. Without an accurate representation of cracking, models predicting beam capacity will always lack robustness, only being able to predict for the limited cases it was developed on. Machine learning models have the flexibility to avoid simplifications but require significant data to accurately learn the mechanics. Hybrid modeling methods, which incorporate machine learning and mechanics have the best chance to create accurate, robust models for predicting shear capacity.

This thesis implements hybrid machine learning-mechanistic methods to attempt to accurately model load-induced cracking in concrete beams without transverse reinforcement. While we were not able to achieve this goal in this thesis, we made substantial progress toward it.

To make this progress, we followed the approach introduced in Chapter 5, which is given in detail now.

First, several hybrid models were surveyed (approach step 1) to determine which could predict crack propagation best. Physics Informed Machine Learning, Physics Informed Neural Networks, and Physics Guided Machine learning are just a few names given to hybrid models developed in Civil Engineering. To determine which would best suit our problem, the models were categorized by functionality.

Next, the Shear Crack Propagation Theory and Critical Shear Crack Theory mechanistic models were evaluated for use in hybridization (approach step 2).

From this, the Critical Shear Crack Theory mechanistic model and the Neural Network machine learning model were used in the Data-Driven Inclusion Method (approach step 3) to accurately predict load-induced cracking. This method allows for the critical crack shape to be learned from beam capacity datasets. Crack shape, kinematics, and aggregate interlock are replaced in the hybrid model because they contain too much mechanistic bias.

The mechanistic consistency of the hybrid model's predictions was then investigated in light of them not matching experimental crack shapes (approach step 4).

Without any standard practices set for how to best combine machine learning and mechanistic models in the Data-Driven Inclusion Method, multiple versions were constructed varying the combinations. These varied combinations were compared, in terms of interpretability and accuracy, against each other and against mechanistic and machine learning models that constituted them (approach step 5).

Additionally, two extra steps were taken because we were not able to fully complete step three, accurately predicting load-induced cracking. Poor performance is associated with the hybrid model not considering multiple cracks, not providing sufficient mechanistic constraint, and containing too much mechanistic bias. To remedy this, we developed a new implementation (approach step 6) that combines a finite crack framework with the Data-Driven Inclusion method. This new implementation allows for multiple cracks to be predicted and evaluated appropriately. Additionally, it includes mechanistic models with low bias. Finally, we evaluated what is needed for sufficient

constraint and designed an experiment to further investigate the role of constraint in making mechanistically accurate predictions (approach step 7). This experiment alters the level of constraint and evaluates the mechanistic consistency of predictions. It also experiments with alternate, looser types of constraints through Mechanistic Learning.

Through these steps, we completed several objectives defined in the thesis proposal. Presented now are the main findings from the completed objectives.

Hybrid modeling methods can be separated by how they incorporate mechanics and are best organized by functionality (how incorporating mechanics helps machine learning). This organization is more robust than the biases proposed by Karniadakis et al (2021). All benefits of hybrid modeling can be defined by the Hybrid Learning theory. Hybrid Learning theory makes two claims: (1) Whether it be by an increase in simulated data or by decreasing the complexity of the model space, hybrid modeling reduces the required data for learning, and (2) Inaccuracies in the mechanistic models (mechanistic bias) decrease the accuracy of the machine learning prediction and reverse the data efficiency so that more data is required. From an analysis of interpretability, we found hybrid models to be interpretable even though their mathematical form is not due to the "black box" effect. The interpretability of hybrid models is nonetheless equivalent to that of the mechanistic models, however, and can lead to more robust interpretations. From a comparison of machine learning and empirical models, we found hybrid models to be very similar to mechanistic models. Finally, we found neural networks to be the best machine learning model for hybrid methods because of their modularity.

We found our hybrid model's predictions to be mechanistically inconsistent because they contain too much mechanistic bias, were not properly constrained and did not represent multiple

cracks. Insufficient constraint caused bad predictions because crack shape and opening were predicted so that residual tensile strength was inaccurately high and the aggregate interlock contribution was not tied to shape or opening, so multiple combinations of crack opening, crack shape, and aggregate interlock capacity could result in an accurate prediction of shear capacity.

Hybrid models with the highest degree of residual connectivity were found to provide the most data efficiency. Increasing residual connectivity allows for more efficient representations of mechanics, requiring much fewer trainable parameters for the same accuracy. Hybrid models had greater accuracy than mechanistic and machine learning models when predicting shear capacity. Hybrid models outperform mechanistic ones because of their flexibility and machine learning ones because of the hybrid learning theory. We found that mechanistic bounding and mechanistic learning can be used simultaneously to further constrain predictions. We consider the hybrid model to have the same interpretability as the mechanistic model and more interpretability than the machine learning model. The interpretability of the hybrid model indicated that it did not represent shear failure mechanics well, and while our initial implementation would not be useful, the accuracy and interpretability of hybrid modeling show its promise for use in structural engineering.

Due to the finite time available in this thesis, we were not able to accurately predict load-induced cracking in concrete beams without shear reinforcement. In the future, we will take the following approach to complete this objective.

First, we will implement the framework in Chapter 10 to remedy issues with mechanistic bias and not predicting multiple cracks. Then we will perform the experiment designed in Chapter 11 to determine the effect of constraint on learning. After constraint is sufficiently investigated, the new

model will be modified so that it is sufficiently constrained. In completing these steps, the new hybrid model will be able to predict load-induced cracking, and shear capacity can be robustly predicted for concrete beams without transverse reinforcement.

Being able to robustly predict the shear capacity of concrete beams without transverse reinforcement will lead to improved efficiency in design and allow us to better understand the failure mechanics of concrete beams. Beam action is prevalent in walls, columns, and slabs, which make up the majority of concrete structures, so designing these structural members knowing their true shear capacity significantly reduces the amount of concrete used in construction, increasing the sustainability of our built environment. By comparing hybrid model predictions with crack shapes from experiments, we can determine mechanics that have not been identified in load-induced cracking or identify mechanics that have not been represented well in other portions of the model.

After successfully implementing hybrid models to predict load-induced cracking and robustly predict shear capacity, hybrid methods can then be applied to columns, trusses, walls, or foundations made of other materials as well to model their complex mechanics better too.

# GLOSSARY OF VARIABLES

Latin

| | |
|---|---|
| $a$ | Shear span |
| $a_c$ | Crack length in the fuselage |
| $a_{crit}$ | The distance along the shear span in which the critical shear crack occurs |
| $a_i, b_i, \dots, f_i$ | Lengths of triangles $abc$ and $def$ that are used to determine crack kinematics |
| $b$ | Beam width |
| $b_n$ | Effective beam width for doweling action |
| $d$ | Beam depth |
| $d_F$ | Height of point F, which is defined by (Cavagnis, et al., 2018), from the flexural reinforcement. |
| $d_{agg}$ | Maximum aggregate size |
| $d_s$ | Diameter of steel reinforcement |
| $f_c$ | Concrete compressive strength |
| $f_{ct}$ | Tensile strength of concrete |
| $f_i, \alpha_i$ | Arbitrary functions and their outputs, respectively |
| $h_F$ | Distance from extreme compression fiber to the tip of a bilinear critical shear crack |
| $h_d$ | The horizontal projection of the delamination crack near the critical crack |
| $h_k$ | The horizontal projection of crack $k$ |
| $k$ | Calibration coefficient |
| $k, c, m$ | the stiffness, damping coefficient, and mass of a single degree of freedom system, respectively |
| $k_b$ | Calibration coefficient representing the effects of delamination |
| $l$ | Crack length |
| $l_1$ | Opening radius for the tip of the vertical crack segment in a bilinear crack |
| $l_2$ | Opening radius for the root of the vertical crack segment in a bilinear crack |
| $l_3$ | Opening radius corresponds to an opening in which no microcracks exist in the vertical crack segment in a bilinear crack |
| $l_A$ | The length of the vertical crack segment in a bilinear crack |
| $l_F$ | The length of the horizontal crack segment in a bilinear crack |
| $l_{F1}$ | Opening radius corresponds to an opening in which no microcracks exist in the horizontal crack segment in a bilinear crack |
| $l_b$ | Tributary area in which cracks affect the critical shear crack. Equivalently the distance from the flexural reinforcement to the elbow of a bilinear critical shear crack (point B) |
| $l_i$ | Length of crack i |
| $n, i$ | Iteration variables |
| $n_m$ | Model space complexity |
| $n_s$ | Number of steel reinforcement strands |

| | |
|---|---|
| $r_F$ | Distance from the application of load and the tip of a bilinear critical shear crack |
| $r_{o,i}$ | The opening radius for crack $i$ |
| $r_{s,i}$ | The sliding radius for crack $i$ |
| $s$ | Depth of a concrete tooth in cantilever action |
| $s_{cr}$ | The spacing of critical cracks along the length of a concrete beam |
| $u_{a,max}$ | Crack width at failure at the level of flexural reinforcement |
| $u_a$ | Horizontal crack opening at the level of reinforcement |
| $u_i, u_i', u_i''$ | Displacement, velocity, and acceleration at timestep $i$, respectively |
| $v_a$ | Vertical crack opening at the level of reinforcement |
| $w$ | Width of crack opening |
| $w_A$ | The opening (Mode I) of the root of the vertical crack segment in a bilinear crack |
| $w_{BF}$ | The opening (Mode I) of the root of the horizontal crack segment in a bilinear crack |
| $w_c$ | Material property representing a crack width in which no microcracks exist |
| $w_p$ | The weights (parameters) of a neural network |
| $x_0$ | Depth of the neutral axis |
| $x_1$ | Distance from crack tip to the neutral axis |
| $y_0, \beta_0$ | Initial crack height and inclination |

Capital Latin

| | |
|---|---|
| $C$ | The complexity of the modeled system |
| $C$ and $m$ | material properties for fracture mechanics |
| $CB_{lower}$ | A lower bound for machine learning crack length predictions |
| $CB_{upper}$ | An upper bound for machine learning crack length predictions |
| $D$ | Size of the in-sample data set |
| $E_{bias}$ | Out-of-sample error from bias |
| $E_c$ | Elastic modulus of concrete |
| $E_s$ | The elastic modulus of steel |
| $E_s$ | Elastic modulus of steel |
| $E_{var}$ | Out-of-sample error from variance |
| $F_{cc}$ | Compressive force results in uncracked concrete |
| $F_{ct}$ | Tensile force resultant in uncracked concrete |
| $F_{e,i}$ | The exciting force of a single degree of freedom system at time step $i$ |
| $F_s$ | Tensile force in steel reinforcement |
| $G_f$ | Fracture energy required to create a cracked surface |
| $M$ | The moment resultant in a virtual section in a beam |
| $M_{CR}$ | A critical moment that causes failure in either the concrete teeth or the remaining arch of a concrete beam |
| $M_{FL}$ | The flexural capacity of a concrete beam |
| $V_{agg}$ | Shear resistance provided by aggregate interlock |
| $V_{conc}$ | Shear resistance provided by the inclined compression zone |

| | |
|---|---|
| $V_{da,0}$ | Maximum possible shear resistance available from doweling action |
| $V_{dowel}$ | Shear resistance provided by doweling action |
| $V_{res}$ | Shear resistance provided by the residual tensile strength |
| $V_{vs}$ | The shear resultant in a virtual section of a beam |
| $V$ | Total shear capacity of a concrete beam |
| $X$ | Input variables for models |
| $Y$ | Output variables for models |
| $Y_{pred}$ | Predicted output variables for models |
| $Y_{true}$ | True output variables for models |

Greek

| | |
|---|---|
| $\beta$ | Crack inclination from the horizontal |
| $\beta_{AB}$ | Crack Inclination for the vertical crack segment in a bilinear crack |
| $\beta_{BF}$ | Crack Inclination for the horizontal crack segment in a bilinear crack |
| $\delta$ | Sliding distance between two cracked faces |
| $\delta y$ | Vertical projection of crack propagation increment due to a load increment |
| $\epsilon_{cr}$ | Strain at the level of the crack tip |
| $\epsilon_d$ | Strain in the delaminated portion of the tensile reinforcement |
| $\epsilon_s$ | Steel strain |
| $\epsilon_{top}$ | Strain in the extreme compression fiber of the beam |
| $\epsilon_{ts}$ | Steel strain in non-delaminated portions of the beam subject to tension stiffening |
| $\theta$ | A property or prediction of a machine learning model |
| $\lambda$ | Strength parameter |
| $\rho$ | Tensile reinforcement ratio |
| $\sigma_1, \sigma_2$ | Primary and secondary principal stresses |
| $\sigma_Y$ | Reinforcement yield strength |
| $\sigma_{ai}, \tau_{ai}$ | Normal and shear stress from aggregate interlock |
| $\sigma_{fpz}$ | Normal stress in fracture process zone |
| $\sigma_s$ | Stress in tensile reinforcement |
| $\sigma_{x0}$ | Normal stress at the crack tip on a plane oriented vertically |
| $\sigma_{z0}$ | Normal stress at the crack tip on a plane oriented horizontally |
| $\tau_0$ | Shear stress at the crack tip on a plane oriented vertically |
| $\phi$ | Cracked section rotation |
| $\xi$ | Variable between 0 and 1 representing the location of a point along a crack |

Capital Greek

| | |
|---|---|
| $\Delta K_t$ | stress intensity factor |
| $\Delta F_s$ | Increase in tensile force in steel reinforcement due to beam action |
| $\Phi$ | Trainable parameters of a regressor |

Functions

| | |
|---|---|
| $elu(\ \ )$ | The exponential linear unit function |
| $L(\ \ )$ | A loss function |
| $ML(\ \ )$ | A machine learning model |
| $Mech(\ \ )$ | A mechanistic model |
| $NN(\ \ )$ | A neural network |
| $R(\ \ )$ | A Regularization Function |
| $relu(\ \ )$ | The rectified linear unit function |
| $\sigma(\ \ )$ | The Sigmoid Function |

# REFERENCES


ACI Committee 318 & American Concrete Institute. (2019) "Building code requirements for structural concrete (aci 318-19) : an aci standard ; commentary on building code requirements for structural concrete (aci 318r-19)." American Concrete Institute.

Baydin, A. G., Pearlmutter, B. A., Radul, A. A., & Siskind, J. M. (2018) "Automatic differentiation in machine learning: a survey." *Journal of Machine Learning Research*, 18, pp. 1-43.

Bažant, Z. P., & Gambarova, P. (1980). "Rough cracks in reinforced concrete." *Journal of the Structural Division*, *106*(4), 819-842.

Beer, F. P., Johnston, E. R., DeWolf, J. T., & Mazurek, D. F. (2017). *Statics and mechanics of materials*. New York: McGraw-Hill Education.

Benhelal, E., Zahedi, G., Shamsaei, E., & Bahadori, A. (2013). "Global strategies and potentials to curb CO2 emissions in cement industry." *Journal of cleaner production*, 51, 142-161.

Bentz, E. (2005). "Explaining the riddle of tension stiffening models for shear panel experiments." *Journal of structural engineering*, 131(9), 1422-1425.

Block, P., Calvo Barentin, C., Ranaudo, F., & Paulson, N. (2019). "Imposing challenges, disruptive changes: rethinking the floor slab." *The materials book: inspired by the 6th lafargeholcim foundation*, 67.

Blomfors, M., Lundgren, K., & Zandi, K. (2021). "Incorporation of pre-existing longitudinal cracks in finite element analyses of corroded reinforced concrete beams failing in anchorage." *Structure and Infrastructure Engineering*, 17(7), pp. 960-976.

Box, G. E. (1979) "Robustness in the strategy of scientific model building." *Robustness in statistics*, pp. 201-236).

Breyer, D. E., Cobeen, K. E., Fridley, K. J., & Pollock, D. G. (2015). *Design of wood structures—ASD/LRFD*. McGraw-Hill Education.

Campana, S., Ruiz, M. F., Anastasi, A., & Muttoni, A. (2013). Analysis of shear-transfer actions on one-way RC members based on measured cracking pattern and failure kinematics. *Magazine of Concrete Research*, 65(6), 386–404.

Cavagnis, F., Ruis, F., Muttoni, A. (2018) "A mechanical model for failures in shear of members without transverse reinforcement based on development of a critical shear crack." *Engineering Structures*, 157, pp. 300-315.

Cavagnis, F., Ruiz, M., Muttoni, A. (2015) "Shear failures in reinforced concrete members without transverse reinforcement: An analysis of the critical shear crack development on the basis of test results." *Engineering Structures*, 103(9), pp. 157-173

Cavagnis, F., Ruiz, M., Muttoni, A. (2017) "An analysis of the shear-transfer actions in reinforced concrete members without transverse reinforcement based on refined experimental measurements." *Structural Concrete*, 19(1), pp. 49-64

Cavagnis, F., Simoes, J., Ruiz, M. (2020) "Shear strength of members without transverse reinforcement based on development of critical shear crack" *ACI Structural Journal*, 117(1), pp. 103-118.

Chakraborty, S., & Adhikari, S. (2021). "Machine learning based digital twin for dynamical systems with multiple time-scales." *Computers & Structures*, 243, 106410.

Charalampakis, A. E., & Papanikolaou, V. K. (2021) "Machine learning design of R/C columns." *Engineering Structures*, 226.

Classen, M. (2020) "Shear Crack Propagation Theory (SCPT) – The mechanical solution to the riddle of shear in RC members without shear reinforcement." *Engineering Structures*, 210.

Dulacska, H. (1972, December). "Dowel action of reinforcement crossing cracks in concrete." In *Journal Proceedings,* 69 (12), 754-757.

El-Ariss, B. (2007). "Behavior of beams with dowel action." *Engineering structures*, 29(6), 899-903.

Eshkevari, S. S., Takáč, M., Pakzad, S. N., & Jahani, M. (2021). "DynNet: Physics-based neural architecture design for nonlinear structural response modeling and prediction." *Engineering Structures*, 229, 111582.

Esteghamati, M. Z., & Flint, M. M. (2021). "Developing data-driven surrogate models for holistic performance-based assessment of mid-rise RC frame buildings at early design." *Engineering Structures*, 245, 112971.

Feng, D., Wang, W., Mangalathu, S. (2021) "Implementing ensemble learning methods to predict the shear strength of RC deep beams with/without web reinforcements" *Engineering Structures*, 235

Ferguson, M. (1956) "Some Implications of Recent Diagonal Tension Tests." *ACI Journal Proceedings*, 53(2), pp. 157-172.

Ferguson, P. (1951) "Diagonal Tension in Reinforced Concrete Beams," *Journal Proceedings*, 48(2), pp. 156-1 to 156-3

Fernández Ruiz, M., Mirzaei, Y., & Muttoni, A. (2013). "Post-punching behavior of flat slabs." *ACI Structural Journal*, 110, 801-812.

Friberg, B. F. (1940). "Design of dowels in transverse joints of concrete pavements." *Transactions of the American Society of Civil Engineers*, *105*(1), 1076-1095.

Gondia, A., Ezzeldin, M., & El-Dakhakhni, W. (2020). "Mechanics-guided genetic programming expression for shear-strength prediction of squat reinforced concrete walls with boundary elements." *Journal of Structural Engineering*, 146(11), 04020223.

Guidotti, R. (2010) "Poinc ̧onnement des planchers-dalles aveccolonnes superpose ́es fortement sollicite ́es." PhD thesis. Ecole Polytechnique Fe ́de ́rale de Lausanne, Lausanne, Switzerland.

Guan, X., Burton, H., Shokrabadi, M., & Yi, Z. (2021). "Seismic drift demand estimation for steel moment frame buildings: From mechanics-based to data-driven models." *Journal of Structural Engineering*, 147(6), 04021058.

Gunaratnam, D., Gero, J. (1994) "Effect of Representation on the Performance of Neural Networks in Structural Engineering Applications." *Computer-Aided Civil and Infrastructure Engineering*, 9(2), pp. 97-108.

Haghighat, E., Raissi, M., Moure, A. (2021) "A physics-informed deep learning framework for inversion and surrogate modeling in solid mechanics." *Computer Methods in Applied Mechanics and Engineering*, 379.

He, K., Zhang, X., Ren, S., & Sun, J. (2016) "Deep residual learning for image recognition." *Proceedings of the IEEE conference on computer vision and pattern recognition*, pp. 770-778.

He, Q., Chen, J. (2020) "A Physics-Constrained Data-Driven Approach Based on Locally Convex Reconstruction for Noisy Database." *Computer Methods in Applied Mechanics and Engineering*, 363.

Hillerborg, A. (1983). "Analysis of one single crack."*F. H. Wittmann (Ed.), Fracture Mechanics of Concrete (Developments in civil engineering),* pp. 223-249.

Hognestad, E. (1951). Study of combined bending and axial load in reinforced concrete members. University of Illinois at Urbana Champaign, College of Engineering. Engineering Experiment Station.

Hordijk, D. (1992) "Tensile and Tensile fatigue behavior of concrete; experiments, modelling and analyses." *Heron*, 37(1), pp 1-79.

Huber, P., Huber, T., & Kollegger, J. (2016). "Investigation of the shear behavior of RC beams on the basis of measured crack kinematics." *Engineering Structures*, 113, 41-58.

Huber, T., Huber, P., & Kollegger, J. (2019). "Influence of aggregate interlock on the shear resistance of reinforced concrete beams without stirrups." *Engineering Structures*, 186, 26-42.

Jacobsen, JS. Poulsen, PN., Olesoen, JF. (2012) "Characterization of mixed mode crack opening in concrete." *Mater Struct*, 45, pp. 107-122.

Jokar, M., & Semperlotti, F. (2021). "Finite element network analysis: A machine learning based computational framework for the simulation of physical systems." *Computers & Structures*, 247, 106484.

Kani, G. (1964). "The Riddle of Shear Failure and its Solution." *Journal Proceedings*, 61(4), pp. 441-468

Karniadakis, G. E., Kevrekidis, I. G., Lu, L., Perdikaris, P., Wang, S., & Yang, L. (2021). "Physics-informed machine learning." *Nature Reviews Physics*, 3(6), pp. 422-440.

Kim, S. H., Song, X., Cho, C., & Lee, C. H. (2021). "Strength prediction of steel CHS X-joints via leveraging finite element method and machine learning solutions." *Journal of Constructional Steel Research*, 176, 106394.

Kirchdoerfer, T., Oritz, M. (2016) "Data-driven computational mechanics." *Computer Methods in Applied Mechanics and Engineering*, 304, pp. 81-101.

Kirchdoerfer, T., Oritz, M. (2017) "Data Driven Computing with noisy material data sets." *Computer Methods in Applied Mechanics and Engineering*, 326, pp. 622-641.

Kirchdoerfer, T., Oritz, M. (2018) "Data-driven computing in dynamics." *International Journal for Numerical Methods in Engineering*, 113(11), pp. 1697-1710.

Košćak, J., Damjanović, D., Bartolac, M., & Duvnjak, I. (2022). "Shear behavior of RC beams without transverse reinforcement: An analysis of crack kinematics and transfer mechanisms based on stereophotogrammetric measurements." *Engineering Structures*, 255, 113886.

Kupfer, HB., Gerstel, KH. (1973) "Behavior of Concrete Under Biaxial Stresses." *Journal of Engineering Mechanics*, 99(4), pp. 853-66.

Leonhardt, F., and Walther. (1961) "Contribution to the Treatement of Shear Problems in Reinforced Concrete" *Beton-und Stahibetonbau* 56(12)

Mangalathu, S., Shin, H., Choi, E. (2021) "Explainable machine learning models for punching shear strength estimation of flat slabs without transverse reinforcement" *Journal of Building Engineering*, 39.

Marí, A., Bairán, J., Cladera, A., Oller, E., & Ribas, C. (2015). "Shear-flexural strength mechanical model for the design and assessment of reinforced concrete beams." *Structure and Infrastructure Engineering*, 11(11), 1399-1419.

Millard, S. G., & Johnson, R. P. (1984). "Shear transfer across cracks in reinforced concrete due to aggregate interlock and to dowel action." *Magazine of concrete research*, *36*(126), 9-21.

Muttoni, A., & Ruiz, M. (2008). "Shear strength of members without transverse reinforcement as function of critical shear crack width." *ACI Structural Journal*, 105, pp. 163-172.

Napolitano, R., Glisic, B. (2020) "Hybrid physics-based modeling and data-driven method for diagnostics of masonry structures." *Computer Aided Civil and Infrastructure Engineering*, 35(5), pp. 483-494.

Ngo, D., & Scordelis, A. C. (1967). "Finite element analysis of reinforced concrete beams." *In Journal Proceedings*, 64 (3), 152-163.

Perez, J., Cladera, A., Rabunal, J. (2012) "Optimization of existing equations using a new Genetic Programming algorithm: Application to the shear strength of reinforced concrete beams." *Advances in Engineering Software*, 50(1), pp. 82-96.

Rackauckas, C., Ma, Y., Martensen, J., Warner, C., Zubov, K., Supekar, R., ... & Edelman, A. (2020) "Universal differential equations for scientific machine learning." arXiv preprint arXiv:2001.04385.

Raissi, M., Perdikaris, P., & Karniadakis, G. E. (2019). "Physics-informed neural networks: A deep learning framework for solving forward and inverse problems involving nonlinear partial differential equations." *Journal of Computational physics*, *378*, 686-707.

Rao, C., Sun, H., & Liu, Y. (2021). "Physics-informed deep learning for computational elastodynamics without labeled data." *Journal of Engineering Mechanics*, 147(8), 04021043.

Reddy, J. N. (2019). *Introduction to the finite element method*. McGraw-Hill Education.

Reineck, K. (1991) "Ultimate shear force of structural concrete members without transverse reinforcement derived from a mechanical model." *Structural Journal*, 88(5), pp. 592-602

Reinhardt, H. (1984) "Fracture Mechanics of an Elastic Softening Material Like Concrete." *Heron*, 29(2), pp. 1-42.

Reinhardt, H., Cornelissen, H., Hordijk, D. (1986) "Tensile Tests and Failure Analysis of Concrete." *Journal of Structural Engineering*, 112(11), pp. 2462-2477.

Ruiz, M. F., Muttoni, A., & Sagaseta, J. (2015). "Shear strength of concrete members without transverse reinforcement: A mechanical approach to consistently account for size and strain effects." *Engineering structures*, 99, 360-372.

Saint-Venant, A. J. C. B. (1855) "Memoire sur la Torsion des Prismes" *Mem. Divers Savants*, 14, pp. 233–560

Schaeffer, H., Tran, G., Ward, R. (2018) "Extracting Sparse High-Dimensional Dynamics from Limited Data." *SIAM Journal on Applied Mathematics*, 78(6), pp. 3279-3295.

Schlaich, J., & Schafer, K. (1991). "Design and detailing of structural concrete using strut-and-tie models." *Structural Engineer*, 69(6), 113-125.

Segui, W. T. (2012). *Steel design*. Cengage Learning.

Shukla, K., Di Leoni, P. C., Blackshire, J., Sparkman, D., & Karniadakis, G. E. (2020). "Physics-informed neural network for ultrasound nondestructive quantification of surface breaking cracks." *Journal of Nondestructive Evaluation*, 39(3), 1-20.

Sofi, F. A., & Steelman, J. S. (2021). "Using committees of artificial neural networks with finite element modeling for steel girder bridge load rating estimation." *In Structures,* 33, 533-553. Elsevier.

Soroushian, P., Obaseki, K., & Rojas, M. C. (1987). "Bearing strength and stiffness of concrete under reinforcing bars." *Materials Journal*, *84*(3), 179-184.

Sun, H., Burton, H. V., & Huang, H. (2021). "Machine learning applications for building structural design and performance assessment: State-of-the-art review." *Journal of Building Engineering*, 33.

Taylor, R. (1960) "Some Shear Tests on Reinforced Concrete Beams without Shear Reinforcement" *Magazine of Concrete Research*, 12(36), pp. 145 -154.

Timoshenko, S. P. (1921). "LXVI. On the correction for shear of the differential equation for transverse vibrations of prismatic bars." *The London, Edinburgh, and Dublin Philosophical Magazine and Journal of Science*, *41*(245), 744-746.

Tipireddy, R., Perdikaris, P., Stinis, P., Tartakovsky, A. (2019) "A comparative study of physics-informed neural network models for learning unknown dynamics and constitutive relations." *CoRR*, abs/1904.04058

Tirassa, M., Ruiz, M. F., & Muttoni, A. (2020). "Influence of cracking and rough surface properties on the transfer of forces in cracked concrete." *Engineering Structures*, *225*, 111138.

Ulaga, T. (2003) "Betonbauteile mit stab-und lamellenbewehrung: verbund-und zuggliedmodellierung." PhD thesis, ETHZ, Zurich, Switzerland.

Vapnik, V. N., & Chervonenkis, A. Y. (2015) "On the uniform convergence of relative frequencies of events to their probabilities." *Measures of complexity*, pp. 11-30.

Vecchio, F. J., & Collins, M. P. (1986). "The modified compression-field theory for reinforced concrete elements subjected to shear." *ACI J.*, 83(2), pp. 219-231.

Vianna, F., Nascimento, R., Dourado, A. (2021) "Estimating model inadequacy in ordinary differential equations with physics-informed neural networks" *Computers and Structures*, 245.

Walraven, J. (1980) "Aggregate Interlock: A Theoretical and Experimental Investigation." Ph.D. thesis, Delft University of Technology, Delft, Netherlands.

Walraven, J. C. (1979). "Experiments on shear transfer in cracks in concrete. Part II: Analysis of results." *Report Stevin Laboratory, Concrete Structures,* 5-79-10.

Walraven, J. C. (1981). "Fundamental analysis of aggregate interlock." *Journal of the Structural Division*, 107(11), 2245-2270.

Walraven, J. C., & Reinhardt, H. W. (1981). "Concrete mechanics. Part A: Theory and experiments on the mechanical behavior of cracks in plain and reinforced concrete subjected to shear loading." *Nasa Sti/recon Technical Report N*, *82*, 25417.

Wang, H., Wu, T. (2020) "Knowledge-Enhanced Deep Learning for Wind-Induced Nonlinear Structural Dynamic Analysis." *Journal of Structural Engineering*, 146(11).

Wight, J. K., & MacGregor, J. G. (2016). *Reinforced concrete*. Pearson Education UK.

Xu, Y., Zheng, B., & Zhang, M. (2021). "Capacity prediction of cold-formed stainless steel tubular columns using machine learning methods." *Journal of Constructional Steel Research*, 182, 106682.

Yang, Y. (2014). Shear behavior of reinforced concrete members without shear reinforcement: a new look at an old problem.

Zararis, P. D., & Papadakis, G. C. (2001). "Diagonal shear failure and size effect in RC beams without web reinforcement." *Journal of structural engineering*, 127(7), 733-742.

Zhang, R., Liu, Y., & Sun, H. (2020). "Physics-guided convolutional neural network (PhyCNN) for data-driven seismic response modeling." *Engineering Structures*, 215, 110704.

Zhang, Z., Sun, C. (2020) "Structural damage identification via physics-guided machine learning: a methodology integrating pattern recognition with finite element model updating" *Structural Health Monitoring*.

Zhang, R., Liu, Y., & Sun, H. (2020). "Physics-informed multi-LSTM networks for metamodeling of nonlinear structures." *Computer Methods in Applied Mechanics and Engineering*, 369, 113226.

Zhang, M., Akiyama, M., Shintani, M., Xin, J., & Frangopol, D. M. (2021). "Probabilistic estimation of flexural loading capacity of existing RC structures based on observational corrosion-induced crack width distribution using machine learning." *Structural Safety*, 91, 102098.

Zsutty, T. C. (1968). "Beam shear strength prediction by analysis of existing data." *Journal Proceedings* 65(11), pp. 943-951.